# Mathematical Modelling, Simulation and Optimization of Gas Dynamics in a Car's Exhaust Pipe

**Dissertation**
**zur Erlangung des Doktorgrades**
**der Fakultät für Mathematik, Informatik**
**und Naturwissenschaften**
**der Universität Hamburg**

vorgelegt
im Fachbereich Mathematik

von
Martin Rafael Rybicki
aus Neustadt

Hamburg, 2014

Als Dissertation angenommen vom Fachbereich
Mathematik der Universität Hamburg

Auf Grund der Gutachten von: Prof. Dr. Ingenuin Gasser
Prof. Dr. Winnifried Wollner
Prof. Dr. Roberto Natalini

Hamburg, den 02.07.2014

Prof. Dr. Armin Iske
Leiter des Fachbereichs Mathematik

## Acknowledgements

I would like to express my deep gratitude to Prof. Dr. Ingenuin Gasser and Jun.-Prof. Dr. Winnifried Wollner, my research supervisors, for their patient guidance and constantly outstanding support during the last years. This work would not have been possible without the time they devoted to me.

I am very grateful for the experience I was able to gather at several conferences, workshops and summer schools during my PhD time. Therefore my special thanks to Prof. Dr. Ingenuin Gasser, Prof. Dr. Michael Hinze and the University of Hamburg who helped me to realize those travels by providing funding.

I thankfully appreciate the support of several colleagues. Nikolaus von Daniels, Dr. Elisabetta Felaco, Dr. Claus Goetz, Libor Kadrnka, Philipp Kunde, Alexander Lohse and Arne Roggensack were constantly available for technical discussions and always willing to help me with their expertise. Moreover, I would like to acknowledge the proofreading by Alexander Lohse and Arne Roggensack, who gave me valuable remarks and advice.

My deepest thanks to my partner Stefanie Wegener and my parents Izabela and Mariusz Rybicki for their loving support.

# Contents

# 1. Introduction

Emissions caused by vehicles have been an important issue over the last five decades. Moreover, it still is of huge relevance, as the reaction to exceptionally high levels of air pollution in Paris on March 17 2014 shows: Cars with even-numbered license plates and commercial vehicles over 3.5 tons were banned from entering the city during that day. The plan of banning the odd-numbered plates on the next day became unnecessary, since the level of pollution was reduced[1].

In order to reduce the exhaust gas pollution, governments in many countries of the world prescribe technical requirements for the production of cars, especially the exhaust system of the car, so that their emissions do not exceed certain limits. One of the first restrictions was introduced by the government of California (USA) in the early 1960s. In 1970 the European Community passed first laws regarding exhaust gas pollution. Today, we are facing the *Euro 6* standard, which will become compulsory in September 2014 in Europe[2].

For the reduction of the concentration of harmful gases in the exhaust gas (e.g., CO, $NO_x$ and $C_xH_y$), there is a classical technical solution, namely the installation of catalytic converters in the exhaust pipe system. The functionality of catalytic converters strongly depends on the temperature in the converters. There is a lower limit (about 300 degrees Celsius) for proper functionality and an upper limit to avoid damages. In particular, right after the engine start there is a critical time interval where the temperature in the converters is not high enough. That is why the cold start phase has a disproportionally high impact on pollutant emission caused by vehicles.

A method of heating the catalysts after starting the engine is the combustion of unburnt gas in the catalytic converters. Modern exhaust systems can control the ratio of oxygen and fuel in the combustion chamber of the engine. By choosing a ratio with more fuel and less oxygen some unburnt fuel flows to the catalytic converters where it can be used for an exothermic reaction.

Computational fluid dynamics (CFD) can help us to understand, predict or even control the flow of exhaust gas through a pipe during the cold start, e.g., with the aim of reducing pollutant emission. Most models concerning fluid dynamics are based on partial differential equations (PDEs). Although popular models like the

[1] `http://en.wikipedia.org/wiki/Road_space_rationing`

[2] `http://europa.eu/legislation_summaries/environment/air_pollution/l28186_en.htm`

*Navier-Stokes equations* or *Euler equations of gas dynamics* have been known for centuries, there is still no sufficient theoretical base, that makes CFD obsolete. In many real world applications computer based simulations are the only possibility to obtain information in reasonable time, without having to perform real experiments.

CFD has a wide range and there is a multitude of models that describe similar phenomena. Complex models that need hours/days/months of computational time on super-computers with thousands of teraflops per second are not always suitable. For applications like parameter-identification or optimal control they produce large costs, since such tasks require multiple model evaluations. Therefore, one would, especially in the case of such tasks, benefit from mathematical models that can deliver accurate information in a short time.

The aim of this thesis is to derive and verify a mathematical model that describes the transient gas dynamics in an exhaust pipe in a correct and numerically efficient way. Subsequently, this model will be needed to answer the question, how to optimally control the inflow of unburnt gas in order to heat up the catalytic converters during the cold start phase.

The mathematical and especially engineering literature on modelling and simulation of exhaust pipes is broad. There are many different issues the research is focused on, from studies of vibrations (see e.g., [JW98, Lin94]) and sound waves in the exhaust pipe system (see e.g., [HDRD11, LT11]) to studies of the dynamics of the temperature in catalytic converters, etc. As already indicated, we focus on the latter issue.

Rjasanow [Rja95] studied the influence of the geometric structure of the exhaust pipe on the heating process of a catalyst. Diverse chemical reactions in the catalytic converter are studied in the textbook of Cumberbatch and Fitt [CF01] with the aim of a better understanding of the heating process after the engine start. Similar models are presented in the book of Friedman and Littman [FL94], where additionally an optimal control problem with respect to the temperature in the catalyst is considered.

There are several multi-dimensional approaches (see e.g., [BHT$^+$, CCDD03]), which are known to be numerically very expensive. These studies are necessary if one is interested in detailed fluid dynamic phenomena in a specific part of the exhaust pipe (with the trade-off of more complex modelling and an enormous increase in computation times).

We focused on one-dimensional models of the gas flow through an exhaust pipe. They are known to be much simpler and still very accurate in predicting certain flow quantities, like temperature and density (see [CH99, LTW09, MSZH11]).

The model of interest for this thesis is the promising model that was studied by Lacoste and Natalini (see [LN04]). There, a fully compressible, one-dimensional approach on the basis of the reactive Euler equation of gas was followed, in order

to model the chemical processes which arise inside an exhaust pipe. The model is described in detail in Section 2.3. However, there is still room for improvement, since this approach has weaknesses when it comes to numerical simulation, in the sense that the computing efficiency suffers.

1. It is known that the flow in an exhaust pipe is always in the small Mach number regime. This can cause severe numerical problems in a fully compressible approach (see [SMT99, GV99]), which lead to large computing costs.

2. The description of the pipe's geometry in [LN04] is realized by a cross section function in the governing equations (see also [Liu82, MSZH11] for such an approach). The strongly varying cross sections lead to very small step sizes for the spatial discretization at the cross overs (and due to the CFL condition also in time[3]).

This thesis is devoted to overcoming these issues and therefore we derive a new, numerically more efficient model on the basis of the Lacoste-Natalini model. We perform two steps to rule out the above mentioned disadvantages.

1. A way out of the delicate small Mach number situation is to use the small Mach number in order to derive an asymptotic model. The advantage is, that such an asymptotic model does not track the propagation of sound waves. Therefore, larger step sizes in time can be realized in the numerical simulation (see also [KSGF09] on this issue). An incompressible approach is not recommended due to the strongly varying temperatures.

2. In order to avoid strongly varying geometry functions, we consider the exhaust pipe as a network of single pipes with constant cross sections. In this way we completely avoid using geometry functions and shift the problem to finding physically meaningful coupling conditions at the vertices. This gives us the opportunity to include *minor loss terms*, which describe pressure losses due to turbulences at the junctions.[4] Coupling conditions for similar problems were discussed, for example, by Gasser and Kraft in [GK08] and by Banda, Herty and Klar [BHK06]. A similar network approach for a part of the exhaust pipe was presented by D'Errico, Ferrari and Onorati in [DFO00], but although pressure losses were mentioned in that work, they have not been taken into account in the numerical realization.

The details on both steps, the network approach and the small Mach number limit, as well as the derivation and presentation of the model of Lacoste and

[3]Details on the CFL condition for our numerical algorithms are given in Subsections 3.3.1 and 3.3.2.

[4]Remark 4 on Page 25 is devoted to this issue.

Natalini, will be given in Chapter 2, which finishes with the proposal of a new asymptotic model.

Clearly, mathematical models have to be verified to convince the reader of their meaningfulness. The new asymptotic model consists of highly non-linear, coupled PDEs on a network, and does not fit into a class of (partly) well understood systems, i.e., it is neither parabolic, elliptic nor hyperbolic. Hence, an analytic approach is a difficult task and was beyond the scope of this thesis. Therefore, we will apply computer based simulations to obtain numerical solutions.

In Chapter 3, we derive and present the numerical algorithm we use, and verify its correctness by studying the numerical convergence of the transient problem towards the analytical stationary solution. Subsequently, we check the accuracy of the model by comparing it to the pre-asymptotic, hyperbolic one, i.e., a well established model. We do not only compare and interpret the results, but also discuss the numerical efficiency. We will deduce a good agreement of the numerical simulations and a drastic advantage for the new model with respect to computing times. In contrast to the established hyperbolic model, which is slower by orders of magnitude, simulations of the asymptotic model run on regular laptop PCs in real time.

Having a numerically efficient and accurate model, we can tackle the mentioned optimization task. We recall that unburnt fuel is used for the heating of the catalytic converter during a cold start. Clearly, there is a competition between reaching the optimal converter temperature fast and using very little unburnt fuel in the exhaust gas. Optimization on such a model is still a highly challenging topic. We only mention representatively some works where similarly complex issues were studied: Herty and Sachers [HS07] studied how to optimally transport gas through pipeline networks by controlling the power of compressor stations. Gugat et al. [GHKL05] considered an optimization task related to traffic flow, whereas the optimal cooling of glass was studied by Frank, Klar and Pinnau in [FKP10].

In Chapter 4, we show how to compute an optimal inflow distribution of unburnt gas (into the exhaust tube) with respect to a cost function, subject to our asymptotic model. The cost functional consists of a tracking-type term for the temperature of the catalytic converter and a penalization term for the consumption of fuel. Since we want to follow the steepest descent direction of the cost functional, we require a gradient which we compute by adjoint calculus. We therefore differentiate the Lagrangian functional, which contains all information about the cost functional and the asymptotic model, with respect to the the control, state and adjoint variables. The technical derivation of the first order optimality conditions is a major part of that chapter. However, it is done only on a formal basis, since we do not know anything about the space of solutions. While this mechanism is well known in the context of elliptic, parabolic and also hyperbolic systems, to our

knowledge it has never been applied to a type of equations like our asymptotic model. We complete Chapter 4 with a discussion about the discretization and the presentation of some numerical examples.

Lastly, we want to mention the Appendix A which is devoted to the nomenclature and should be considered whenever one loses track of the notation.

Part of the results in this thesis have been published in:

[GR13] I. Gasser, M. Rybicki: *Modelling and simulation of gas dynamics in an exhaust pipe*, Applied Mathematical Modelling, vol. 37 (5), 2747–2764, 2013.
`http://dx.doi.org/10.1016/j.apm.2012.06.010`

[GRW14a] I. Gasser, M. Rybicki, W. Wollner: *Modelling, simulation and optimization of gas dynamics in an exhaust pipe*, In *Hyperbolic Problems: Theory, Numerics, Applications (Proceedings of the 14th International Conference on Hyperbolic Problems held in Padova, June 25–29, 2012)*, vol. 8, 907–914, 2014.

[GRW14b] I. Gasser, M. Rybicki, W. Wollner: *Optimal control of the temperature in a catalytic converter*, Computers and Mathematics with Applications, vol. 67 (8), 1521–1544, 2014.
`http://dx.doi.org/10.1016/j.camwa.2014.02.006`

The content of the first publication [GR13] is embedded in Chapters 2 and 3, whereas the fourth Chapter consists of the issues discussed in the last publication [GRW14b]. The contribution to the Proceedings of the Conference HYP2012 [GRW14a] contains a compact overview over all main issues of this thesis, namely modelling, simulation and optimization of gas dynamics in an exhaust pipe.

# 2. Modelling

The aim of this chapter is to derive a mathematical model that describes the dynamics of exhaust gas in a car's exhaust pipe. In Section 2.1, we explain roughly what an exhaust pipe in a car consists of and how catalytic converters work. Then, we present and partly motivate the model of Lacoste and Natalini in Section 2.3, which describes the gas dynamics in an exhaust pipe. Starting from their model, we derive a new, numerically more efficient, model in the remaining sections of this chapter. The key steps to our goal are a *network approach* (Section 2.4) and a *low Mach number limit* (Section 2.5).

The major content of this chapter, namely the derivation of a new asymptotic model on a network of pipes (Sections 2.4 and 2.5), has been published in [GR13][1].

## 2.1. The application's background[2]

The cause of a car's movement is the transformation of *chemical energy* into *mechanical energy*, mostly *kinetic energy*. Whereas chemical energy is the potential of releasing (or absorbing) energy through chemical reactions, kinetic energy is the energy of motion. In this case, the chemical energy is stored in a high-energy fluid, the *fuel*. There are many chemical components in this fluid. Furthermore, they differ from fuel to fuel (e.g., diesel and benzine). However, we just consider a reference reaction of a hydrocarbon molecule with oxygen, i.e., an *oxidation* of $\mathrm{C}_x\mathrm{H}_y$, which represents the explosion of fuel in a combustion chamber:

$$\mathrm{C}_x\mathrm{H}_y + \left(x + \frac{y}{4}\right)\mathrm{O}_2 \to x\mathrm{CO}_2 + \frac{y}{2}\mathrm{H}_2\mathrm{O} + \Delta_R H, \tag{R1}$$

where $\Delta_R H$ denotes the reaction enthalpy, which represents the heat release due to the combustion. Reaction (R1) is of course a rough simplification of all the (partly still unknown) complex inside reactions in the combustion process. Since the considered oxidation is of *exothermic* nature, we have $\Delta_R H > 0$. The rise of temperature and pressure of the gas mixture in the combustion chamber is

[1] Using the published content in this thesis is in agreement with the copy rights of the publisher: `http://www.elsevier.com/journal-authors/author-rights-and-responsibilities`.

[2] The content of this section is taken from the book *Handbuch Verbrennungsmotor* [vBS05].

transformed into kinetic energy of the piston. We explain this in more detail in the following paragraph.

We consider a *four stroke cycle engine*. Such an engine has four stages/strokes, where one stroke represents a complete and vertically directed movement of the piston in the combustion chamber (see also Figure 2.1):

1. **Intake stroke:** In this stage the exhaust valve is closed and the inlet valve is open. The piston moves down and creates a depression, which causes an intake of the fuel-air mixture.

2. **Compression stroke:** Both valves are closed. The piston moves up and compresses the mixture.

3. **Combustion stroke:** The piston reaches its top position and the mixture its highest compression. At this point the spark plug emits a spark which ignites the fuel-air mixture. The explosion/oxidation (R1) takes places. The heat release leads to a large increase of temperature and pressure, which pushes the piston down.

4. **Exhaust stroke:** After the piston reaches the bottom position the exhaust valve opens. The piston moves up again and pushes the burnt gas mixture out of the combustions chamber into the exhaust pipe.

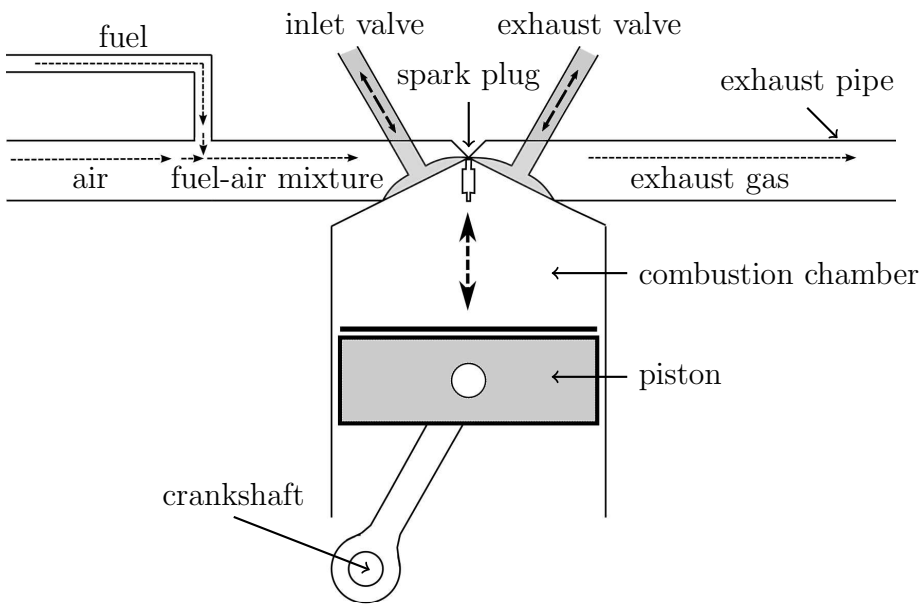


Figure 2.1.: Combustion engine

Modern cars are equipped with more than one combustion chamber. Usually there are at least four cylinders with shifted strokes, in order to provide a smooth impulse on the crankshaft.

## Catalytic converters

The products of the combustion of the fuel-air mixture are ejected into the exhaust pipe. Some unwanted chemical products are toxic, such as carbon monoxide (CO), carbon hydrides ($C_xH_y$) or nitrogen oxides ($NO_z$). Therefore, one is interested in transforming those harmful gases into less harmful gases, before emitting them into the environment. For this purpose *catalytic converters* are essential components in cars' exhaust systems. A catalyst is a substance which reduces the activation energy of certain chemical reactions, by providing alternative reaction channels, without being consumed by the reactants. Thus, with the help of catalysts chemical reactions can occur under conditions which are not sufficient for the reactions without the catalyst. The reactions we consider are:

- Oxidation of $C_xH_y$ and CO:

$$\begin{gathered} C_xH_y + \left(x + \frac{y}{4}\right) O_2 \rightarrow xCO_2 + \frac{y}{2}H_2O \\ 2CO + O_2 \rightarrow 2CO_2 \\ CO + H_2O \rightarrow CO_2 + H_2 \end{gathered}$$

- Reductions of $NO_z$:

$$\begin{gathered} 2NO_z + 2zCO \rightarrow N_2 + 2zCO_2 \\ 2NO_z + 2zH_2 \rightarrow N_2 + 2zH_2O \\ \left(2x + \frac{y}{2}\right) NO_z + zC_xH_y \rightarrow \left(x + \frac{y}{4}\right) N_2 + xzCO_2 + \frac{yz}{2}H_2O \end{gathered}$$

A catalytic converter which supports the oxidation of carbon monoxide (CO) and carbon hydrides ($C_xH_y$) as well as the reduction of nitrogen oxides ($NO_z$), is called *three-way catalyst* (TWC). Such a TWC in a car's exhaust pipe, that reduces the activation energy of the above mentioned reactions, typically consists of several components. A honeycomb-like structured ceramic block serves as a carrier. Its channels are coated with noble metals. This coating is called *wash coat*, and consists mainly of platinum (Pt), palladium (Pd) and rhodium (Rh). The oxidations and reductions mentioned above, take place on the surface of this noble metal coating. To this end, the honeycomb structure is chosen to provide a large surface area. With this construction technique (honeycomb structure with many small channels)

catalytic converters can reach surface areas up to a hundred square metres. Due to this structure a local friction force acts on the bypassing fluids.

A crucial quantity for the sufficient transformation of harmful into less harmful gases is the temperature of the catalytic converter. Although the activation temperature for the oxidations and reductions is reduced by the catalyst, it is still far above the mean outside temperature. The temperature which ensures that the reactions take place in a desired order of magnitude is called *light off temperature* $\tilde{T}_{lo} \approx 550 - 600\text{K}$. As long as this temperature is not reached, neither the reduction of $NO_z$, nor the oxidations of CO and $C_xH_y$ occur on a significant scale. This is especially a problem for a cold start of the car. During this phase the concentration of unwanted molecules in the emitted exhaust gas is highest. That is why the cold start phase has a disproportionally high impact on the exhaust gas emission caused by vehicles (see [GHH10]).

Therefore, one is interested in heating up the catalytic converter as fast as possible. An electric heating for the catalyst is not a reasonable option, due to the low available voltage of 12 V. A better and in practice often applied method is to use some unburnt fuel from the explosion in the combustion chamber for an exothermic reaction in the converter.

### How does unburnt fuel reach the catalytic converter?

In order to have enough unburnt fuel for the exothermic reaction in the catalyst, one needs to choose the $\lambda$-*ratio* to be less than one. The $\lambda$-ratio is the ratio between the air mass which is in the combustion chamber during the combustion stroke, and the *stoichiometric* air mass, i.e., $\lambda = m_{\text{air}}/m_{\text{air}}^{\text{st}}$. The stoichiometric air mass is needed for a complete combustion, so that neither unburnt fuel nor unburnt air leaves the combustion chamber in the exhaust stroke. The stoichiometric amount of air for 1 kg of petrol (diesel) is 14.7 kg (14.5 kg) of air. The $\lambda$-ratio can be controlled by an electronic control unit. Thus, by choosing $\lambda < 1$, i.e., letting not enough air into the combustion chamber for a complete combustion of fuel, unburnt fuel can enter the exhaust pipe in the exhaust stroke. This reactant can be used for an exothermic reaction in the catalytic converter and therefore reduce the time until the light off temperature $\tilde{T}_{lo}$ is reached.

### Where does the oxygen for the exothermic reaction (R1) come from?

Since $\lambda < 1$ the gas mixture in the exhaust pipe does not contain any unburnt air. However, oxidations, such as the exothermic reaction (R1), need oxygen. The supply of $O_2$ is ensured by the injection of *secondary air*. By this procedure air is injected into the exhaust pipe by an electrical pump and circumvents the absence of oxygen for the exothermic oxidation. Figure 2.2 shows the impact of secondary

air on the temperature in the catalytic converter after a cold start.

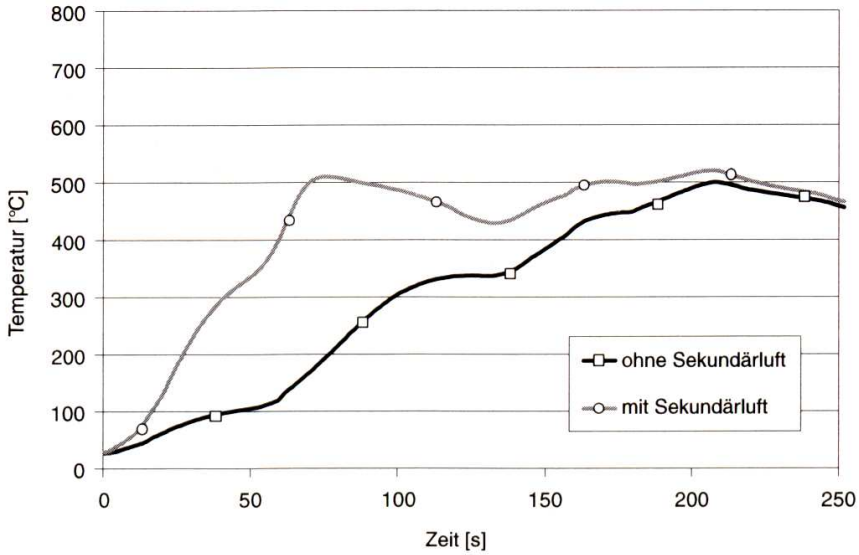


Figure 2.2.: Time evolution of a catalyst's temperature with (black graph, □) and without (grey graph, ○) secondary air (from [vBS05], page 711).

## Mufflers

Like in the case of gas emission, the legislative authorities prescribes compulsory critical levels for the noises produced by cars. *Muffler* devices are designed to reduce this noise. Some mufflers are filled with materials that absorb the noise, whereas others contain perforated pipes and chambers which are arranged so that the sound waves are reflected back towards the engine.

There are several studies on how to reduce this noise, dealing with the vibrations produced by the exhaust pipe (see e.g., [JW98, Lin94]) or sound waves (see e.g., [HDRD11, LT11])). However, in our application we will not be interested in noise emission issues and therefore keep this paragraph on mufflers short.

## The whole exhaust pipe

We finalize this section with an overview of the geometrical structure of the whole exhaust pipe. Due to the heat of the engine one is interested in building the catalytic converter as close to the engine as possible. This ensures high temperature of the catalyst. However, due to the lack of space near the engine one can only

build small catalytic converters next to it. Since such a small converter is not sufficient to match the critical levels for gas emission, a second catalyst is installed in many exhaust pipes (see Figure 2.3)

Our considered exhaust pipe will consist of two catalytic converters and two mufflers.

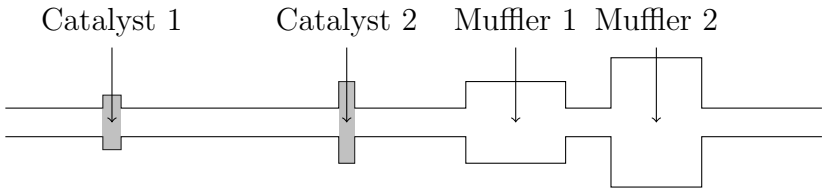


Figure 2.3.: Considered exhaust pipe: consists of two catalytic converters and two mufflers

## 2.2. The pipe's geometry

The domain in which we want to describe the transient gas dynamics with mathematical models, is a car's exhaust pipe. We assume the pipe to be rotationally symmetric. The data of the considered pipe's geometry is taken from [LN04, Pet07] and can be found in Table 2.1 and is illustrated in Figure 2.4. The pipe has a length of $\tilde{L} = 3.6$m and consists of $n_P = 9$ pipes with each a constant radius, including two catalytic converters and two mufflers. Since the mufflers will be physically treated as empty pipes, we only discriminate between pipes that do and pipes that do not have a catalytic converter. For this purpose we introduce the indicator mapping $\tilde{\chi} : \{1, \dots, n_P\} \to \{0, 1\}$, where

$$\tilde{\chi}^i = \begin{cases} 1, & \text{if pipe } i \text{ has a catalyst,} \\ 0, & \text{otherwise.} \end{cases} \tag{2.1}$$

As already mentioned in the introduction, the presented models will all be one-dimensional. This is known to be much simpler in terms of numerical simulation, but still very accurate in predicting flow quantities (see e.g., [CH99, GS02, BHK06, BGH11, GF13]. We render this more precisely by the following assumption.

**Assumption 1.** *Let $\tilde{y}^*(\tilde{x}, \tilde{x}_2, \tilde{x}_3, \tilde{t})$ be an arbitrary physical quantity (such as density, temperature, pressure) and $\tilde{\mathbf{u}}^*(\tilde{x}, \tilde{x}_2, \tilde{x}_3, \tilde{t})$ the velocity field at time $\tilde{t}$ and at a given point $(\tilde{x}, \tilde{x}_2, \tilde{x}_3)$ in the exhaust pipe. We assume now that all physical quantities are homogeneous in the cross section and the velocity field has only non-vanishing entries along the pipe, i.e.,*

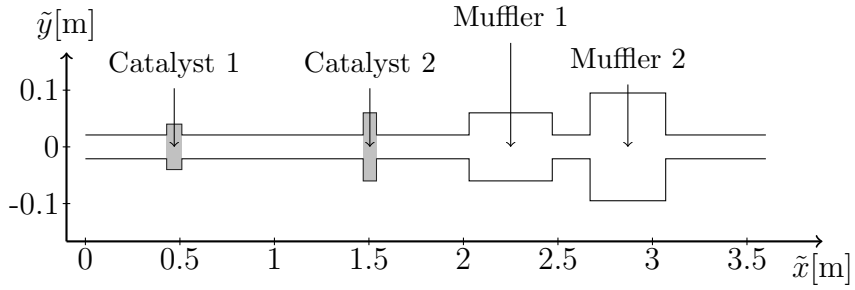


Figure 2.4.: Cross section of the considered exhaust pipe with two catalysts and two mufflers (see Table 2.1 for data)

*(A1) For fixed $\tilde{x}$ and $\tilde{t}$ all physical quantities $\tilde{y}^*(\tilde{x}, \tilde{x}_2, \tilde{x}_3, \tilde{t})$ are constant for all $(\tilde{x}_2, \tilde{x}_3)$ in the exhaust pipe. Instead of $\tilde{y}^*(\tilde{x}, \tilde{x}_2, \tilde{x}_3, \tilde{t})$, from now on we will write $\tilde{y}(\tilde{x}, \tilde{t})$.*

*(A2) The $\tilde{x}_2$ and $\tilde{x}_3$ component of the velocity field $\tilde{\mathbf{u}}$ vanish for all $\tilde{x}$ and $\tilde{t}$:*

$$\tilde{\mathbf{u}}(\tilde{x}, \tilde{t}) = \left(\tilde{u}(\tilde{x}, \tilde{t}), 0, 0\right)^T .$$

Assumption (A1) can be motivated by considering the variable's mean values over the cross section area.

## 2.3. Model proposed by Lacoste and Natalini

In this section, we present the model by Lacoste and Natalini, which was developed in 2004 in collaboration with the Italian car supplier *Magneti Marelli* (see [LN04]). For the correct formulation of this model we need a smooth cross section function $\tilde{A} : [0, \tilde{L}] \to \mathbb{R}$. Therefore, small intervals of length $\tilde{\alpha} = 0.03$m were introduced, in order to connect two different radii $r^i$ and $r^{i+1}$ via a third order polynomial $\tilde{r}_{\tilde{\alpha}}^{i+\frac{1}{2}}$, obeying the following conditions:

$$\tilde{r}_{\tilde{\alpha}}^{i+\frac{1}{2}}\left(\tilde{x}^{i+\frac{1}{2}} - \frac{\tilde{\alpha}}{2}\right) = \tilde{r}^i, \qquad \tilde{r}_{\tilde{\alpha}}^{i+\frac{1}{2}}\left(\tilde{x}^{i+\frac{1}{2}} + \frac{\tilde{\alpha}}{2}\right) = \tilde{r}^{i+1},$$

$$\left(\tilde{r}_{\tilde{\alpha}}^{i+\frac{1}{2}}\right)'\left(\tilde{x}^{i+\frac{1}{2}} - \frac{\tilde{\alpha}}{2}\right) = 0, \qquad \left(\tilde{r}_{\tilde{\alpha}}^{i+\frac{1}{2}}\right)'\left(\tilde{x}^{i+\frac{1}{2}} + \frac{\tilde{\alpha}}{2}\right) = 0,$$

where

$$\tilde{x}^{i+\frac{1}{2}} = \sum_{j=1}^{i} \tilde{L}^j \tag{2.2}$$

| pipe number $i$ | length [m] $\tilde{L}^i$ | radius [m] $\tilde{r}^i$ | catalyst $\tilde{\chi}^i$ |
|---|---|---|---|
| 1 | 0.415 | 0.021 | 0 |
| 2 | 0.12 | 0.04 | 1 |
| 3 | 0.93 | 0.021 | 0 |
| 4 | 0.1 | 0.06 | 1 |
| 5 | 0.45 | 0.021 | 0 |
| 6 | 0.47 | 0.06 | 0 |
| 7 | 0.17 | 0.021 | 0 |
| 8 | 0.43 | 0.095 | 0 |
| 9 | 0.515 | 0.021 | 0 |
| sum | $\tilde{L} = 3.6$ | - | 2 |

Table 2.1.: Geometrical data of the considered exhaust pipe. The indicator mapping $\tilde{\chi}^i$ denotes, whether pipe $i$ does or does not have a catalytic converter. For the illustration of the pipe see Figure 2.4

is the connection point between the $i$-th and $(i+1)$-th pipe. This leads to the following polynomial

$$\tilde{r}_{\tilde{\alpha}}^{i+\frac{1}{2}}(\tilde{x}) = -2\frac{\tilde{r}^{i+1} - \tilde{r}^i}{\tilde{\alpha}^3}\left(\tilde{x} - \tilde{x}^{i+\frac{1}{2}} + \frac{\tilde{\alpha}}{2}\right)^3 + 3\frac{\tilde{r}^{i+1} - \tilde{r}^i}{\tilde{\alpha}^2}\left(\tilde{x} - \tilde{x}^{i+\frac{1}{2}} + \frac{\tilde{\alpha}}{2}\right)^2 + \tilde{r}^i$$

for $\tilde{x} \in I_{\tilde{\alpha}}^{i+\frac{1}{2}}$, with

$$I_{\tilde{\alpha}}^{i+\frac{1}{2}} := \left[\tilde{x}^{i+\frac{1}{2}} - \frac{\tilde{\alpha}}{2}, \tilde{x}^{i+\frac{1}{2}} + \frac{\tilde{\alpha}}{2}\right]. \tag{2.3}$$

See Figure 2.5 for the illustration of such a polynomial. Finally the cross section and the diameter are defined by

$$\tilde{A}(\tilde{x}) := \pi\tilde{r}(\tilde{x})^2, \qquad \tilde{d}(\tilde{x}) := 2\tilde{r}(\tilde{x}), \tag{2.4}$$

where

$$\tilde{r}(\tilde{x}) := \begin{cases} \tilde{r}_{\tilde{\alpha}}^{i+\frac{1}{2}}(\tilde{x}), & \text{if } \tilde{x} \in I_{\tilde{\alpha}}^{i+\frac{1}{2}}, \\ \tilde{r}^i, & \text{if } \tilde{x} \in \left(\tilde{x}^{i-\frac{1}{2}} + \frac{\tilde{\alpha}}{2}, \tilde{x}^{i+\frac{1}{2}} - \frac{\tilde{\alpha}}{2}\right). \end{cases} \tag{2.5}$$

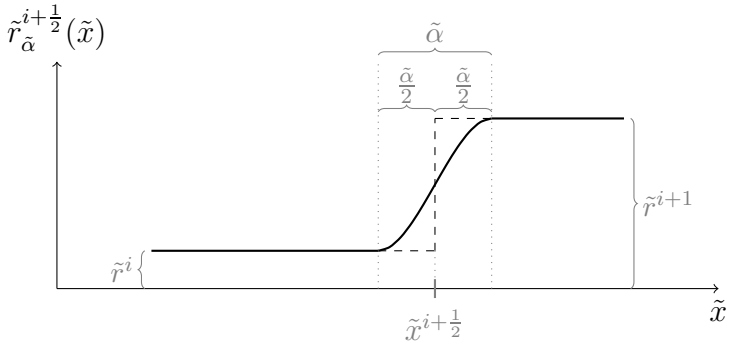


Figure 2.5.: Cubic polynomial $\tilde{r}_{\tilde{\alpha}}^{i+\frac{1}{2}}(\tilde{x})$ for smooth change of the pipe's radius

### System of equations

We will start from the well known Euler equation in a pipe with a variable cross section, i.e.,

$$\begin{aligned}(\tilde{A}\tilde{\rho})_{\tilde{t}} + (\tilde{A}\tilde{\rho}\tilde{u})_{\tilde{x}} &= 0,\\ (\tilde{A}\tilde{\rho}\tilde{u})_{\tilde{t}} + (\tilde{A}\tilde{\rho}\tilde{u}^2 + \tilde{A}\tilde{p})_{\tilde{x}} &= -\tilde{A}_{\tilde{x}}\tilde{p},\\ (\tilde{A}\tilde{\rho}\tilde{E})_{\tilde{t}} + (\tilde{A}\tilde{\rho}\tilde{u}\tilde{E} + \tilde{A}\tilde{u}\tilde{p})_{\tilde{x}} &= 0.\end{aligned}$$

See e.g., the textbook of Whitham [Whi74, Section 8.1, Page 265] for details. The model of Lacoste and Natalini consists of the reactive[3] Euler equations with right hand sides. We now present those in detail.

- **Conservation of mass**
  Let $\tilde{\rho}(\tilde{x}, \tilde{t})$ and $\tilde{u}(\tilde{x}, \tilde{t})$ be the density and the flow velocity of the gas mixture at point $\tilde{x}$ and time $\tilde{t}$, respectively. Since there are neither sinks nor sources in the exhaust pipe[4], the total mass should stay conserved over space and time, i.e.,

$$\boxed{(\tilde{A}\tilde{\rho})_{\tilde{t}} + (\tilde{A}\tilde{\rho}\tilde{u})_{\tilde{x}} = 0.} \tag{2.6}$$

- **Reaction equation**
  It is assumed, that there are only two chemical states in the gas mixture, i.e., burnt and unburnt gas. Although there is a multitude of other chemical

[3]The additional specification "reactive" implies, that the fluid consists of more than one component and that there are additional equations for those components of the fluid.

[4]Secondary air is neglected.

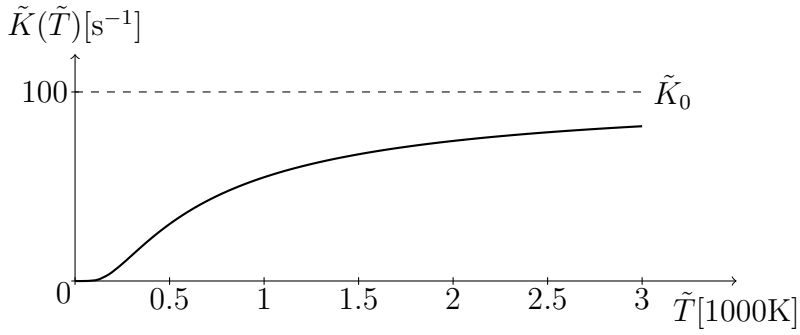


Figure 2.6.: Arrhenius' law with $\tilde{K}_0 = 100\mathrm{s}^{-1}$ and $\tilde{T}^+ = 600\mathrm{K}$

components involved in the reaction, this strongly simplified approach works very well in the model, since one is only interested in the overall heat release of all chemical reactions together (see [CCDD03, CS08] or even [FW66]).

So, let $\tilde{z}(\tilde{x}, \tilde{t})$ be the ratio of unburnt gas in the gas mixture at point $\tilde{x}$ and time $\tilde{t}$. Thus, the product $\tilde{\rho}\tilde{z}$ stands for the density of the unburnt gas in the mixture. The conserved form of the reaction equation would be (analogously to the conservation of mass equation)

$$(\tilde{A}\tilde{\rho}\tilde{z})_{\tilde{t}} + (\tilde{A}\tilde{\rho}\tilde{z}\tilde{u})_{\tilde{x}} = 0.$$

However, the ratio of unburnt gas is not conserved, but reduced by only one exothermic reaction in the catalytic converters. Furthermore, it is assumed that this reaction with a temperature dependent reaction rate $\tilde{K}(\tilde{T})$ is irreversible, where $\tilde{T} = \tilde{T}(\tilde{x}, \tilde{t})$ stands for the temperature of the gas mixture. The reaction rate is modelled by *Arrhenius'* law[5]:

$$\tilde{K}(\tilde{T}) := \tilde{K}_0 \exp\left(-\frac{\tilde{T}^+}{\tilde{T}}\right), \tag{2.7}$$

where $\tilde{T}^+ = 600\mathrm{K}$ and $\tilde{K}_0 = 100\mathrm{s}^{-1}$ represent the activation temperature and the limit reaction rate at infinitely high temperature, often called *pre-exponential factor*, respectively. See Figure 2.6 for the illustration of Arrhenius' law. Note that this reaction happens only in the catalytic converters.

[5]The more common formulation of the Arrhenius' law is the one with activation energy $\tilde{E}^+$ and the ideal gas constant $\tilde{R}$: $\tilde{K}(\tilde{T}) = \tilde{K}_0 \exp\left(-\tilde{E}^+/(R\tilde{T})\right)$. Hence, with $R\tilde{T}^+ = \tilde{E}^+$ the above used formulation is equivalent.

Therefore, one needs an indicator function[6] $\tilde{\chi}_f : [0, \tilde{L}] \to \{0, 1\}$ with

$$\tilde{\chi}_f(\tilde{x}) = \begin{cases} 1, & \text{if } \tilde{x} \text{ is in a catalyst,} \\ 0, & \text{otherwise.} \end{cases} \tag{2.8}$$

The chemical reaction happens on the surface of the catalytic converter. Hence, the sink of unburnt fuel $\tilde{\rho}\tilde{z}$ is modelled by the term $-\tilde{\chi}_f \tilde{A}\tilde{\rho}\tilde{z}\tilde{K}(\tilde{T})$. Finally, one ends up with the following reaction equation:

$$\boxed{(\tilde{A}\tilde{\rho}\tilde{z})_{\tilde{t}} + (\tilde{A}\tilde{\rho}\tilde{z}\tilde{u})_{\tilde{x}} = -\tilde{\chi}_f \tilde{A}\tilde{\rho}\tilde{z}\tilde{K}(\tilde{T}).} \tag{2.9}$$

- **Momentum balance**
  Let $\tilde{p}(\tilde{x}, \tilde{t})$ be the pressure of the gas mixture at point $\tilde{x}$ and time $\tilde{t}$. If the momentum was a conserved quantity, the following equation would hold:

  $$(\tilde{A}\tilde{\rho}\tilde{u})_{\tilde{t}} + (\tilde{A}\tilde{\rho}\tilde{u}^2)_{\tilde{x}} + \tilde{A}\tilde{p}_{\tilde{x}} = 0.$$

  It is worth remarking, that the conservation of momentum cannot be written in conservation form, due to the fact that the pipe's cross section is not constant. For more details see the Appendix B.1.

  The physical effects that take place are the wall friction (with the wall friction coefficient $\xi = 0.0241$) and friction due to the honeycomb structure of the catalytic converter (with friction coefficient $\tilde{C}_c = 800\text{s}^{-1}$). For the wall friction a quadratic friction law is chosen, whereas it is postulated that the surface friction has linear behaviour.

  $$\boxed{(\tilde{A}\tilde{\rho}\tilde{u})_{\tilde{t}} + (\tilde{A}\tilde{\rho}\tilde{u}^2)_{\tilde{x}} + \tilde{A}\tilde{p}_{\tilde{x}} = -\frac{\xi}{4}\pi\tilde{d}\tilde{\rho}\frac{\tilde{u}|\tilde{u}|}{2} - \tilde{\chi}_f \tilde{C}_c \tilde{A}\tilde{\rho}\tilde{u}.} \tag{2.10}$$

- **Energy balance**
  Let $\tilde{\rho}(\tilde{x}, \tilde{t})\tilde{E}(\tilde{x}, \tilde{t})$ be the total energy density at point $\tilde{x}$ and time $\tilde{t}$. It consists of the internal energy density $\tilde{c}_v\tilde{\rho}(\tilde{x}, \tilde{t})\tilde{T}(\tilde{x}, \tilde{t})$ and the kinetic energy density $\tilde{\rho}(\tilde{x}, \tilde{t})\frac{\tilde{u}(\tilde{x},\tilde{t})^2}{2}$, i.e.,

  $$\tilde{E} = \tilde{c}_v\tilde{T} + \frac{\tilde{u}^2}{2},$$

  where $\tilde{c}_v = 717.7\frac{\text{m}^2}{\text{s}^2\text{K}}$ is the specific heat at constant volume of the gas mixture. Then, according to the Euler equation of gas dynamics in a variable pipe, the conservation of energy would be

  $$(\tilde{A}\tilde{\rho}\tilde{E})_{\tilde{t}} + (\tilde{A}\tilde{\rho}\tilde{u}\tilde{E} + \tilde{A}\tilde{u}\tilde{p})_{\tilde{x}} = 0.$$

[6] Note that the indicator mapping $\tilde{\chi} : \{1, \ldots, n_P\} \to \{0, 1\}$ (see (2.1)) is a discrete mapping, whereas the indicator function $\tilde{\chi}_f : [0, \tilde{L}] \to \{0, 1\}$ (see (2.8)) is a real function.

As the momentum, the energy is not a conserved quantity. First, there is a loss of energy due the heat exchange with the wall (heat exchange coefficient $\tilde{h} = 100\frac{\mathrm{m}^2}{\mathrm{s}^2\mathrm{K}}$), where the wall temperature $\tilde{T}_{\mathrm{Wall}}$ is computed by the mean value of the constant outer temperature $\tilde{T}_{\mathrm{out}} = 290.28\mathrm{K}$[7] and the gas temperature, i.e.,

$$\tilde{T}_{\mathrm{Wall}}(\tilde{x}, \tilde{t}) = \frac{1}{2}\left(\tilde{T}(\tilde{x}, \tilde{t}) + \tilde{T}_{\mathrm{out}}\right). \tag{2.11}$$

Second, there is an energy gain due to the exothermic reaction in the catalysts (specific heat release coefficient $\tilde{q}_0 = 5 \cdot 10^6 \frac{\mathrm{m}^2}{\mathrm{s}^2}$). Finally, one receives the balance law for the energy:

$$\boxed{(\tilde{A}\tilde{\rho}\tilde{E})_{\tilde{t}} + (\tilde{A}\tilde{\rho}\tilde{u}\tilde{E} + \tilde{A}\tilde{u}\tilde{p})_{\tilde{x}} = -\tilde{h}\pi\tilde{d}(\tilde{T} - \tilde{T}_{\mathrm{Wall}}) + \tilde{\chi}_f\tilde{q}_0\tilde{A}\tilde{\rho}\tilde{z}\tilde{K}(\tilde{T}).} \tag{2.12}$$

- **Ideal gas law**
  Since there are five unknowns (density, velocity, pressure, temperature and ratio of unburnt gas) and only four equations so far, one needs another condition. As the equation of state the *ideal gas law* is chosen, i.e.,

$$\boxed{\tilde{p} = \tilde{R}\tilde{\rho}\tilde{T},} \tag{2.13}$$

  where $\tilde{R} = 287.08\frac{\mathrm{m}^2}{\mathrm{s}^2\mathrm{K}}$ is the ideal gas constant.

So the final model presented in [LN04] and the master thesis of Petrucci [Pet07], consisting of conservation of mass (2.6), a momentum (2.10) and energy balance (2.12), a reaction equation for the chemical reaction in the catalytic converters (2.9) and the ideal gas law (2.13), forming the so-called *reactive Euler equations of gas dynamics through a variable pipe* with right hand sides, is the following:

$$\boxed{\begin{aligned}
(\tilde{A}\tilde{\rho})_{\tilde{t}} + (\tilde{A}\tilde{\rho}\tilde{u})_{\tilde{x}} &= 0,\\
(\tilde{A}\tilde{\rho}\tilde{u})_{\tilde{t}} + (\tilde{A}\tilde{\rho}\tilde{u}^2)_{\tilde{x}} + \tilde{A}\tilde{p}_{\tilde{x}} &= -\frac{\xi}{4}\pi\tilde{d}\tilde{\rho}\frac{\tilde{u}|\tilde{u}|}{2} - \tilde{\chi}_f\tilde{C}_c\tilde{A}\tilde{\rho}\tilde{u},\\
(\tilde{A}\tilde{\rho}\tilde{E})_{\tilde{t}} + (\tilde{A}\tilde{\rho}\tilde{u}\tilde{E} + \tilde{A}\tilde{u}\tilde{p})_{\tilde{x}} &= -\tilde{h}\pi\tilde{d}(\tilde{T} - \tilde{T}_{\mathrm{Wall}}) + \tilde{\chi}_f\tilde{q}_0\tilde{A}\tilde{\rho}\tilde{z}\tilde{K}(\tilde{T}),\\
(\tilde{A}\tilde{\rho}\tilde{z})_{\tilde{t}} + (\tilde{A}\tilde{\rho}\tilde{z}\tilde{u})_{\tilde{x}} &= -\tilde{\chi}_f\tilde{A}\tilde{\rho}\tilde{z}\tilde{K}(\tilde{T}),\\
\tilde{p} &= \tilde{R}\tilde{\rho}\tilde{T}
\end{aligned}} \tag{2.14}$$

[7] The value corresponds to the initial condition of a cold start. By this choice we the heat exchange vanishes at $\tilde{t} = 0$.

in $\Omega := (0, \tilde{L}) \times (0, \infty)$ with **initial conditions**

$$\begin{aligned} \tilde{\rho}(\tilde{x}, 0) &= \tilde{\rho}_{ic}(\tilde{x}), \quad \tilde{u}(\tilde{x}, 0) = \tilde{u}_{ic}(\tilde{x}), \\ \tilde{p}(\tilde{x}, 0) &= \tilde{p}_{ic}(\tilde{x}), \quad \tilde{z}(\tilde{x}, 0) = \tilde{z}_{ic}(\tilde{x}) \end{aligned} \tag{2.15}$$

on $\Gamma_{ic} := (0, \tilde{L}) \times \{\tilde{t} = 0\}$ and inflow **boundary conditions**

$$\begin{array}{rcl} \tilde{p}(0, \tilde{t}) & = & \tilde{p}_{bc,l}(\tilde{t}), \\ \left.\begin{array}{rcl} \tilde{\rho}(0, \tilde{t}) & = & \tilde{\rho}_{bc,l}(\tilde{t}), \\ \tilde{z}(0, \tilde{t}) & = & \tilde{z}_{bc,l}(\tilde{t}), \end{array}\right\} \text{ if } \tilde{u}(0, \tilde{t}) > 0, \end{array} \qquad \begin{array}{rcl} \tilde{p}(\tilde{L}, \tilde{t}) & = & \tilde{p}_{bc,r}(\tilde{t}), \\ \left.\begin{array}{rcl} \tilde{\rho}(\tilde{L}, \tilde{t}) & = & \tilde{\rho}_{bc,r}(\tilde{t}), \\ \tilde{z}(\tilde{L}, \tilde{t}) & = & \tilde{z}_{bc,r}(\tilde{t}), \end{array}\right\} \text{ if } \tilde{u}(\tilde{L}, \tilde{t}) < 0 \end{array} \tag{2.16}$$

on $\Gamma_{bc} := \{0, \tilde{L}\} \times [0, \infty)$.

**Remark 1.** *This is not exactly the model that was proposed by Lacoste and Natalini. The formulation varies slightly (e.g., in notation). All differences are listed in the Appendix B.2.*

This model was studied numerically by Lacoste and Natalini. Prior to this, the values for the parameters $\tilde{C}_c$ and $\tilde{h}$ were calibrated by a least squares adjustment with data that was provided by Magenti Marelli (see [LN04]).

The model has two drawbacks when it comes to numerical simulations, which both lead to relatively high computation times. These are:

(D1) Large changes of the cross section on small intervals lead to large derivatives in $A$ and therefore to a fine spatial grid. Additionally, for reasons of numerical stability, the step sizes in time and space have to be coupled (e.g., by the CFL condition[8]). Hence, large derivatives in $A$ also demand a finer time grid.

(D2) Our main purpose is to describe the temperature development in the exhaust pipe. However, this model unnecessarily tracks the sound waves in the gas dynamics. Therefore, in the numerical realization of explicit schemes, one is forced to use small step sizes in time, in order to fulfil the CFL condition, which is geared to the largest speed, i.e., the speed of the sound waves. (see details explained in Subsection 3.4.1)

[8]Details on the CFL condition for our numerical algorithms are given in Sections 3.3.1 and 3.3.2.

## 2.4. Network approach

In order to avoid the problem mentioned in (D1), one can consider the whole exhaust pipe as a network of single pipes, each having a constant cross section (see Figure 2.7). Each pipe $i \in \{1, \ldots, n_P = 9\}$ represents an individual computational domain, which has its own set of equations to describe the physics in the pipe, discriminating between pipes that have a catalytic converter ($\tilde{\chi}^i = 1$), and pipes that do not ($\tilde{\chi}^i = 0$).

These distinct "sub-models" (individual domains and sets of equations) have to interact/communicate with their neighbours. Therefore, it is necessary to prescribe *coupling conditions*, which connect those 9 "sub-models" in a physically meaningful way to one overall model for the whole exhaust pipe


Figure 2.7.: Single pipes with constant cross sections

By this approach we do not need a space dependent and smooth cross section function $\tilde{A} = \tilde{A}(\tilde{x})$ anymore. Furthermore, the length of the intervals $I_{\tilde{\alpha}}^{i+\frac{1}{2}}$ can be set to $\tilde{\alpha} = 0$ (see (2.3)).

Before we present the sub-model and discuss the coupling conditions, we first introduce the network notation.

### 2.4.1. Network notation

We now introduce a notation for the network. At first sight this notation seems to be quite complicated, but it is necessary to state meaningful coupling conditions in a simple way. We will derive conditions like in [GK08] in all their generality in subsection 2.4.3. Afterwards, we will use the simple structure of the considered network, where we always have only two pipes at each junction.
So, let $N_V = \{1, \ldots, n_V\}$ be the set of all junctions (vertices) and $N_P = \{1, \ldots, n_P\}$ the set of all pipes (edges), where $n_V, n_P \in \mathbb{N}$ denote the number of junctions and pipes, respectively. The quantities in the $i$-th pipe are given by

| | |
|---|---|
| $\tilde{A}^i, \tilde{d}^i, \tilde{L}^i$ | cross section, diameter, length, |
| $\tilde{\rho}^i, \tilde{z}^i, \tilde{u}^i, \tilde{p}^i, \tilde{T}^i$ | density, ratio of unburnt gas, velocity, pressure, temperature, |
| $\tilde{y}_l^i(\tilde{t}) := \tilde{y}^i(0, \tilde{t})$ | left value of the physical quantity $\tilde{y}^i$, |
| $\tilde{y}_r^i(\tilde{t}) := \tilde{y}^i(\tilde{L}^i, \tilde{t})$ | right value of the physical quantity $\tilde{y}^i$. |

For each vertex $j \in N_V$ let $P^j \subset N_P$ be the set of all pipes, which are connected with the vertex $j$. We now define two maps, that are used to express the geometrical relation among pipes:

$$\begin{aligned} P : N_P \times N_V &\to \{l, r, 0\} \\ (i,j) &\mapsto \begin{cases} l, & \text{if vertex } j \text{ lies to the left of pipe } i, \\ r, & \text{if vertex } j \text{ lies to the right of pipe } i, \\ 0, & \text{if vertex } j \text{ is not connected to pipe } i, \end{cases} \end{aligned} \tag{2.17}$$

and

$$\begin{aligned} \operatorname{sgn} : N_P \times N_V &\to \{-1, 0, 1\} \\ (i,j) &\mapsto \begin{cases} -1, & \text{if } P(i,j) = r, \\ 0, & \text{if } P(i,j) = 0, \\ 1, & \text{if } P(i,j) = l. \end{cases} \end{aligned} \tag{2.18}$$

These maps are required for a proper definition of the coupling conditions.

**Remark 2.** *For the geometry of the exhaust pipe we consider (see Figure 2.4 and Table 2.1) this means that* $n_P = 9$ *and* $n_V = 8$. *The matrix* $(\operatorname{sgn}(i,j))_{(i,j)} \in \mathbb{R}^{n_P \times n_V}$ *has the following simple form:*

$$\begin{pmatrix} -1 & 0 & 0 & 0 & 0 & 0 & 0 & 0 \\ 1 & -1 & 0 & 0 & 0 & 0 & 0 & 0 \\ 0 & 1 & -1 & 0 & 0 & 0 & 0 & 0 \\ 0 & 0 & 1 & -1 & 0 & 0 & 0 & 0 \\ 0 & 0 & 0 & 1 & -1 & 0 & 0 & 0 \\ 0 & 0 & 0 & 0 & 1 & -1 & 0 & 0 \\ 0 & 0 & 0 & 0 & 0 & 1 & -1 & 0 \\ 0 & 0 & 0 & 0 & 0 & 0 & 1 & -1 \\ 0 & 0 & 0 & 0 & 0 & 0 & 0 & 1 \end{pmatrix}$$

### 2.4.2. A model for a single pipe

The considered spatial domain $[0, \tilde{L}^i]$ is the $i$-th pipe. The governing equations for the gas dynamics in a single pipe remain basically the same as for the whole pipe, i.e., we describe the physics with the model of Lacoste and Natalini (2.14). However, instead of using the indicator function $\tilde{\chi}_f$, we now use the indicator mapping $\tilde{\chi}$. Furthermore, the cross section function of the $i$-th pipe $\tilde{A}^i$ is constant. We can therefore simply divide by this term, and have the following reformulation

of the Lacoste-Natalini model for a single pipe with constant cross section:

$$\begin{aligned}
\tilde{\rho}^i_{\tilde{t}} + (\tilde{\rho}^i \tilde{u}^i)_{\tilde{x}} &= 0, \\
(\tilde{\rho}^i \tilde{u}^i)_{\tilde{t}} + (\tilde{\rho}^i (\tilde{u}^i)^2 + \tilde{p}^i)_{\tilde{x}} &= -\frac{\xi}{\tilde{d}^i} \tilde{\rho}^i \frac{\tilde{u}^i |\tilde{u}^i|}{2} - \tilde{\chi}^i \tilde{C}_c \tilde{\rho}^i \tilde{u}^i, \\
(\tilde{\rho}^i \tilde{E}^i)_{\tilde{t}} + (\tilde{\rho}^i \tilde{u}^i \tilde{E}^i + \tilde{u}^i \tilde{p}^i)_{\tilde{x}} &= -\frac{4\tilde{h}}{\tilde{d}^i} (\tilde{T}^i - \tilde{T}^i_{\text{Wall}}) + \tilde{\chi}^i \tilde{q}_0 \tilde{\rho}^i \tilde{z}^i \tilde{K}(\tilde{T}^i), \\
(\tilde{\rho}^i \tilde{z}^i)_{\tilde{t}} + (\tilde{\rho}^i \tilde{z}^i \tilde{u}^i)_{\tilde{x}} &= -\tilde{\chi}^i \tilde{\rho}^i \tilde{z}^i \tilde{K}(\tilde{T}^i), \\
\tilde{p}^i &= \tilde{R} \tilde{\rho}^i \tilde{T}^i
\end{aligned} \tag{2.19}$$

for all pipes $i = 1, \ldots, n_P$ and $(\tilde{x}, \tilde{t}) \in \Omega^i := (0, \tilde{L}^i) \times (0, \tilde{t}_{\text{end}})$. As a consequence of the formulation of the model on single pipes with constant cross sections, we have to restate the initial and boundary condition. Basically, both stay the same, but we have to adjust them to the new notation. So let $\tilde{y}_{ic}$ be the initial condition of an arbitrary physical quantity $\tilde{y}$ in the old formulation of the model (2.14). Then, the initial condition for the $i$-th pipe is the following[9]:

$$\tilde{y}^i(\tilde{x}, 0) = \tilde{y}^i_{ic}(\tilde{x}) = \tilde{y}_{ic}(\tilde{x}^{i-\frac{1}{2}} + \tilde{x})$$

for all pipes $i = 1, \ldots, n_P$ and $\tilde{x} \in (0, \tilde{L}^i)$. Hence, the initial conditions for the model (2.19) are

$$\begin{aligned}
\tilde{\rho}^i(\tilde{x}, 0) &= \tilde{\rho}^i_{ic}(\tilde{x}), \quad \tilde{u}^i(\tilde{x}, 0) = \tilde{u}^i_{ic}(\tilde{x}), \\
\tilde{p}^i(\tilde{x}, 0) &= \tilde{p}^i_{ic}(\tilde{x}), \quad \tilde{z}^i(\tilde{x}, 0) = \tilde{z}^i_{ic}(\tilde{x})
\end{aligned} \tag{2.20}$$

for all pipes $i = 1, \ldots, n_P$ and $\tilde{x} \in (0, \tilde{L}^i)$.

The boundary conditions also remain the same, i.e., we prescribe pressure boundary conditions as well as inflow boundary conditions for density and ratio of unburnt gas at the left hand side end of the pipe $i = 1$ and the right hand side end of the pipe $i = n_P = 9$, i.e.,

$$\begin{aligned}
\tilde{p}^1(0, \tilde{t}) &= \tilde{p}_{bc,l}(\tilde{t}), \\
\left.\begin{aligned}
\tilde{\rho}^1(0, \tilde{t}) &= \tilde{\rho}_{bc,l}(\tilde{t}), \\
\tilde{z}^1(0, \tilde{t}) &= \tilde{z}_{bc,l}(\tilde{t}),
\end{aligned}\right\} &\text{ if } \tilde{u}^1(0, \tilde{t}) > 0
\end{aligned} \tag{2.21}$$

and

$$\begin{aligned}
\tilde{p}^{n_P}(\tilde{L}^{n_P}, \tilde{t}) &= \tilde{p}_{bc,r}(\tilde{t}), \\
\left.\begin{aligned}
\tilde{\rho}^{n_P}(\tilde{L}^{n_P}, \tilde{t}) &= \tilde{\rho}_{bc,r}(\tilde{t}), \\
\tilde{z}^{n_P}(\tilde{L}^{n_P}, \tilde{t}) &= \tilde{z}_{bc,r}(\tilde{t}),
\end{aligned}\right\} &\text{ if } \tilde{u}^{n_P}(\tilde{L}^{n_P}, \tilde{t}) < 0
\end{aligned} \tag{2.22}$$

for all $i = 1, \ldots, n_P$ and $\tilde{t} \in [0, \infty)$.

[9] Recall that $\tilde{x}^{i-\frac{1}{2}}$ is the connection point between the $(i-1)$-th and $i$-th pipe (see (2.2)).

**Remark 3.** *Now, one can easily detect the necessity of coupling conditions, because each pipe requires boundary data at its left hand side and right hand side end. However, boundary conditions are only partly given to the two outer pipes.*

### 2.4.3. Coupling conditions

In this subsection, we first want to state the coupling condition for a general network, before we exploit the considered network's structure.

Let us consider a single vertex $j \in N_V$ and all the pipes $i$ which are connected to this vertex, i.e., $i \in P^j$. In order to connect the models for the single pipes, we have to define some coupling conditions. Since we have four unknowns[10] $(\tilde{\rho}, \tilde{z}, \tilde{u}, \tilde{p})$ we need four coupling conditions.

(CC1) The **conservation of mass flux** at every vertex $j \in N_V$ is the first coupling condition one would come up with. Indeed this is physically meaningful and used in similar cases. Equivalently we can state that the sum over all $i \in P^j$ of the flux $\operatorname{sgn}(i,j)\tilde{\rho}^i_{P(i,j)}\tilde{u}^i_{P(i,j)}\tilde{A}^i$ has to vanish.

$$\sum_{i \in P^j} \operatorname{sgn}(i,j)\tilde{\rho}^i_{P(i,j)}\tilde{u}^i_{P(i,j)}\tilde{A}^i = 0 \qquad \forall j \in N_V. \tag{2.23}$$

(CC2) Since there is no combustion at the junctions, the **conservation of unburnt gas flux** at every vertex $j \in N_V$ seems to be a reasonable coupling condition, i.e., the sum over all $i \in P^j$ of the unburnt gas flux $\operatorname{sgn}(i,j)\tilde{\rho}^i_{P(i,j)}\tilde{z}^i_{P(i,j)}\tilde{u}^i_{P(i,j)}\tilde{A}^i$ has to vanish.

$$\sum_{i \in P^j} \operatorname{sgn}(i,j)\tilde{\rho}^i_{P(i,j)}\tilde{z}^i_{P(i,j)}\tilde{u}^i_{P(i,j)}\tilde{A}^i = 0 \qquad \forall j \in N_V. \tag{2.24}$$

(CC3) Since we will have large changes in the cross section, one can easily guess that the momentum is not a quantity which is conserved at a vertex. It is obvious that the kinetic energy cannot be preserved. Hence, we assume that there is no temperature loss at the junctions, so that the **conservation of internal energy flux** at each vertex $j \in N_V$ holds, i.e., the sum over all $i \in P^j$ of the internal energy flux $\operatorname{sgn}(i,j)\tilde{\rho}^i_{P(i,j)}\tilde{T}^i_{P(i,j)}\tilde{u}^i_{P(i,j)}\tilde{A}^i$ has to vanish.

$$\sum_{i \in P^j} \operatorname{sgn}(i,j)\tilde{\rho}^i_{P(i,j)}\tilde{T}^i_{P(i,j)}\tilde{u}^i_{P(i,j)}\tilde{A}^i = 0 \qquad \forall j \in N_V. \tag{2.25}$$

[10] The fifth unknown $\tilde{T}$ can be deduced from the density and pressure with the help of the ideal gas law (2.13).

(CC4) Finally we have to state a **coupling condition for the pressure**. Let us first assume that there is good "mixing" at each vertex, such that for every pressure $\tilde{p}^i_{P(i,j)}$ for $i \in P^j$ the equation

$$\tilde{p}^j_V = \tilde{p}^i_{P(i,j)}$$

holds, where $\tilde{p}^j_V$ is the pressure at vertex $j$ (see [GK08]).
However, these are not the "correct" coupling conditions for this model. Since we will have large differences in the cross section (sudden expansions and contractions), one has to include physical pressure losses, the so-called *minor loss terms*, at the junctions in the mathematical coupling conditions. So let us assume that the pressure loss is given by a quantity $\tilde{f}^{i,j}_{ext}$, which depends on the geometrical structure of pipe $i$ connected to the vertex $j$ and the flow direction[11]. Then our coupling conditions would be of the form

$$\tilde{p}^j_V = \tilde{p}^i_{P(i,j)} - \operatorname{sgn}(i,j)\tilde{f}^{i,j}_{ext} \qquad \forall i \in P^j, \tag{2.26}$$

where

$$\tilde{f}^{i,j}_{ext} \begin{cases} > 0, & \text{if } \tilde{u}^i_{P(i,j)} \geq 0, \\ < 0, & \text{if } \tilde{u}^i_{P(i,j)} < 0. \end{cases}$$

These four conditions are not sufficient in the case of a general network (see [GK08]), but are just right for our special network (the exhaust pipe). The reason for this is, that we always have one ingoing and one outgoing pipe. In the case of at least two outgoing pipes, we would have to declare what the inflow conditions for $\tilde{\rho}$ and $\tilde{z}$ for each pipe are. In general one can make the assumption of a "good mixture" (like we have done for the pressure above) and declare for each outgoing pipe the same boundary conditions for density and ratio of unburnt gas.

### Exploiting the network structure

Since we have only pipe-to-pipe connections in the considered exhaust pipe, we can strongly simplify the coupling conditions.

Conservation of mass flux

$$\tilde{\rho}^i_r \tilde{u}^i_r \tilde{A}^i = \tilde{\rho}^{i+1}_l \tilde{u}^{i+1}_l \tilde{A}^{i+1} \qquad \forall i = 1, \ldots, n_P - 1. \tag{2.27}$$

Conservation of unburnt gas flux

$$\tilde{\rho}^i_r \tilde{z}^i_r \tilde{u}^i_r \tilde{A}^i = \tilde{\rho}^{i+1}_l \tilde{z}^{i+1}_l \tilde{u}^{i+1}_l \tilde{A}^{i+1} \qquad \forall i = 1, \ldots, n_P - 1. \tag{2.28}$$

[11] In the following subsection we only give information on the computation of the minor loss term for the case of pipe-to-pipe connections.

Conservation of internal energy flux

$$\tilde{\rho}_r^i \tilde{T}_r^i \tilde{u}_r^i \tilde{A}^i = \tilde{\rho}_l^{i+1} \tilde{T}_l^{i+1} \tilde{u}_l^{i+1} \tilde{A}^{i+1} \qquad \forall i = 1, \dots, n_P - 1. \tag{2.29}$$

Coupling condition for the pressure

$$\tilde{p}_r^i = \tilde{p}_l^{i+1} + \tilde{f}_{ext}^i \qquad \forall i = 1, \dots, n_P - 1. \tag{2.30}$$

Using the first coupling condition, one can simplify the second and third one to the conservation of ratio of unburnt gas and temperature, i.e.,

$$\tilde{z}_r^i = \tilde{z}_l^{i+1}, \qquad \tilde{T}_r^i = \tilde{T}_l^{i+1}.$$

We will use this formulation in the summary of the models (Section 2.6).

**Remark 4.** *In the case of pipe-to-pipe connections (see [BHK06]) there are formulas that model the minor loss term $\tilde{f}_{ext}^j$ for pipe expansions and contractions. Whether a pipe-to-pipe connection is a (sudden) expansion or contraction (see Figure 2.8) depends on the flow direction of the fluid. For the following remark, we will state the formulas assuming a positive flow direction for all times, i.e., $\tilde{u} > 0$. However, a formulation for unknown flow directions is also possible.*

1. *Due to the difficulty of the physics at a junction there is no theory, but empirical models combined with measurements for the minor loss term $\tilde{f}_{ext}^j$. However, a good approximation for this term is given in the textbooks [Cra82] and [Mul04]:*

$$\tilde{f}_{ext}^j = \begin{cases} \left(1 - \frac{\tilde{d}_j^2}{\tilde{d}_{j+1}^2}\right)^2 \phi_E(\theta) \tilde{\rho}_r^j \frac{(\tilde{u}_r^j)^2}{2}, & \text{if } \tilde{d}_j < \tilde{d}_{j+1} \text{ (expansion)}, \\ \frac{1}{2}\left(1 - \frac{\tilde{d}_{j+1}^2}{\tilde{d}_j^2}\right) \phi_C(\theta) \tilde{\rho}_l^{j+1} \frac{(\tilde{u}_l^{j+1})^2}{2}, & \text{if } \tilde{d}_j > \tilde{d}_{j+1} \text{ (contraction)}. \end{cases} \tag{2.31}$$

   *The parameter $\tilde{d}_j$ denotes the diameter of the $j$-th pipe. The first, geometry dependent term is called $K$-factor in the literature. Note that we will always have to use the velocity in the pipe with the smaller diameter for the computation of the kinetic energy. The angle-dependent functions $\phi_E$ and $\phi_C$ are factoring the pressure loss coefficient due to the angle $\theta$ ($\theta = \pi$ stands for a sudden expansion or contraction).*

$$\phi_E(\theta) = \begin{cases} 2.6 \sin(\frac{\theta}{2}), & \text{if } 0 \le \theta < \frac{\pi}{4}, \\ 1, & \text{if } \frac{\pi}{4} \le \theta \le \pi, \end{cases} \quad \phi_C(\theta) = \begin{cases} 1.6 \sin(\frac{\theta}{2}), & \text{if } 0 \le \theta < \frac{\pi}{4}, \\ \sqrt{\sin(\frac{\theta}{2})}, & \text{if } \frac{\pi}{4} \le \theta \le \pi. \end{cases}$$

2. *Since the geometry of the exhaust pipe we consider includes only sudden expansions and contractions (i.e., $\theta = \pi$), the angle dependent term in the $K$-factor in* (2.31) *is equal to 1.*

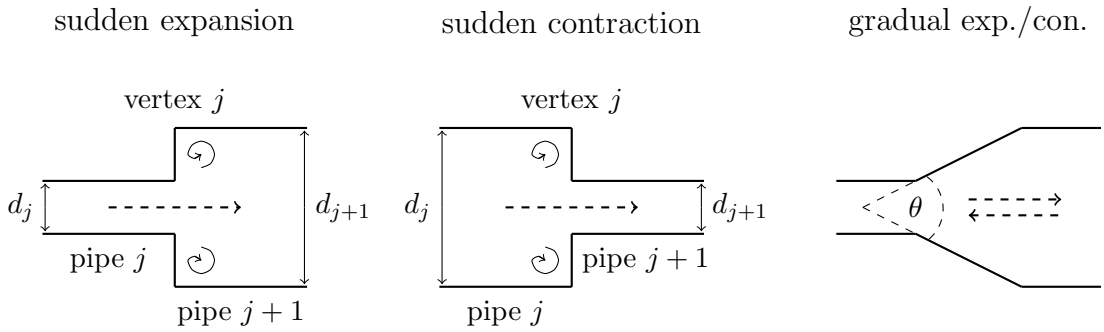


Figure 2.8.: Coupling conditions for the pressure at a sudden/gradual expansion or contraction. The dashed arrow represents the flow direction.

3. *Note that these terms describing the pressure losses are mostly derived by experiments. Therefore, it is not too surprising that one can find contradictions in the literature concerning minor losses. The approximations we use from [Cra82] and [Mul04] claim that the pressure loss grows monotonically with increasing angle $\theta$. In contrast, it is said in [Whi79] that for some angles $\theta \in (\frac{2}{9}\pi, \frac{1}{3}\pi)$ the pressure loss in a gradual expansion is even higher than in the case of a sudden expansion.*

4. *In Subsection 3.4.2 we will show an example, where we compare the numerical results of the gas flow with and without inclusion of the minor loss term.*

## 2.5. Asymptotic model

**Notation 1.** *In this section, we cease to denote the variables affiliation to a certain pipe by a superscript, i.e., instead of $\tilde{y}^i$ we just write $\tilde{y}$. The only exception will be the paragraphs in which we discuss the coupling conditions.*

This section is devoted to the problem (D2)[12], and to derive a model that does not track sound waves, since they are not of interest for this application.

A widely accepted and well studied approach for this intent is considering the flow to be *incompressible* (see the paper of Klainerman and Majda [KM82] or the textbook of Lions [Lio98]). However, the incompressible derivation of the Euler or Navier-Stokes equations is only valid if there is no or just small heat exchange and density and temperature remain unchanged. Hence, an incompressible approach

[12] Unnecessarily tracking sound waves.

is not applicable for our problem, where temperatures of up to 1200 K can be reached in the catalytic converter.

Another well studied technique is the *small Mach number limit* (see the article by Codina and Principe [CP09] for an overview). The Mach number $M$ of a fluid flow is the ratio of the flow velocity and the fluid's speed of sound. This approach uses the fact that this parameter $M$ is small and performs a limit process, where $M$ tends to zero. With a multiple scale analysis one can still keep physical features of the original system and study acoustic phenomena for instance (see [Mei99]). We are not interested in acoustic problems in this application. On the contrary, we explicitly want to exclude those and restrict ourselves to a single scale analysis, so that we can have larger step sizes in time (see Subsection 3.4.1). This leads us to a new asymptotic model that does not track the propagation of sound waves, but preserves the physical behaviour of gas density, ratio of unburnt gas, velocity, temperature and pressure, i.e., all quantities we are interested in.

### 2.5.1. Scaling

The first step is to scale the system (2.19). So far all physical quantities were unscaled. This was denoted by the tilde symbol ($\sim$) on top of the variable. In order to obtain a dimension-free, scaled model, we have to introduce reference values for each physical quantity (see Table 2.2) and replace each unscaled physical quantity ($\tilde{y}(\tilde{x}, \tilde{t})$), by the product of its scaled counterpart ($y(x, t)$) and its reference value ($\tilde{y}_{\text{ref}}$), i.e.,

$$\tilde{y}(\tilde{x}, \tilde{t}) = \tilde{y}_{\text{ref}} \cdot y(x, t).$$

This also has consequences for the derivatives. We consider the scaled independent variables as functions of the unscaled independent variables, i.e.,

$$x = x(\tilde{x}) = \frac{\tilde{x}}{\tilde{x}_{\text{ref}}}, \qquad t = t(\tilde{t}) = \frac{\tilde{t}}{\tilde{t}_{\text{ref}}}.$$

Hence, the derivative of an unscaled quantity has the following form

$$\tilde{y}_{\tilde{x}}(\tilde{x}, \tilde{t}) = \frac{\tilde{y}_{\text{ref}}}{\tilde{x}_{\text{ref}}} y_x(x, t), \qquad \tilde{y}_{\tilde{t}}(\tilde{x}, \tilde{t}) = \frac{\tilde{y}_{\text{ref}}}{\tilde{t}_{\text{ref}}} y_t(x, t).$$

| quantity | unit | reference quantity | reference value |
|---|---|---|---|
| $\tilde{t}$ | s | $\tilde{t}_{\text{ref}} = \tilde{x}_{\text{ref}}/\tilde{u}_{\text{ref}}$ | 0.36 |
| $\tilde{x}$ | m | $\tilde{x}_{\text{ref}} = \tilde{L}$ | 3.6 |
| $\tilde{\rho}$ | kg/m$^3$ | $\tilde{\rho}_{\text{ref}}$ | 1.2 |
| $\tilde{u}$ | m/s | $\tilde{u}_{\text{ref}}$ | 10 |
| $\tilde{p}$ | kg/(ms$^2$) | $\tilde{p}_{\text{ref}}$ | $10^5$ |
| $\tilde{T}$ | K | $\tilde{T}_{\text{ref}} = \tilde{p}_{\text{ref}}/(\tilde{R}\tilde{\rho}_{\text{ref}})$ | 290.28 |
| $\tilde{z}$ | - | $\tilde{z}_{\text{ref}}$ | 0.1 |

Table 2.2.: Reference values for the physical quantities

By proper manipulation we obtain a new dimensionless, scaled system (2.32),

$$\begin{aligned}
\rho_t + (\rho u)_x &= 0, \\
(\rho u)_t + (\rho u^2)_x + \frac{1}{\varepsilon} p_x &= -C_f \rho \frac{u|u|}{2} - \chi C_c \rho u, \\
\left(\rho T + \varepsilon(\gamma-1)\rho\frac{u^2}{2}\right)_t + \left(\rho u T + \varepsilon(\gamma-1)\rho\frac{u^3}{2} + (\gamma-1)up\right)_x & \\
&= -h(T - T_{\text{Wall}}) + \chi q_0 \rho z K(T), \\
(\rho z)_t + (\rho u z)_x &= -\chi \rho z K(T), \\
p &= \rho T,
\end{aligned} \tag{2.32}$$

where the parameter $\varepsilon$ is defined by $\varepsilon := \frac{\tilde{\rho}_{\text{ref}}\tilde{u}_{\text{ref}}^2}{\tilde{p}_{\text{ref}}} = 0.012$. The remaining dimensionless parameters are defined as follows:

$$\begin{aligned}
C_f &:= \frac{\xi \tilde{x}_{\text{ref}}}{\tilde{d}}, & C_c &:= \frac{\tilde{C}_c \tilde{x}_{\text{ref}}}{\tilde{u}_{\text{ref}}}, & \gamma - 1 &= \frac{\tilde{R}}{\tilde{c}_v}, \\
h &:= \frac{4\tilde{h}\tilde{x}_{\text{ref}}}{\tilde{d}\tilde{\rho}_{\text{ref}}\tilde{u}_{\text{ref}}\tilde{c}_v}, & q_0 &:= \frac{\tilde{\rho}_{\text{ref}}\tilde{z}_{\text{ref}}\tilde{q}_0 R}{\tilde{p}_{\text{ref}}\tilde{c}_v}, & K(T) &:= \frac{\tilde{x}_{\text{ref}}}{\tilde{u}_{\text{ref}}}\tilde{K}(\tilde{T}_{\text{ref}}T).
\end{aligned} \tag{2.33}$$

In the dimensionless version of our model the scaled parameters $C_f, C, h$ and $q_0$ represent the frictions in the pipe and in the catalytic converter, the rate of heat exchange as well as the rate of heat release by the combustion of unburnt gas, respectively.

### Scaling the initial, boundary and coupling conditions

Of course, one has to scale the initial, boundary and coupling conditions as well. This task is trivial for most of the conditions. However, in the case of the coupling condition for the pressure (2.30), one has to be more careful, since the kinetic energy appears in the pressure loss term $\tilde{f}^j_{ext}$ (see (2.31)). Hence, the scaled version will have also the small parameter $\varepsilon$:

$$p_r^i = p_l^{i+1} + \varepsilon f_{ext}^i \qquad \forall i = 1, \dots, n_P - 1. \tag{2.34}$$

For a positive flow direction, i.e., $u^i > 0 \ \forall i = 1, \dots, n_P$, the scaled version of the minor loss term is

$$f_{ext}^j = \begin{cases} \left(1 - \frac{d_j^2}{d_{j+1}^2}\right)^2 \phi_E(\theta) \rho_r^j \frac{(u_r^j)^2}{2}, & \text{if } d_j < d_{j+1} \text{ (expansion)}, \\ \frac{1}{2}\left(1 - \frac{d_{j+1}^2}{d_j^2}\right) \phi_C(\theta) \rho_l^{j+1} \frac{(u_l^{j+1})^2}{2}, & \text{if } d_j > d_{j+1} \text{ (contraction)}. \end{cases} \tag{2.35}$$

## 2.5.2. Low Mach number asymptotics

The Mach number $M$ is defined by the quotient of the speed of fluid $\tilde{u}$ and the speed of sound $\tilde{c}$.

$$M = \frac{\tilde{u}}{\tilde{c}} \qquad \text{and} \qquad \tilde{c} = \sqrt{\frac{\gamma \tilde{p}}{\tilde{\rho}}} \tag{2.36}$$

with $\gamma = 1.4$ the adiabatic exponent. Thus, the parameter $\varepsilon$ can by rewritten:

$$\varepsilon = \frac{\tilde{\rho}_{\text{ref}} \tilde{u}_{\text{ref}}^2}{\tilde{p}_{\text{ref}}} = \gamma \tilde{u}_{\text{ref}}^2 \left(\sqrt{\frac{\tilde{\rho}_{\text{ref}}}{\gamma \tilde{p}_{\text{ref}}}}\right)^2 = \gamma \frac{\tilde{u}_{\text{ref}}^2}{\tilde{c}_{\text{ref}}^2} = \gamma M_{\text{ref}}^2.$$

Therefore, we will call our asymptotic limit a small Mach number limit.

The first step in deriving the asymptotic model is to expand the physical quantities asymptotically, by writing

$$y(x,t) = y_0(x,t) + \varepsilon y_1(x,t) + \mathcal{O}(\varepsilon^2). \tag{2.37}$$

We perform this asymptotic expansion for every physical quantity, i.e., $\rho, u, p, T$ and $z$. Due to the inverse of the small parameter $\varepsilon$ in the momentum balance, we start the limit process with the momentum balance. Plugging in the asymptotic expansions of the physical variables and multiplying the equation by $\varepsilon$ leads to

$$\varepsilon \left[(\rho_0 u_0)_t + (\rho_0 u_0^2)_x + (p_1)_x\right] + (p_0)_x = -\varepsilon \left[C_f \rho_0 \frac{u_0 |u_0|}{2} + \chi C_c \rho_0 u_0\right] + \mathcal{O}(\varepsilon^2).$$

After taking limit $\varepsilon \to 0$ and considering the rest of the dimensionless parameters fixed, we deduce that the spatial derivative of the zeroth order pressure term vanishes, i.e.,

$$(p_0)_x = 0.$$

Hence, the pressure in zeroth order, often called *thermodynamic pressure*, is space-independent in this low Mach number limit. The following assumption will simplify the setting even more.

**Assumption 2.**

*(A3) The thermodynamic pressure $p_0$ is time-independent, i.e.,*

$$(p_0)_t = 0.$$

The above assumption is physically meaningful if the boundary conditions for the pressure do not vary strongly over time. Due to constant outside pressure this is immediately clear for the right hand side boundary condition. In our later numerical examples (such as in the numerical examples of [LN04]), we also have a constant boundary condition for the pressure at the pipe's entrance. As a consequence of this assumption the pressure in leading order is a constant, i.e.,

$$p_0 = const. \tag{2.38}$$

In the next step of deriving the asymptotic model, we substitute all physical quantities by their asymptotic expansion and immediately take the limit ($\varepsilon \to 0$), without multiplying the equation by $\varepsilon$. We deduce:

1. The asymptotic conservation of mass:

$$(\rho_0)_t + (\rho_0 u_0)_x = 0.$$

2. The momentum balance: With $p_0 = const$ we have

$$(\rho_0 u_0)_t + (\rho_0 u_0^2 + p_1)_x = -C_f \rho_0 \frac{u_0|u_0|}{2} - \chi C_c \rho_0 u_0.$$

3. The asymptotic ideal gas law:

$$p_0 = \rho_0 T_0. \tag{2.39}$$

   Since $p_0$ is a constant, the gas temperature in leading order is the inverse of the density in leading order times the constant $p_0$.

4. The asymptotic energy balance:

$$(\rho_0 T_0)_t + (\rho_0 u_0 T_0 + (\gamma - 1) u_0 p_0)_x = -h(T_0 - T_{\text{Wall}}) + \chi q_0 \rho_0 z_0 K(T_0).$$

   Since $\rho_0 T_0 = p_0$ is a constant, the time derivatives in the energy equation vanish and the spatial derivatives simplify to

$$\gamma p_0 (u_0)_x = -h(T_0 - T_{\text{Wall}}) + \chi q_0 \rho_0 z_0 K(T_0).$$

5. The asymptotic reaction equation:

$$(\rho_0 z_0)_t + (\rho_0 u_0 z_0)_x = -\chi \rho_0 z_0 K(T_0).$$

All physical quantities but the pressure appear only in the zeroth order of its asymptotic expansion. The pressure splits into two components: a *thermodynamic pressure* $p_0$ and a *mechanical pressure* $p_1$. The first one is, as already mentioned above, a constant given by outer atmospheric constraints. On the other hand, $p_1$ is determined from the inner pipe's mechanics.

From now on, we will omit the subscripts of the terms of the asymptotic expansion for all quantities except the pressure, since only $p$ has a contribution of its zeroth and first order expansion terms in the asymptotic model.

Hence, in the low Mach number limits we have to solve a system of equations for $\rho, z, u, T$ and $p_1$, which is the following asymptotic model:

$$\begin{aligned}
\rho_t + (\rho u)_x &= 0, \\
(\rho u)_t + (\rho u^2 + p_1)_x &= -C_f \rho \frac{u|u|}{2} - \chi C_c \rho u, \\
u_x &= \frac{1}{\gamma p_0} \left[ -h(T - T_{\text{Wall}}) + \chi q_0 \rho z K(T) \right], \\
(\rho z)_t + (\rho u z)_x &= -\chi \rho z K(T), \\
p_0 &= \rho T.
\end{aligned} \tag{2.40}$$

### The asymptotic initial, boundary and coupling conditions

Since we are now dealing with boundary and coupling conditions, the affiliation of a variable to a pipe is crucial. Therefore, we resurrect the superscript notation for the pipe number for this discussion.

In order to deliver the appropriate initial, boundary and coupling conditions for the asymptotic model, we also expand those asymptotically and take the limit $\varepsilon \to 0$.

These computations are trivial for the initial and boundary conditions of density, velocity and ratio of unburnt gas. However, this is not the case for the pressure.

We immediately observe, that the zeroth order initial and boundary conditions for the pressure have to be constant and even identical. This constant, representing the zero order term of the initial and boundary functions for the pressure, will be the outside pressure ($p_0 = 1 \Leftrightarrow \tilde{p}_0 = 1\text{bar}$). For the first order pressure term we have

$$p_1^i(x,0) = (p_{ic}^i)_1(x) \qquad \forall i = 1,\dots,n_P$$

and

$$p_1^1(0,t) = (p_{bc,l})_1(t), \qquad p_1^{n_P}(L^{n_P},t) = (p_{bc,r})_1(t),$$

where $(p_{ic}^i)_1$ and $(p_{bc,\cdot})_1$ are the first order term in the asymptotic expansion (see (2.37)) of the functions $p_{ic}^i$ and $p_{bc,\cdot}$ (see (2.20) - (2.22) for unscaled version of these functions). [13]

Having finished the consideration of the initial and boundary conditions, we now have to deal with the coupling conditions, which change qualitatively in the performed low Mach number limit.

We restrict ourselves to the network structure of the considered exhaust pipe, with only pipe-to-pipe connections.

Let us start with the coupling condition for the pressure (2.34). For leading order we deduce, that all pressure constants in all pipes have to be identical, i.e.,

$$p_0^i = p_0 \qquad \forall i = 1.\dots n_P. \tag{2.41}$$

The pressure loss term $f_{ext}^j$ appears only in the first order expansion. The condition states

$$p_{1,r}^i = p_{1,l}^{i+1} + f_{ext}^i \qquad \forall i = 1,\dots,n_P - 1. \tag{2.42}$$

We continue with the conservation of internal energy (2.29). The product of density and temperature equals (according to the ideal gas law) the pressure constant $p_0^i$. As we have just learned from (2.41) the pressure in leading order is the same in every pipe. Hence, the products of density and temperature cancel out of the coupling condition. We are simply left with

$$u_r^i A^i = u_l^{i+1} A^{i+1} \qquad \forall i = 1,\dots,n_P - 1. \tag{2.43}$$

This has an impact on the conservation of mass. Since the products of velocity and cross section area at the intersections are identical, the coupling condition (2.27) reduces to the conservation of density, i.e.,

$$\rho_r^i = \rho_l^{i+1} \qquad \forall i = 1,\dots,n_P - 1. \tag{2.44}$$

[13] See Subsection 3.3.2 how to compute the first order boundary conditions for numerical simulations.

We finalize the coupling conditions for the asymptotic model with the conservation of unburnt gas (2.28). With the help of (2.43) and (2.44) we deduce the conservation of ratio of unburnt gas at the junctions, i.e.,

$$z_r^i = z_l^{i+1} \qquad \forall i = 1, \dots, n_P - 1. \tag{2.45}$$

### 2.5.3. Reformulation of the asymptotic model

We will reformulate the current version of the asymptotic model to match the boundary conditions[14] in an easier way. There are at least two possibilities of rewriting the system (2.40). First, one can differentiate the asymptotic momentum equation with respect to the spatial variable $x$. By this way we would end up with a second order differential equation for $p_1$. This method was applied in [GS02], where a related problem - a model for fire in tunnels - was studied.

Another way to rewrite the system in order to meet the boundary conditions, is the spatial integration of asymptotic momentum and energy balance. This reformulation was first used by Gasser and Steinrück in [GS06b] (later also in [GB12] and [GF13]) for an extension of the tunnel fire model on networks. In this subsection, we will use the second reformulation technique, since it has major advantages:

1. Integrating is numerically and analytically less critical than differentiating.

2. We will reduce the number of unknowns, since the pressure variable will only appear at its evaluation at the pipe's boundaries. Hence, mathematically we reduce the number of required boundary conditions to two. However, the boundary data for the pressure is still needed, since it will appear as a parameter in the reformulated momentum balance.

3. The velocity $u(x,t)$ will be decomposed into the sum of an unknown space-independent variable $v(t)$ and a functional, that depends on density and ratio of unburnt gas. Hence, if we first solve numerically the equations for $\rho$ and $z$, we will be only left with an integro-differential equation instead of a PDE for the velocity.

We start the reformulation with the definition of the energy gain and loss term $q[\rho, z]$, which consists of the right hand side of the asymptotic energy balance:

$$q[\rho, z](x,t) := \frac{1}{\gamma p_0}\big( - h(T(x,t) - T_{\text{Wall}}(x,t)) + \chi q_0 \rho(x,t) z(x,t) K(T(x,t))\big). \tag{2.46}$$

[14] Two boundary conditions for the pressure, no boundary condition for the velocity.

Next we integrate the asymptotic energy balance (third equation of (2.40)) with respect to the space variable. Hence, we obtain a time dependent variable $v$ - the space independent velocity component:

$$u(x,t) = v(t) + \int_0^x q[\rho, z](\xi, t)d\xi =: v(t) + Q[\rho, z](x,t). \tag{2.47}$$

As the above equation already defines, we denote the spatial potential of the energy gain and loss term with $Q[\rho, z]$. The values of $q[\rho, z]$ and $Q[\rho, z]$ are unknown since they depend on density and ratio of unburnt gas. However, we write just $q$ and $Q$ to keep the notation simple.

Now we have finished the preparation for the main step, i.e., adopting the momentum balance to the boundary conditions. We therefore integrate the second equation of (2.40) over the spatial domain.

$$\int_0^L \rho u_t dx + \int_0^L \rho u u_x dx + p_{1,r} - p_{1,l} = -\int_0^L C_f \rho \frac{u^2}{2} dx - \int_0^L \chi C_c \rho u dx,$$

where $p_{1,l}$ and $p_{1,r}$ are, according to the fundamental theorem of calculus, the spatial evaluation of the first order pressure at the left and right end of the pipe.

Substituting the velocity $u$ by $v + Q$, we are able to extract $v$ and its time derivatives from the integrals. Isolating the time derivative of $v$ leads us to the following integro-differential equation.

$$\begin{aligned} v_t = \frac{1}{\int_0^L \rho dx} \Bigg[ & p_{1,l} - p_{1,r} - \int_0^L \rho Q_t dx - \int_0^L \rho(v+Q) q dx \\ & - C_f \int_0^L \frac{\rho(v+Q)|v+Q|}{2} dx - \chi C_c \int_0^L \rho(v+Q)\, dx \Bigg]. \end{aligned} \tag{2.48}$$

Plugging $u = v + Q$ and $u_x = q$ into the equations for $\rho$ and $z$ of system (2.40) completes our reformulated asymptotic model.

$$\begin{aligned} \rho_t + (v+Q)\rho_x &= -q\rho, \\ z_t + (v+Q) z_x &= -\chi z K(T). \end{aligned} \tag{2.49}$$

The resulting system consists of two partial differential equations, one integro-differential equation and an algebraic closing relation $p_0 = \rho T$ for the unknowns $\rho, z, T$ and $v$.

### Initial condition for $v$

As far as the initial data is concerned we can transform the initial condition for $u$ into a condition for $v$ by

$$v_{ic} = u_{ic}(0). \tag{2.50}$$

For compatibility reason we have to demand for all $x \in [0, L]$

$$\begin{aligned} u_{ic}(x) &= v_{ic} + Q[\rho_{ic}, z_{ic}](x) \\ &= v_{ic} + \frac{1}{\gamma p_0} \int_0^x -h(T_{ic}(\xi) - T_{\text{Wall}}(\xi, 0)) + \chi q_0 \rho_{ic}(\xi) z_{ic}(\xi) K(T_{ic}(\xi)) d\xi \end{aligned} \tag{2.51}$$

with $T_{ic} = p_0/\rho_{ic}$. Otherwise we would violate the asymptotic energy balance $u_x(x, 0) = q(x, 0)$.

## 2.6. Summary

After a quick introduction into the application's background, we motivated and presented the model of Lacoste and Natalini from [LN04], and shortly discussed the drawbacks of this formulation. We overcame those drawbacks by two steps.

First, we treated the exhaust pipe as a network (see Section 2.4), and therefore got rid of the cross section function $A$. Clearly, we won flexibility in the discretization, since refinements around the cross overs are not required anymore. On the other hand, we had to state coupling conditions, which, in turn, gave the opportunity to include pressure loss terms easily. We call the thereby derived intermediate model *full Euler model*, and use the abbreviation **FE**. It consists of the state equations (2.32), accompanied by the scaled version of the initial (2.20) and boundary conditions (2.21) - (2.22) as well as the coupling conditions (2.27) - (2.30).

Second, we performed a low Mach number limit to rule out sound waves, which will enable us to have fast numerical simulations. We call our final formulation *asymptotic model*, and abbreviate it by **AM**. It consists of the equations (2.48) - (2.49). The corresponding initial, boundary and coupling conditions were derived in Sections 2.5.2 and 2.5.3 on the basis of the above stated conditions for the full Euler model.

The complete model descriptions of FE and AM are summarized on the following pages. For both models we consider the same geometry - the exhaust pipe (see Table 2.1 or Figure 2.4).

## FE - Full Euler model on a network

$$\boxed{\begin{aligned}
\rho_t^i + (\rho^i u^i)_x &= 0,\\
(\rho^i u^i)_t + \left(\rho^i (u^i)^2 + \frac{1}{\varepsilon} p^i\right)_x &= -C_f^i \rho^i \frac{u^i|u^i|}{2} - \chi^i C_c \rho^i u^i,\\
\left(\rho^i T^i + \varepsilon(\gamma-1)\rho^i \frac{(u^i)^2}{2}\right)_t + \left(\rho^i u^i T^i + \varepsilon(\gamma-1)\rho \frac{(u^i)^3}{2} + (\gamma-1) u^i p^i\right)_x &\\
= -h^i(T^i - T^i_{\text{Wall}}) + \chi^i q_0 \rho^i z^i K(T^i),&\\
(\rho^i z^i)_t + (\rho^i u^i z^i)_x &= -\chi^i \rho^i z^i K(T^i),\\
p^i &= \rho^i T^i
\end{aligned}} \tag{2.52}$$

for all pipes $i = 1, \ldots, n_P$ and $(x,t) \in (0, L^i) \times (0, \infty)$, initial conditions

$$\boxed{\begin{aligned}
\rho^i(x,0) &= \rho^i_{ic}(x), \quad u^i(x,0) = u^i_{ic}(x),\\
p^i(x,0) &= p^i_{ic}(x), \quad z^i(x,0) = z^i_{ic}(x)
\end{aligned}} \tag{2.53}$$

for all pipes $i = 1, \ldots, n_P$ and $x \in (0, L^i)$, boundary conditions

$$\boxed{\begin{aligned}
p^1(0,t) &= p_{bc,l}(t),\\
\left.\begin{aligned}\rho^1(0,t) &= \rho_{bc,l}(t),\\ z^1(0,t) &= z_{bc,l}(t),\end{aligned}\right\} &\text{ if } u^1(0,t) > 0
\end{aligned}} \tag{2.54}$$

and

$$\boxed{\begin{aligned}
p^{n_P}(L^{n_P},t) &= p_{bc,r}(t),\\
\left.\begin{aligned}\rho^{n_P}(L^{n_P},t) &= \rho_{bc,r}(t),\\ z^{n_P}(L^{n_P},t) &= z_{bc,r}(t),\end{aligned}\right\} &\text{ if } u^{n_P}(L^{n_P},t) < 0
\end{aligned}} \tag{2.55}$$

for all $t \in [0, \infty)$ and coupling conditions

$$\boxed{\begin{aligned}
\rho^i_r(t) u^i_r(t) A^i = \rho^{i+1}_l(t) u^{i+1}_l(t) A^{i+1}, &\quad z^i_r(t) = z^{i+1}_l(t),\\
T^i_r(t) = T^{i+1}_l(t), &\quad p^i_r(t) = p^{i+1}_l(t) + \varepsilon f^i_{ext}(t)
\end{aligned}} \tag{2.56}$$

for all pipes $i = 1, \ldots, n_P - 1$ and $t \in [0, \infty)$, where

$$T^i_{\text{Wall}}(x,t) := \frac{1}{2}(T^i(x,t) + T_{out}), \qquad K(T^i) = \frac{\tilde{K}_0 \tilde{x}_{\text{ref}}}{\tilde{u}_{\text{ref}}} \exp\left(-\frac{\tilde{T}^+}{\tilde{T}_{\text{ref}} T^i}\right).$$

## AM - Asymptotic model on a network

$$\boxed{\begin{aligned}
&\rho_t^i + (v^i + Q^i)\rho_x^i = -q^i\rho^i,\\
&z_t^i + (v^i + Q^i)z_x^i = -\chi^i z^i K(T^i),\\
&\qquad v_t^i = \frac{1}{\int_0^{L^i}\rho^i dx}\Bigg[p_{1,l}^i - p_{1,r}^i - \int_0^{L^i}\rho^i Q_t^i dx - \int_0^{L^i}\rho^i(v^i+Q^i)q^i dx\\
&\qquad\qquad - C_f^i\int_0^{L^i}\frac{\rho^i(v^i+Q^i)|v^i+Q^i|}{2}dx - \chi^i C_c\int_0^{L^i}\rho^i(v^i+Q^i)\,dx\Bigg],\\
&\qquad p_0 = \rho^i T^i
\end{aligned}} \tag{2.57}$$

for all pipes $i = 1, \ldots, n_P$ and $(x,t) \in (0, L^i) \times (0, \infty)$, initial conditions

$$\boxed{\rho^i(x,0) = \rho_{ic}^i(x), \quad z^i(x,0) = z_{ic}^i(x), \quad v^i(0) = v_{ic}^i} \tag{2.58}$$

for all pipes $i = 1, \ldots, n_P$ and $x \in (0, L^i)$, boundary conditions

$$\boxed{\begin{array}{rcl} p_1^1(0,t) &=& (p_{bc,l})_1(t),\\ \left.\begin{array}{rcl}\rho^1(0,t) &=& \rho_{bc,l}(t),\\ z^1(0,t) &=& z_{bc,l}(t),\end{array}\right\} & \text{if} & u^1(0,t) > 0\end{array}} \tag{2.59}$$

and

$$\boxed{\begin{array}{rcl} p_1^{n_P}(L^{n_P},t) &=& (p_{bc,r})_1(t),\\ \left.\begin{array}{rcl}\rho^{n_P}(L^{n_P},t) &=& \rho_{bc,r}(t),\\ z^{n_P}(L^{n_P},t) &=& z_{bc,r}(t),\end{array}\right\} & \text{if} & u^{n_P}(L^{n_P},t) < 0\end{array}} \tag{2.60}$$

for all $t \in [0, \infty)$ and coupling conditions

$$\boxed{\begin{array}{ll} \rho_r^i(t) = \rho_l^{i+1}(t), & z_r^i(t) = z_l^{i+1}(t),\\ u_r^i(t)A^i = u_l^{i+1}(t)A^{i+1}, & p_{1,r}^i(t) = p_{1,l}^{i+1}(t) + f_{ext}^i(t)\end{array}} \tag{2.61}$$

for all pipes $i = 1, \ldots, n_P - 1$ and $t \in [0, \infty)$, where

$$q^i(x,t) := \frac{1}{\gamma p_0}\big(-h^i(T^i(x,t) - T_{\text{Wall}}^i(x,t)) + \chi^i q_0 \rho^i(x,t) z^i(x,t) K(T^i(x,t))\big),$$

$$u^i(x,t) = v^i(t) + Q^i(x,t), \qquad Q^i(x,t) := \int_0^x q^i(\xi,t)d\xi.$$

# 3. Numerical simulations

The key aspect of this chapter is to show by numerical examples, that the asymptotic model is a justified approximation of the full Euler model. On the way towards this goal, we start with a short discussion about the difficulty of providing an existence theory for both considered transient models, FE and AM. However, we will present solutions to a simplified stationary asymptotic model. After explaining the numerical treatment, we use the knowledge of the explicit stationary solution to verify the correct convergence of the algorithm for the transient asymptotic model. Lastly, we will compare costs and results of the numerical schemes of both models.

The comparison of numerical costs and numerical solutions of both, the hyperbolic (FE) and asymtotic model (AM) (Section 3.4), has been published in [GR13][1].

## 3.1. Remarks on the existence of solutions of models FE and AM

Although providing an existence theory for the asymptotic and/or full Euler model was not within the scope of this thesis, we want to discuss shortly the difficulties of this delicate task for both models.

There is a lot of literature on existence and uniqueness of related one-dimensional hyperbolic problems. The variety diminishes when the equations are not governing only one pipe, but a network of pipes. Assuming there exists a solution for a considered problem, it is not trivial to expand this solution to the network case. We mention as a reference example only the paper of Banda, Herty and Klar [BHK06], since it comes close to the full hyperbolic system we consider. There, the isothermal[2] Euler equations were studied. A linear equation of state gave a linear dependence between pressure and density to model transport of gases through pipes. Under certain assumptions they could show for a simplified setting of only pipe to pipe intersection with identical diameters, that there exists a unique

[1] Using the published content in this thesis is in agreement with the copy rights of the publisher: `http://www.elsevier.com/journal-authors/author-rights-and-responsibilities`.

[2] constant temperature

transient solution to the Riemann problem. However, the governing equations of the problem in [BHK06] and our hyperbolic problem differ strongly. Since we are dealing with a multi-component and non-isothermal flow, we have two additional equations. Since in our setting not all eigenvalues are distinct, our problem is not *strictly hyperbolic*, but only *hyperbolic* (see Subsection 3.3.1 for details). This complicates the attempt to (uniquely) solve a Riemann problem. Additionally, we consider complex physical (and partly local) phenomena, which are described by the right hand sides of the equations. And lastly, although minor loss terms are mentioned in [BHK06], they are neglected in the analysis. Hence, we are dealing with a more complex problem and cannot easily extend the results given in [BHK06].

In the case of the asymptotic model, the task might be even more challenging. Since we left the hyperbolic regime by performing the small Mach number limit, we have to abstain from the possibly helping literature on this topic. The literature on existence theory of limits of the (multi-component) Euler equations concentrates on the incompressible case. However, there is an article by Gasser and Steinrück [GS06b] in which existence theory for a related transient problem, a model that describes fire in tunnels, was studied. In contrast to our asymptotic model, this model, which was derived in [GS02] in a similar small Mach number limit, describes a single-component fluid flow with a given heat source $q$. Due to this fact, and under the assumption of a given solution for the space-independent velocity component $v$, one is able to compute the characteristic curves which have the speed $u = v + Q$ and show the existence of a unique solution for the transport equation. This step is the basis for the global existence and uniqueness result for the whole problem with a fixed point argument. However, the aggregated energy gain $Q$, depends on the density $\rho$ and ratio of unburnt gas $z$, and is therefore unknown. This makes solving by the method of characteristics impossible in our case. Furthermore, the considered spatial domain in [GS06b] is a single tunnel/pipe. The existence of a solution for the tunnel fire model on a network is currently investigated in the PhD thesis of Roggensack [Rog14].

## 3.2. The stationary problem

In this section we consider a simplified stationary problem originating from the asymptotic model (2.57) - (2.61). The aim is to use the unique analytical results with the purpose of verifying the convergence of the algorithm applied to the transient model. Details on this can be found in Subsection 3.3.3. First, before starting the analysis, we want to state the simplified transient model, since we will use it in that section for the verification of the algorithm. Starting from the asymptotic model, we simplify it by applying the following steps:

- We have only one gas component (no equation for $z$).
- There are no catalytic converters, i.e., $\chi^i = 0 \; \forall i = 1, \dots, n_P$.

Thus, the governing transient equations are:

$$\begin{aligned} &\rho_t^i + (v^i + Q^i)\rho_x^i = -q^i\rho^i, \\ &v_t^i = \frac{1}{\int_0^{L^i} \rho^i dx} \left[ \Delta p_1^i - \int_0^{L^i} \rho^i Q_t^i + \rho^i(v^i + Q^i)q^i + C_f^i \frac{\rho^i(v^i + Q^i)|v^i + Q^i|}{2} dx \right] \end{aligned} \tag{3.1}$$

for all pipes $i = 1, \dots, n_P$ and $(x,t) \in (0, L^i) \times (0, \infty)$. Despite omitting the conditions for the ratio of unburnt gas $z$, we keep the initial, inflow boundary and coupling conditions from the original formulation. We denote by $\Delta p_1^i := p_{1,l}^i - p_{1,r}^i$, the pressure difference in the $i$-th pipe. As a consequence of $\chi^i = 0$, the energy balance term $q^i$ (compare (2.46)) reduces to

$$q^i(x,t) := -\frac{h^i}{2\gamma p_0} \left( \frac{p_0}{\rho^i(x,t)} - T_{out} \right). \tag{3.2}$$

### 3.2.1. A simplified stationary problem for a single pipe

We first concentrate on the single pipe scenario, i.e., $n_P = 1$. The pipe's scaled length[3] is denoted by $L$. By setting all time derivatives to zero, we obtain the *stationary problem* for a single pipe:

$$\begin{aligned} &(v + Q)\rho_x = -q\rho, \\ &\Delta p_1 = \int_0^L \rho(v + Q)q dx + C_f \int_0^L \frac{\rho(v + Q)|v + Q|}{2} dx \end{aligned} \tag{3.3}$$

with boundary condition $\rho(x_0) = \rho_{bc}$, where $x_0$ is either the left end ($x_0 = 0$) or right end ($x_0 = L$) of the pipe.

For the purpose of a simpler formulation, it makes sense to rewrite the system (3.3) in the way it was done in [GS02] for the related tunnel fire model. Using the identity

$$(v(t) + Q(x,t))_x = q(x,t)$$

[3] In a model for a single pipe, one usually takes the pipe's unscaled length $\tilde{L}$ as a spatial reference value, such that the scaled length of the pipe is $L = 1$. However, we want to apply the results of this subsection to the network case. Therefore, a careful analysis with a variable length $L$ is required (see Section 2.5.1 for details on scaling).

we obtain, that the product of $v + Q$ and $\rho$ must be a constant:

$$((v+Q)\rho)_x = 0 \;\Rightarrow\; (v+Q)\rho =: m = const.$$

By this condition and the definition of $q$ (see (3.2)), we obtain the reformulation of our model[4]:

$$\boxed{\begin{aligned} \rho_x &= \frac{h}{2\gamma p_0 m}\rho\left(p_0 - \rho \cdot T_{out}\right), \\ \Delta p_1 &= m\int_0^L q dx + C_f \frac{m|m|}{2}\int_0^L \frac{1}{\rho}dx \end{aligned}} \tag{3.4}$$

with boundary conditions

$$\rho(0) = \rho_{bc,l}, \quad \text{if } m > 0, \qquad\qquad \rho(L) = \rho_{bc,r}, \quad \text{if } m < 0. \tag{3.5}$$

**Proposition 1.** *The ODE of (3.4) with $x \in [0, \infty)$ has two stationary points:*

$$\rho_*^0 = 0, \qquad\qquad \rho_*^+ = p_0/T_{out}.$$

*The stability depends on the sign of $m$:*

$$\begin{aligned} m > 0 &\Rightarrow \rho_*^0 \text{ unstable and } \rho_*^+ \text{ asymptotically stable}, \\ m < 0 &\Rightarrow \rho_*^0 \text{ asymptotically stable and } \rho_*^+ \text{ unstable}. \end{aligned}$$

*Proof.* A simple phase portrait proves the statement. □

We will discriminate between two cases, namely neglecting and considering heat exchange with the wall. In the first setting, i.e., $h = 0$, we prove unique existence. However, this is not possible in the case $h > 0$, where at least two solutions exist.

### The case $h = 0$

In the case where we have no heat exchange with the wall, i.e., $h = 0$, the term $q$ vanishes. Hence, the stationary problem simplifies to

$$\begin{aligned} \rho_x &= 0, \\ \Delta p_1 &= C_f \frac{m|m|}{2}\int_0^L \frac{1}{\rho}dx \end{aligned} \tag{3.6}$$

[4]The case $m = 0$ is not of interest, since this is only possible if $\Delta p_1 = 0$. However, in our (physically motivated) setting, this will not be the case.

with the inflow boundary condition (3.5). As a consequence of the first equation, we obtain $\rho(x) = \rho_{bc}$ for all $x \in [0,1]$, where $\rho_{bc}$ is either the left or the right boundary condition. With this information, we deduce from the second equation

$$m|m| = \frac{2\Delta p_1 \rho_{bc}}{C_f L} \;\Leftrightarrow\; m = \begin{cases} \sqrt{\dfrac{2\Delta p_1 \rho_{bc,l}}{C_f L}}, & \text{if } \Delta p_1 > 0, \\ -\sqrt{\dfrac{2|\Delta p_1| \rho_{bc,r}}{C_f L}}, & \text{if } \Delta p_1 < 0. \end{cases}$$

So the unique solution of the system (3.6) (in the physical variables $\rho$ and $v$) is

$$\rho(x) = \begin{cases} \rho_{bc,l}, & \text{if } \Delta p_1 > 0, \\ \rho_{bc,r}, & \text{if } \Delta p_1 < 0, \end{cases} \qquad v = \begin{cases} \sqrt{\dfrac{2\Delta p_1}{C_f L \rho_{bc,l}}}, & \text{if } \Delta p_1 > 0, \\ -\sqrt{\dfrac{2|\Delta p_1|}{C_f L \rho_{bc,r}}}, & \text{if } \Delta p_1 < 0 \end{cases} \tag{3.7}$$

for all $x \in [0, L]$.

**The case $h > 0$**

In the case of positive heat exchange with the wall, the situation is more delicate. Even in the simple setting (single pipe, only one gas component, no catalytic converter) there are at least two solutions to the problem (3.4) as the following results show.

**Proposition 2.** *The $k \in \mathbb{N}$ non-vacuum smooth solutions to the stationary problem* (3.4) *with boundary conditions* (3.5) *are given by*

$$\rho(x) = \frac{p_0}{(p_0/\rho_{bc} - T_{out}) \exp\left(-\dfrac{h}{2\gamma m} x\right) + T_{out}},$$

*if and only if there exist $k$ solutions to the problem*

$$\Delta p_1 = F(m)$$

*with*

$$F(m) := \left(\frac{1}{\rho_{bc}} - \frac{T_{out}}{p_0}\right) m^2 \left(\exp\left(-\frac{hL}{2\gamma m}\right) - 1\right)\left(1 - \frac{\gamma C_f}{h}|m|\right) + \frac{C_f L T_{out}}{2p_0} m|m|.$$

*Furthermore, the sign of a solution $m^*$ to $\Delta p_1 = F(m^*)$ determines, whether we have to use the left or right boundary condition.*

*Proof.* We know from Proposition 1, that $\rho_{bc} = 0$ and $\rho_{bc} = p_0/T_{out}$ are stationary solutions of the ODE of (3.4). So let us exclude those cases for the further computation. Moreover, we know also from Proposition 1, that with $\rho_{bc} \in (0, p_0/T_{out})$ or $\rho_{bc} \in (p_0/T_{out}, \infty)$, a solution of $\rho$ will not leave these intervals for all $x \in (0, \infty)$.

Since this ODE has a Lipschitz-continuous right hand side, we know that there exists a unique solution with parameter $m$. With separation of variables (see Appendix C.1 for detailed computation) we find the solution

$$\rho(x) = \frac{p_0}{(p_0/\rho_{bc} - T_{out}) \exp\left(-\frac{h}{2\gamma m}x\right) + T_{out}}.$$

The algebraic equation of (3.4) delivers a condition for $m$:

$$\begin{aligned}\Delta p_1 &= m \int_0^L q dx + C_f \frac{m|m|}{2} \int_0^L \frac{1}{\rho} dx \\ &= m \cdot \left( -\frac{h}{2\gamma} \int_0^L \frac{1}{\rho} dx + \frac{hLT_{out}}{2\gamma p_0} \right) + C_f \frac{m|m|}{2} \int_0^L \frac{1}{\rho} dx. \end{aligned} \tag{3.8}$$

Since the constant $m$ appears in the solution of $\rho$, we have to compute the following integral:

$$\begin{aligned}\int_0^L \frac{1}{\rho} dx &= \int_0^L \frac{1}{p_0}(p_0/\rho_{bc} - T_{out}) \exp\left(-\frac{h}{2\gamma m}x\right) + \frac{T_{out}}{p_0} dx \\ &= \frac{LT_{out}}{p_0} + \left(\frac{1}{\rho_{bc}} - \frac{T_{out}}{p_0}\right) \left[ -\frac{2\gamma m}{h} \exp\left(-\frac{h}{2\gamma m}x\right) \right]_{x=0}^{x=L} \\ &= \frac{LT_{out}}{p_0} - \frac{2\gamma}{h} \left(\frac{1}{\rho_{bc}} - \frac{T_{out}}{p_0}\right) m \left( \exp\left(-\frac{hL}{2\gamma m}\right) - 1 \right).\end{aligned}$$

Plugging this into (3.8) leads to

$$\begin{aligned}\Delta p_1 &= \left(\frac{1}{\rho_{bc}} - \frac{T_{out}}{p_0}\right) m^2 \left( \exp\left(-\frac{hL}{2\gamma m}\right) - 1 \right) \\ &\quad + \frac{C_f LT_{out}}{2p_0} m|m| - \frac{\gamma C_f}{h} \left(\frac{1}{\rho_{bc}} - \frac{T_{out}}{p_0}\right) m^2|m| \left( \exp\left(-\frac{hL}{2\gamma m}\right) - 1 \right) \\ &= \left(\frac{1}{\rho_{bc}} - \frac{T_{out}}{p_0}\right) m^2 \left( \exp\left(-\frac{hL}{2\gamma m}\right) - 1 \right) \left(1 - \frac{\gamma C_f}{h}|m|\right) + \frac{C_f LT_{out}}{2p_0} m|m|.\end{aligned}$$

□

Thus, the existence and uniqueness of the solution of the system (3.4) depends on the existence and uniqueness of the solution of $\Delta p_1 = F(m)$. We state two results that under certain assumptions show that there are at least two solution to $\Delta p_1 = F(m)$, one with a positive and one with a negative flow direction.

**Proposition 3.** *If $\Delta p_1 > 0$, then there exists an $m^+ > 0$ with $F(m^+) = \Delta p_1$.*

**Proposition 4.** *If $p_0 > \rho_{bc} T_{out}$, there exists, regardless of the sign of $\Delta p_1$, an $m^- < 0$ with $F(m^-) = \Delta p_1$.*

In terms of our application, the parameter constellation $p_0 > \rho_{bc} T_{out}$ is realistic. Usually the scaled thermodynamic pressure $p_0$ and outside temperature $T_{out}$ are equal to 1. Furthermore the boundary condition for the density $\rho_{bc}$ is less than 1, since it describes the high temperature fluid entering the exhaust pipe.

*Proof of Proposition 3.* Let us define $G^+(m)$:

$$G^+(m) := -\Delta p_1 + \underbrace{(-abm^2 + am)}_{=:g_1^+(m)} \underbrace{m(\exp(-cm^{-1}) - 1)}_{=:g_2^+(m)} + dm^2$$

for $m > 0$ with

$$a := \frac{1}{\rho_{bc}} - \frac{T_{out}}{p_0}, \qquad b := \frac{\gamma C_f}{h}, \qquad c := \frac{hL}{2\gamma}, \qquad d := \frac{C_f L T_{out}}{2p_0}.$$

First, we instantly see that

$$\lim_{m \searrow 0} G^+(m) = -\Delta p_1 < 0.$$

In the following we will prove that the limit $\lim_{m\to\infty} G^+(m) = +\infty$, and hence there exists at least one root of $G^+$, since $m \mapsto G^+(m)$ is continuous for $m > 0$. All parameters $\rho_{bc}, T_{out}, p_0, C_f$ and $h$ have positive sign. So it is obvious, that $b, c$ and $d$ are positive as well. Only the sign of $a$ depends on the relation between $\rho_{bc}, T_{out}$ and $p_0$.

(i) If $p_0 = \rho_{bc} T_{out}$, the parameter $a = 0$ and we would have $g_1^+(m) = 0$. With $dm^2 \to \infty$ as $m \to \infty$ the statement is proven.

(ii) For the case $p_0 > \rho_{bc} T_{out}$, we have $a > 0$. Let us first check the sign of $g_2^+$.

$$0 < m < \infty \Leftrightarrow -\infty < -cm^{-1} < 0 \Leftrightarrow 0 < \exp(-cm^{-1}) < 1.$$

Thus, $g_2^+(m) < 0$.

The only root of $g_1^+$ is $m = b^{-1}$. The parameter $a$ is positive, and therefore we know that

$$g_1^+(m) \begin{cases} > 0, & \text{if } m \in (0, b^{-1}), \\ < 0, & \text{if } m \in (b^{-1}, \infty). \end{cases}$$

Hence, we get

$$\lim_{m\to\infty} g_1^+(m) g_2^+(m) > 0 \qquad \Rightarrow \qquad \lim_{m\to\infty} G^+(m) = \infty.$$

(iii) For the case $p_0 < \rho_{bc} T_{out}$, we have $a < 0$. Let us first check $g_2^+$.

$$g_2^+(m) = m\left(\sum_{k=0}^{\infty} \frac{(-cm^{-1})^k}{k!} - 1\right) = -c + \frac{c^2 m^{-1}}{2} \mp \ldots \overset{m\to\infty}{\longrightarrow} -c.$$

Since $g_2^{+\prime}(m) = \exp(-cm^{-1})(cm^{-1} - 1) < 0$ for all $m > c$ and $g_2^+(m) < 0$ for all $m > 0$, we can deduce that $|g_2^+(m)| < c$ for all $m > c$. So now the following estimation is true for all $m > \max\{b^{-1}, c\}$.

$$|g_1^+(m) g_2^+(m)| < |ac(-bm^2 + m)| < |abc| m^2.$$

Plugging in the definitions of $a, b$ and $c$, we obtain

$$|abc| = \left|\left(\frac{1}{\rho_{bc}} - \frac{T_{out}}{p_0}\right) \frac{\gamma C_f}{h} \frac{h}{2\gamma}\right| = \frac{C_f}{2}\left|\frac{1}{\rho_{bc}} - \frac{T_{out}}{p_0}\right| < \frac{C_f T_{out}}{2p_0} = d,$$

since

$$-\frac{T_{out}}{p_0} < \frac{1}{\rho_{bc}} - \frac{T_{out}}{p_0} < \frac{T_{out}}{p_0} \Leftrightarrow p_0 < 2\rho_{bc} T_{out}.$$

□

*Proof of Proposition 4.* The proof is similar to the previous one. We will also use the same definitions of $a, b, c, d$. With

$$G^-(m) := -\Delta p_1 + \underbrace{(abm^2 + am)}_{=:g_1^-(m)} \underbrace{m(\exp(-cm^{-1}) - 1)}_{=:g_2^-(m)} - dm^2$$

we will show:

1. $\lim\limits_{m\nearrow 0} G^-(m) = +\infty$,

2. $\lim_{m\to-\infty} G^-(m) = -\infty$.

Then, an $m^- \in (-\infty, 0)$ with $G^-(m^-) = 0$ must exist, since $G^-$ is continuous for $m < 0$.

1. We have $\exp(-cm^{-1}) > 1$ for all $m < 0$. Therefore $g_2^-(m) < 0$. Furthermore, $g_1^-(m) = am(bm+1) < 0$ for all $m > -b^{-1}$. Thus, the product $g_1^- g_2^- > 0$ for all $m \in (-b^{-1}, 0)$. Finally with
$$\lim_{m\nearrow 0} \exp(-cm^{-1}) = \infty$$
we obtain the statement.

2. As already discussed $g_2^- < 0$ for all $m < 0$. The only root of $g_1^-$ is $m = -b^{-1}$. Therefore we know that
$$g_1^-(m) \begin{cases} > 0, & \text{if } m \in (-\infty, -b^{-1}), \\ < 0, & \text{if } m \in (-b^{-1}, 0). \end{cases}$$
Hence, we get
$$\lim_{m\to-\infty} g_1^-(m) g_2^-(m) < 0 \qquad \Rightarrow \qquad \lim_{m\to\infty} G^+(m) = -\infty.$$

□

### 3.2.2. A simplified stationary problem for a network of pipes

We want to extend our results to the case of a network of pipes. Like in our application we will only consider a pipe-to-pipe structure. The number of pipes is arbitrary, i.e., $n_P \in \mathbb{N}$. We consider only the case $h = 0$, since we can ensure existence of a unique solution here. Furthermore, for the sake of simplicity we neglect minor loss terms, i.e., $f_{ext} = 0$.

So the governing equations of the problem stationary problem on a network of $n_P$ pipes with no heat exchange and no pressure loss at the vertices are

$$\begin{aligned} \rho_x^i &= 0, \\ \Delta p_1^i &= C_f^i \frac{m^i|m^i|}{2} \int_0^{L^i} \frac{1}{\rho^i} dx \end{aligned} \tag{3.9}$$

for $i = 1, \ldots, n_P$ and with the boundary condition

$$\rho^1(0) = \rho_{bc,l}, \quad \text{if } m^1 > 0, \qquad \rho^{n_P}(L^{n_P}) = \rho_{bc,r}, \quad \text{if } m^{n_P} < 0, \tag{3.10}$$

$$p_1^1(0) = (p_{bc,l})_1, \qquad p_1^{n_P}(L^{n_P}) = (p_{bc,r})_1. \tag{3.11}$$

For our setting, i.e., no equation for $z$ and no pressure losses at the junctions, the coupling conditions (2.61) reduce to

$$\rho_r^i = \rho_l^{i+1}, \qquad A^i u_r^i = A^{i+1} u_r^{i+1}, \qquad p_{1,r}^i = p_{1,l}^{i+1}. \tag{3.12}$$

As we know from (3.7), the stationary solution for any pipe $i \in \{1, \dots, n_P\}$ is:

$$\rho^i(x) = \rho_{const}^i \;\; \forall\, x \in [0, L^i], \qquad v^i = \begin{cases} \sqrt{\dfrac{2\Delta p_1^i}{C_f^i L^i \rho_{const}^i}}, & \text{if } \Delta p_1^i > 0, \\ -\sqrt{\dfrac{2|\Delta p_1^i|}{C_f^i L^i \rho_{const}^i}}, & \text{if } \Delta p_1^i < 0. \end{cases} \tag{3.13}$$

With the help of the coupling condition for the density, we immediately conclude, that $\rho_{const}^i = \rho_{const}$ for all $i = 1, \dots, n_P$. From the coupling condition for the velocity $u$ we can deduce, that the flow direction has to be uniform in all pipes. Thus, only one of the two boundary conditions for the density is used, i.e.,

$$\rho_{const} = \rho_{bc} = \begin{cases} \rho_{bc,l}, & \text{if } u > 0, \\ \rho_{bc,r}, & \text{if } u < 0. \end{cases}$$

Whether we have to choose the left or right boundary condition, cannot be answered yet.

In order to determine $v^i$ for all $i = 1, \dots, n_P$ we need to know all pressure values at the vertices. However, the only pressure values we know are given by the boundary condition. Therefore, we have to determine pressure values at the junctions. We will do this with the help of the coupling conditions.

Multiplying the terms of the second coupling condition with their absolute values leads to the following identity:

$$A^i u_r^i |A^i u_r^i| = A^{i+1} u_l^{i+1} |A^{i+1} u_l^{i+1}| \quad \Leftrightarrow \quad (A^i)^2 u_r^i |u_r^i| = (A^{i+1})^2 u_l^{i+1} |u_l^{i+1}|.$$

Since the heat exchange rate $h = 0$ vanishes, we have no heat source term $q$. Therefore, we deduce that $u^i = v^i$ for all $i = 1, \dots, n_P$. With the formulation of the coupling condition we are able to plug in the analytic solution of $v^i$ without knowing the sign of the pressure difference $\Delta p_1^i$.

$$(A^i)^2 \frac{2\Delta p_1^i}{C_f^i L^i \rho_{bc}} = (A^{i+1})^2 \frac{2\Delta p_1^{i+1}}{C_f^{i+1} L^{i+1} \rho_{bc}}.$$

We will split the term $\Delta p_1^i$ in the difference of the left and right pressure value in the $i$-th pipe.

$$\frac{(A^i)^2}{C_f^i L^i} \left(p_{1,l}^i - p_{1,r}^i\right) = \frac{(A^{i+1})^2}{C_f^{i+1} L^{i+1}} \left(p_{1,l}^{i+1} - p_{1,r}^{i+1}\right).$$

By $p^i_{1,V}$ we denote the vertex pressure in first order at the vertex $i$, which is connecting the pipes $i$ and $i+1$. Then, with the coupling condition for the pressure, we deduce $p^i_{1,r} = p^i_{1,V} = p^{i+1}_{1,l}$. We manipulate the above equality and obtain

$$\frac{(A^i)^2}{C^i_f L^i} p^{i-1}_{1,V} + \left( -\frac{(A^i)^2}{C^i_f L^i} - \frac{(A^{i+1})^2}{C^{i+1}_f L^{i+1}} \right) p^i_{1,V} + \frac{(A^{i+1})^2}{C^{i+1}_f L^{i+1}} p^{i+1}_{1,V} = 0. \tag{3.14}$$

Hence, in order to determine the unknown pressure values at the vertices, we have to solve an $n_V \times n_V$ linear system with a symmetric tridiagonal matrix, where $n_V = n_P - 1$ stands for the number of vertices.

$$\begin{pmatrix} f^1 & e^2 & & \\ e^2 & \ddots & \ddots & \\ & \ddots & \ddots & e^{n_V} \\ & & e^{n_V} & f^{n_V} \end{pmatrix} \begin{pmatrix} p^1_{1,V} \\ \vdots \\ \vdots \\ p^{n_V}_{1,V} \end{pmatrix} = \begin{pmatrix} -e^1 (p_{bc,l})_1 \\ 0 \\ \vdots \\ 0 \\ -e^{n_V+1} (p_{bc,r})_1 \end{pmatrix}, \tag{3.15}$$

where $(p_{bc,l})_1$ and $(p_{bc,l})_1$ denote the left and right boundary condition for the mechanical pressure (first order of the asymptotic expansion) and

$$e^i := \frac{(A^i)^2}{C^i_f L^i}, \qquad f^i := -e^i - e^{i+1}.$$

The matrix in (3.15) is regular, since it is *irreducible* and *weakly diagonally dominant*[5]. Furthermore, the vertex pressure mapping $i \mapsto p^i_{1,V}$ is monotone, where the direction of decrease is determined by the boundary conditions. This assures us, that the flow direction is uniform in all pipes. We specify this in the following

**Proposition 5.** *Let* $p^0_{1,V} := (p_{bc,l})_1$ *and* $p^{n_V+1}_{1,V} := (p_{bc,r})_1$. *Then*

$$\begin{aligned} p^0_{1,V} > p^{n_V+1}_{1,V} &\Rightarrow p^i_{1,V} > p^{i+1}_{1,V}, \quad \forall i = 0, \dots, n_V, \\ p^0_{1,V} = p^{n_V+1}_{1,V} &\Rightarrow p^i_{1,V} = p^{i+1}_{1,V}, \quad \forall i = 0, \dots, n_V, \\ p^0_{1,V} < p^{n_V+1}_{1,V} &\Rightarrow p^i_{1,V} < p^{i+1}_{1,V}, \quad \forall i = 0, \dots, n_V. \end{aligned}$$

*Proof.* We prove the statement for the case $p^0_{1,V} > p^{n_V+1}_{1,V}$ indirectly. The proof for the other two cases is analogue.

Let us assume, that for an index $j \in \{1, \dots, n_V\}$ the relation $p^j_{1,V} \leq p^{j+1}_{1,V}$ holds. Then $p^{j-1}_{1,V} \leq p^j_{1,V}$ must hold, since $p^{j-1}_{1,V} > p^j_{1,V}$ would lead to the following contradiction.

[5] See Appendix C.2 for definitions and proof.

As we know from (3.14), the vertex pressure $p_{1,V}^j$ is a weighted mean of its neighbouring vertex pressure values $p_{1,V}^{j-1}$ and $p_{1,V}^{j+1}$, i.e.,

$$p_{1,V}^j = \frac{e^j p_{1,V}^{j-1} + e^{j+1} p_{1,V}^{j+1}}{e^j + e^{j+1}} \;\Rightarrow\; \min\{p_{1,V}^{j-1}, p_{1,V}^{j+1}\} \leq p_{1,V}^j \leq \max\{p_{1,V}^{j-1}, p_{1,V}^{j+1}\}$$

with $e^i > 0$ for all $i = 1, \ldots, n_P$. Since $p_{1,V}^{j-1}$ cannot be the smaller neighbouring vertex pressure of $p_{1,V}^j$, the vertex pressure to the right, $p_{1,V}^{j+1}$, must act (in addition to being an upper boundary) as a lower boundary for the vertex pressure $p_V^j$. As a consequence, $p_{1,V}^j = p_{1,V}^{j+1}$ must hold. Using the equality in the above stated identity, leads to a contradiction with the assumption $p_{1,V}^{j-1} > p_{1,V}^j$:

$$p_{1,V}^j = \frac{e^j p_{1,V}^{j-1} + e^{j+1} p_{1,V}^j}{e^j + e^{j+1}} \quad \Leftrightarrow p_{1,V}^j = p_{1,V}^{j-1}.$$

Therefore, $p_{1,V}^{j-1} > p_{1,V}^j$ cannot be true and we must have $p_{1,V}^{j-1} \leq p_{1,V}^j$.

For the same reasons $p_{1,V}^{j+1} \leq p_{1,V}^{j+2}$ must hold. Following this procedure for the other vertices, we finally arrive at

$$p_{1,V}^0 \leq \ldots \leq p_{1,V}^{j-1} \leq p_{1,V}^j \leq p_{1,V}^{j+1} \leq p_{1,V}^{j+2} \leq \ldots \leq p_{1,V}^{n_V+1}$$

in contradiction to $p_{1,V}^0 > p_{1,V}^{n_V+1}$. □

This result ensures the unique existence of the simplified stationary problem and therefore gives rise to the following

**Theorem 1.** *Consider the simplified stationary problem* (3.9) - (3.12)*, i.e., without considering catalytic converters ($\chi = 0$), heat exchange ($h = 0$) and minor loss terms ($f_{ext} = 0$). If the underlying network has exactly two edges (pipes) per vertex (junction), then there exists a unique solution of* (3.9) - (3.12) *which can be computed explicitly.*

## 3.3. Numerical treatment

We present the discretization for the considered models FE and AM. The choice of the discretization is motivated by its purpose, namely a fair comparison of the numerical results and costs of both models. Therefore, we basically apply first-order upwind schemes. In this section we explain the discretization of each model in detail.

The discretization of the spatial domain will be the same for both models. We uniformly distribute $J \in \mathbb{N}$ spatial grid points among all pipes. We denote the

constant spatial step size by $\Delta x := x_j - x_{j-1}$. However, the step sizes in time are not constant, since they depend on CFL conditions (see Algorithms 1 and 2 as well as Subsection 3.4.1). We therefore denote the time step size by a superscript, i.e., $\Delta t^{n+\frac{1}{2}}$, indicating that this is the step size between time grid point $t^n$ and $t^{n+1}$.

### 3.3.1. Numerical treatment of the hyperbolic model FE

As already mentioned we use an upwind scheme for the numerical simulations. In most literature (like in the textbooks of LeVeque [LeV92] and Toro [Tor09]) upwind methods are derived for linear systems, but can be adopted in various ways to the nonlinear case. We use a simple first order upwind scheme with flux vector splitting as it was proposed by Courant, Isaacson and Rees in [CIR52] (see also [SW81, SMT93]). Additionally, we divide the hyperbolic balance law

$$U_t(x,t) + F(U(x,t))_x = G(U(x,t))$$

into two sub-problems, a homogeneous conservation law and an ordinary differential equation for the source term:

$$\begin{aligned} &\text{Problem A:} \quad U_t(x,t) + F(U(x,t))_x = 0, \\ &\text{Problem B:} \quad U_t(x,t) = G(U(x,t)). \end{aligned}$$

The idea of such an approach, which is often called *fractional-step method*, is to combine two numerical solvers in an alternating manner. The advantage is, that we can use standard methods for both problems. Deriving an unsplit method based on the same ideas while incorporating the source term directly can be more difficult (see [LeV02] for details).

We start with the numerical scheme for the homogeneous conservation law

$$U_t(x,t) + F(U(x,t))_x = 0 \tag{3.16}$$

with $U \in \mathbb{R}^d$. Assuming smoothness of the functions $F : V \subset \mathbb{R}^d \to \mathbb{R}^d$ and $U(x,t)$, we can rewrite the equation (3.16) using the chain rule. We arrive at the quasi-linear formulation, where $A(U)$ denotes the Jacobian matrix of $F(U)$:

$$U_t(x,t) + A(U(x,t))U_x(x,t) = 0. \tag{3.17}$$

Let $\Lambda(U) = (\lambda_1(U), \ldots, \lambda_d(U))$ denote the eigenvalues of the matrix $A(U)$. We assume the conservation law to be hyperbolic, i.e., the matrix $A(U)$ has only real eigenvalues and is diagonalizable in the form

$$A(U) = R(U)\Lambda(U)L(U),$$

where $R(U)$ and $L(U)$ denote the matrices containing the right and left eigenvectors, respectively. Since systems of conservation laws may have waves that travel in opposite directions, the following definitions are required:

$$\begin{aligned}
\lambda_i^+(U) &:= \max\{\lambda_i(U), 0\}, & \lambda_i^-(U) &:= \min\{\lambda_i(U), 0\},\\
\Lambda^+(U) &:= \operatorname{diag}(\lambda_1^+(U), \dots, \lambda_n^+(U)), & \Lambda^-(U) &:= \operatorname{diag}(\lambda_1^-(U), \dots, \lambda_n^-(U)),\\
A^+(U) &:= R(U)\Lambda^+(U)L(U), & A^-(U) &:= R(U)\Lambda^-(U)L(U).
\end{aligned}$$

Thus, the numerical algorithm for the conservation law is

$$U_j^{n+1} = U_j^n - \Delta t^{n+\frac{1}{2}} \left( A^+(U_j^n)\frac{U_j^n - U_{j-1}^n}{\Delta x} + A^-(U_j^n)\frac{U_{j+1}^n - U_j^n}{\Delta x} \right).$$

For the numerical treatment of the ordinary differential equation we use the explicit Euler method. Hence, our numerical algorithm for the hyperbolic balance law is

$$\begin{aligned}
U_j^* &= U_j^n - \Delta t^{n+\frac{1}{2}} \left( A^+(U_j^n)\frac{U_j^n - U_{j-1}^n}{\Delta x} + A^-(U_j^n)\frac{U_{j+1}^n - U_j^n}{\Delta x} \right),\\
U_j^{n+1} &= U_j^* + \Delta t^{n+\frac{1}{2}}\, G(U_j^*),
\end{aligned} \tag{3.18}$$

where $U_j^n$ is the numerical approximation of $U(x_j, t_n)$. The method is still first order accurate. We can simply check this by substituting $U_j^*$ in the second equation. Assuming smoothness of $G$ we can perform a Taylor expansion and find

$$U_j^{n+1} = U_j^n - \Delta t^{n+\frac{1}{2}} V_j^n + \Delta t^{n+\frac{1}{2}} \left( G(U_j^n) + \Delta t^{n+\frac{1}{2}} B(U_j^n) V_j^n + \mathcal{O}\left( (\Delta t^{n+\frac{1}{2}})^2 \right) \right)$$

with

$$V_j^n := A^+(U_j^n)\frac{U_j^n - U_{j-1}^n}{\Delta x} + A^-(U_j^n)\frac{U_{j+1}^n - U_j^n}{\Delta x}$$

and $B$ the Jacobian matrix of $G$.

The time step size $\Delta t^{n+\frac{1}{2}}$ is determined by the CFL condition for the upwind scheme (3.18)

$$\Delta t^{n+\frac{1}{2}} \le c_N \frac{\Delta x}{\lambda_{\max}^n} \qquad \text{with} \qquad \lambda_{\max}^n := \max_{\substack{j=1,\dots,J\\ k\in\{1,2,3,4\}}} \left\{ \left| \lambda_k(U_j^n) \right| \right\} \tag{3.19}$$

and $c_N$ denoting the Courant number[6]

[6] For stability purposes the Courant number $c_N$ is chosen in the interval $(0, 1]$.

### Conservation form of the FE model

For better readability, we cease to use the superscript notation for the variables' affiliation to a pipe. In the literature the computation of eigenvalues and eigenvectors of related systems (e.g., Euler equations) relies on the unscaled version of those systems. Therefore, we also consider the unscaled version of the full Euler model (see (2.19)). This is denoted by the $\sim$ symbol on top of the variables.

$$
\begin{aligned}
\tilde{\rho}_{\tilde{t}} + (\tilde{\rho}\tilde{u})_{\tilde{x}} &= 0, \\
(\tilde{\rho}\tilde{u})_{\tilde{t}} + (\tilde{\rho}\tilde{u}^2 + \tilde{p})_{\tilde{x}} &= -\frac{\xi}{\tilde{d}}\tilde{\rho}\frac{\tilde{u}|\tilde{u}|}{2} - \tilde{\chi}\tilde{C}_c\tilde{\rho}\tilde{u}, \\
(\tilde{\rho}\tilde{E})_{\tilde{t}} + (\tilde{\rho}\tilde{u}\tilde{E} + \tilde{u}\tilde{p})_{\tilde{x}} &= -\frac{4\tilde{h}}{\tilde{d}}(\tilde{T} - \tilde{T}_{\text{Wall}}) + \tilde{\chi}\tilde{q}_0\tilde{\rho}\tilde{z}\tilde{K}(\tilde{T}), \\
(\tilde{\rho}\tilde{z})_{\tilde{t}} + (\tilde{\rho}\tilde{z}\tilde{u})_{\tilde{x}} &= -\tilde{\chi}\tilde{\rho}\tilde{z}\tilde{K}(\tilde{T}), \\
\tilde{p} &= \tilde{R}\tilde{\rho}\tilde{T}.
\end{aligned}
$$

The equations in conservation form are

$$
U_t + F(U)_x = G(U) \tag{3.20}
$$

with

$$
\begin{aligned}
U &:= (U_1, U_2, U_3, U_4)^T := (\tilde{\rho}, \tilde{\rho}\tilde{u}, \tilde{\rho}\tilde{E}, \tilde{\rho}\tilde{z})^T, \\
F(U) &:= \begin{pmatrix} U_2 \\ (\gamma-1)U_3 + \dfrac{3-\gamma}{2}\dfrac{U_2^2}{U_1} \\ \gamma\dfrac{U_2U_3}{U_1} + \dfrac{1-\gamma}{2}\dfrac{U_2^3}{U_1^2} \\ \dfrac{U_2U_4}{U_1} \end{pmatrix}, \\
G(U) &:= \begin{pmatrix} 0 \\ -\dfrac{\xi}{\tilde{d}}U_2\left|\dfrac{U_2}{2U_1}\right| - \tilde{\chi}\tilde{C}_cU_2 \\ -\dfrac{4\tilde{h}}{\tilde{d}}(\tilde{T}(U) - \tilde{T}_{\text{Wall}}) + \tilde{\chi}\tilde{q}_0U_4\tilde{K}(\tilde{T}(U)) \\ -\tilde{\chi}U_4\tilde{K}(\tilde{T}(U)) \end{pmatrix}, \\
\tilde{T}(U) &:= \frac{1}{\tilde{c}_v}\left(\frac{U_3}{U_1} - \frac{1}{2}\frac{U_2^2}{U_1^2}\right).
\end{aligned}
$$

The Jacobian of $F(U)$ has the form

$$A(U) = \begin{pmatrix} 0 & 1 & 0 & 0 \\ -\frac{3-\gamma}{2}\frac{U_2^2}{U_1^2} & (3-\gamma)\frac{U_2}{U_1} & (\gamma-1) & 0 \\ -\gamma\frac{U_2U_3}{U_1^2} + (\gamma-1)\frac{U_2^3}{U_1^3} & \gamma\frac{U_3}{U_1} - \frac{3(\gamma-1)}{2}\frac{U_2^2}{U_1^2} & \gamma\frac{U_2}{U_1} & 0 \\ -\frac{U_2U_4}{U_1^2} & \frac{U_4}{U_1} & 0 & \frac{U_2}{U_1} \end{pmatrix}$$
$$= \begin{pmatrix} 0 & 1 & 0 & 0 \\ -\frac{3-\gamma}{2}\tilde{u}^2 & (3-\gamma)\tilde{u} & (\gamma-1) & 0 \\ \frac{\gamma-1}{2}\tilde{u}^3 - \tilde{u}\tilde{H} & -(\gamma-1)\tilde{u}^2 + \tilde{H} & \gamma\tilde{u} & 0 \\ -\tilde{u}\tilde{z} & \tilde{z} & 0 & \tilde{u} \end{pmatrix}$$

with

$$\tilde{H} := \tilde{E} + \frac{\tilde{p}}{\tilde{\rho}} = \frac{\tilde{u}^2}{2} + \frac{\tilde{c}^2}{\gamma-1},$$

where $\tilde{c}$ denotes the speed of sound[7]. Then the eigenvalues of $A(U)$ are

$$\lambda_1 = \tilde{u} - \tilde{c}, \qquad \lambda_2 = \lambda_3 = \tilde{u}, \qquad \lambda_4 = \tilde{u} + \tilde{c}.$$

Since the eigenvalues are not distinct, the system (3.20) is hyperbolic, but *not* strictly hyperbolic. We require the matrices $R = (r_1, r_2, r_3, r_4)$ and $L = (l_1, l_2, l_3, l_4)^T$ for our discritization, where $r_i = r_i(U)$ and $l_i = l_i(U)$ denote the right and left eigenvectors of $A(U)$, i.e.,

$$r_1 = \begin{pmatrix} 1 \\ \tilde{u} - \tilde{c} \\ \tilde{H} - \tilde{c}\tilde{u} \\ \tilde{z} \end{pmatrix}, \quad r_2 = \begin{pmatrix} 1 \\ \tilde{u} \\ \frac{\tilde{u}^2}{2} \\ 0 \end{pmatrix}, \quad r_3 = \begin{pmatrix} 0 \\ 0 \\ 0 \\ 1 \end{pmatrix}, \quad r_4 = \begin{pmatrix} 1 \\ \tilde{u} + \tilde{c} \\ \tilde{H} + \tilde{c}\tilde{u} \\ \tilde{z} \end{pmatrix}$$

[7] The definition of the speed of sound is $\tilde{c} := \sqrt{\gamma\tilde{p}/\tilde{\rho}}$ (compare (2.36)).

and

$$
\begin{aligned}
l_1 &= \left( \frac{\tilde{u}}{2\tilde{c}} + \frac{\tilde{u}^2}{2(2\tilde{H}-\tilde{u}^2)}, \quad -\frac{\tilde{u}}{2\tilde{H}-\tilde{u}^2} - \frac{1}{2\tilde{c}}, \quad \frac{1}{2\tilde{H}-\tilde{u}^2}, \quad 0 \right), \\
l_2 &= \left( 2 - \frac{2\tilde{H}}{2\tilde{H}-\tilde{u}^2}, \quad \frac{2\tilde{u}}{2\tilde{H}-\tilde{u}^2}, \quad -\frac{2}{2\tilde{H}-\tilde{u}^2}, \quad 0 \right), \\
l_3 &= \left( -\frac{\tilde{u}^2\tilde{z}}{2\tilde{H}-\tilde{u}^2}, \quad \frac{2\tilde{u}\tilde{z}}{2\tilde{H}-\tilde{u}^2}, \quad -\frac{2\tilde{z}}{2\tilde{H}-\tilde{u}^2}, \quad 1 \right), \\
l_4 &= \left( \frac{\tilde{u}^2}{2(2\tilde{H}-\tilde{u}^2)} - \frac{\tilde{u}}{2\tilde{c}}, \quad \frac{1}{2\tilde{c}} - \frac{\tilde{u}}{2\tilde{H}-\tilde{u}^2}, \quad \frac{1}{2\tilde{H}-\tilde{u}^2}, \quad 0 \right).
\end{aligned}
\tag{3.21}
$$

#### Unknowns at the boundaries and vertices

Neither the boundary conditions at the left nor at the right hand side represent a known state $U_l$ or $U_r$ (compare (2.54) and (2.55)), since some entries (depending on the flow direction) are unknown. We compute these unknowns by solving linearized Riemann problems. This is presented in detail in the Appendix C.3. A similar challenge occurs at the vertices, where we have even less information than at the boundaries. Therefore, we also solve linearized Riemann problems at the junctions, and use the coupling conditions to determine the unknowns. The technical computations are shifted to the Appendix C.4.

**Algorithm 1** (Numerical simulation of FE)**.** *Suppose the numerical solution is known at time step $t^n$. In order to compute the numerical solution at the next time step $t^{n+1}$ the following steps are required:*

1. *compute a time step size $\Delta t^{n+\frac{1}{2}}$ by the CFL condition* (3.19) *and set $t^{n+1} = t^n + \Delta t^{n+\frac{1}{2}}$;*

2. *compute the numerical solution at $t^{n+1}$ for each pipe ($i = 1, \ldots, n_P$) by the fractional-step method* (3.18)*, consisting of the explicit upwind scheme with flux vector splitting and the explicit Euler method;*

3. *solve linearized Riemann problems at the left boundary of pipe $i = 1$ and the right boundary of pipe $i = n_P$. Furthermore, solve linearized Riemann problems at all inner vertices by applying the coupling conditions (see Appendix C.3 and C.4 for details).*

### 3.3.2. Numerical treatment of the asymptotic model AM

For the numerical simulation of the asymptotic model we have to solve the dimensionless system (2.57) for each single pipe $i = 1, \ldots, n_P$, and fulfil the coupling

conditions (2.61), the initial conditions (2.58) and the boundary conditions at the entrance (2.59) and exit of the exhaust pipe (2.60).

First, we take care of the numerical treatment of the transport PDEs of the asymptotic model. Therefore, let us consider a partial differential equation of the form

$$y_t(x,t) + a(x,t)y_x(x,t) = b(x,t,y) \tag{3.22}$$

on $(0,1) \times (0,\infty)$ with initial and inflow boundary conditions

$$\begin{aligned} y(x,0) &= y_{ic}(x), \\ y(0,t) &= y_{bc;l}(t), \qquad \text{if } a(0,t) > 0, \\ y(1,t) &= y_{bc;r}(t), \qquad \text{if } a(1,t) < 0 \end{aligned}$$

for all $x \in (0,1)$ and all $t \in [0,\infty)$. The discretization of the equation (3.22) is given by the following explicit upwind scheme (see e.g., [GRS07]), i.e,

$$y_j^{n+1} = y_j^n + \Delta t^{n+\frac{1}{2}} \left( -(a_j^n)^+ \frac{y_j^n - y_{j-1}^n}{\Delta x} - (a_j^n)^- \frac{y_{j+1}^n - y_j^n}{\Delta x} + b_j^n \right), \tag{3.23}$$

where $y_j^n$ is the numerical approximation of $y(x_j, t^n)$ and

$$(a_j^n)^- = \min\{0, a_j^n\}, \qquad\qquad (a_j^n)^+ = \max\{0, a_j^n\}.$$

A necessary condition for stability of the scheme is the CFL condition for the upwind scheme (3.23)

$$\Delta t^{n+\frac{1}{2}} \leq c_N \frac{\Delta x}{a_{\max}^n} \qquad \text{with} \qquad a_{\max}^n := \max_{j=1,\dots,J} \{|a_j^n|\} \tag{3.24}$$

and $c_N$ denoting the Courant number.

The first two PDEs for the density $\rho^i$ and the ratio of unburnt gas $z^i$ can be discretized by (3.23). For the integro-differential equation for the space-independent velocity component $v^i$, we need a different scheme. In order to stay consistent with the time discretization in the upwind scheme, we use the explicit Euler scheme

$$v^{n+1} = v^n + \Delta t^{n+\frac{1}{2}} \frac{1}{\int_0^L \rho(x,t^n)dx} \left[ p_{1_l}(t^n) - p_{1_r}(t^n) + f(t^n) \right], \tag{3.25}$$

where $f(t^n)$ gathers all remaining terms of the right hand side, i.e.,

$$f = -\int_0^L \rho Q_t + \rho(v+Q)q + C_f \frac{\rho(v+Q)|v+Q|}{2} + \chi C_c \rho(v+Q)\, dx. \tag{3.26}$$

The spatial integrals in (3.25) and (3.26) (and also for the numerical computation of $Q^i$) are approximated by the box rule

$$\int_0^L y(x)dx \approx \frac{L}{J}\sum_{j=1}^{J} y_j. \tag{3.27}$$

The time derivative of $Q$ (first term in the integral in equation (3.26)) is discretized by forward differences, i.e.,

$$Q_t \approx \frac{Q^{n+1} - Q^n}{\Delta t^{n+\frac{1}{2}}}.$$

### Unknowns at the vertices

Since now the discretization of the differential equations for the asymptotic model is done, we need to deal with the problem, that the pressure values at the inner vertices are not known. In the hyperbolic case we determined the unknowns by solving linearized Riemann problems. However, since we are not in a hyperbolic setting any more, this technique cannot be applied. We want to avoid dealing with an $n_V$-dimensional fixed point problem for each time step, when calculating the unknown pressure values at the vertices including the minor loss terms. Therefore, we will use an explicit approach for the computation of the vertex pressure (see also [GK08]).

We are dealing again with the coupling conditions, and therefore we have to use the superscript notation to denote the variables' affiliation to a pipe. In order to avoid double super-indices (pipe affiliation and discretization), we write $y(t)$ in this subsection and mean the numerical solution at time step $t$.

Using the explicit Euler method for the ODE for the time step $t + \Delta t$ for a pipe $i \in \{1, \ldots, n_P\}$, we end up with

$$v^i(t + \Delta t) = v^i(t) + \Delta t \frac{f^i[v, \rho, z](t)}{R^i(t)} + \Delta t \frac{p^i_{1,l}(t) - p^i_{1,r}(t)}{R^i(t)}, \tag{3.28}$$

where $R^i(t)$ approximates the spatial integral of $\rho^i$ over $x \in [0, L^i]$. The functional $f^i$ depends on known values of the quantities $v^i, \rho^i$ and $z^i$ at the time step $t$ (see (3.26)).

Plugging (3.28) into the asymptotic formulation of conservation of internal en-

ergy (2.43) at time step $t + \Delta t$ and using $u^i = v^i + Q^i$ we deduce

$$\left( v^i(t) + \Delta t \frac{f^i(t)}{R^i(t)} + \Delta t \frac{p^i_{1,l}(t) - p^i_{1,r}(t)}{R^i(t)} + Q^i_r(t + \Delta t) \right) A^i$$
$$= \left( v^{i+1}(t) + \Delta t \frac{f^{i+1}(t)}{R^{i+1}(t)} + \Delta t \frac{p^{i+1}_{1,l}(t) - p^{i+1}_{1,r}(t)}{R^{i+1}(t)} + Q^{i+1}_l(t + \Delta t) \right) A^{i+1}.$$

Note, that in order to evaluate $Q^i = Q^i[\rho^i, z^i]$ at time step $t + \Delta t$, one needs to have the numerical solution of $\rho^i$ and $z^i$ at time step $t + \Delta t$. This is possible, since the computation of $\rho^i$ and $z^i$ at time step $t + \Delta t$ does not require the vertex pressure values at time step $t$.

Before we use the coupling condition for the pressure, let us rearrange this equation so that we can read it as a linear equation for the pressure values

$$\begin{aligned} & \left( v^{i+1}(t) + \Delta t \frac{f^{i+1}(t)}{R^{i+1}(t)} + Q^{i+1}_l(t + \Delta t) \right) \frac{A^{i+1}}{\Delta t} \\ - & \left( v^i(t) + \Delta t \frac{f^i(t)}{R^i(t)} + Q^i_r(t + \Delta t) \right) \frac{A^i}{\Delta t} \\ = & \frac{A^i}{R^i(t)} \left( p^i_{1,l}(t) - p^i_{1,r}(t) \right) - \frac{A^{i+1}}{R^{i+1}(t)} \left( p^{i+1}_{1,l}(t) - p^{i+1}_{1,r}(t) \right). \end{aligned}$$

By $p^i_{1,V}$ we denote the first order pressure in the $i$-th vertex and it should coincide with the right first order pressure value in the $i$-th pipe. Together with the coupling condition for the pressure $p^i_{1,V} = p^i_{1;r} = p^{i+1}_{1,l} + f^i_{ext}$ (compare (2.34)) we finally obtain

$$\begin{aligned} & \left( v^{i+1}(t) + \Delta t \frac{f^{i+1}(t)}{R^{i+1}(t)} + Q^{i+1}_l(t + \Delta t) - \Delta t \frac{f^i_{ext}}{R^{i+1}(t)} \right) \frac{A^{i+1}}{\Delta t} \\ - & \left( v^i(t) + \Delta t \frac{f^i(t)}{R^i(t)} + Q^i_r(t + \Delta t) - \Delta t \frac{f^{i-1}_{ext}}{R^i(t)} \right) \frac{A^i}{\Delta t} \\ = & \frac{A^i}{R^i(t)} p^{i-1}_{1,V}(t) + \left( -\frac{A^i}{R^i(t)} - \frac{A^{i+1}}{R^{i+1}(t)} \right) p^i_{1,V}(t) + \frac{A^{i+1}}{R^{i+1}(t)} p^{i+1}_{1,V}(t) \end{aligned} \tag{3.29}$$

with $p^0_{1,V} = (p_{bc,l})_1$, $p^{n_V+1}_{1,V} = (p_{bc,r})_1$ and $f^0_{ext} = 0$. In order to extract solutions $p^i_{1,V}$ for all vertices $i = 1, \ldots, n_V$ we have to solve the corresponding linear system

$$\mathbf{P_M}(t) \mathbf{p_{1,V}}(t) = \mathbf{g}(t) \tag{3.30}$$

with the tridiagonal, symmetric $n_V \times n_V$ matrix $\mathbf{P_M}(t)$ and the right hand side

vector $\mathbf{g} \in \mathbb{R}^{n_V}$

$$\mathbf{P_M}(t) = \begin{pmatrix} b^1(t) & a^2(t) & & \\ a^2(t) & \ddots & \ddots & \\ & \ddots & \ddots & a^{n_V}(t) \\ & & a^{n_V}(t) & b^{n_V}(t) \end{pmatrix}, \qquad \mathbf{g}(t) = \begin{pmatrix} g^1(t) \\ \vdots \\ \vdots \\ g^{n_V}(t) \end{pmatrix}$$

with

$$a^i(t) := \frac{(A^i)^2}{R^i(t)}, \qquad b^i(t) := -a^i(t) - a^{i+1}(t).$$

The components of the vector $\mathbf{g}$ consist of the left hand sides of (3.29). The matrix $\mathbf{P_M}(t)$ is regular for the same reasons as the matrix in (3.15) (irreducible and weakly diagonally dominant[8]). As long as we have non-vacuum solutions this is true for all times $t \in (0, \infty)$.

**Remark 5.** *A similar scheme for a general network for a related problem (fire in tunnels) is derived in [GK08]. There, it is also shown, that the corresponding linear system is uniquely solvable, if there is at least one pipe/tunnel connected to the outside, i.e., there must be at least one boundary condition.*

*In [GR13] the same scheme with minor loss terms is derived. However, one would have to model the pressure losses differently in the case of a general network. This could not be done by* (2.31).

### Determination of the first order pressure boundary data

We prescribe initial boundary conditions in physically measurable quantities. In the case of the space-independent velocity component $v$ we gave details about the extraction of an initial condition in (2.50). Now, we have to do this also in the case of the boundary condition for the mechanical pressure $p_1$. In the Subsection 3.4.2, in which we present numerical examples, we will prescribe boundary conditions for the pressure $p$. We extract the information for the first order term by

$$p_{1,bc,\cdot} = \frac{p_{bc,\cdot} - p_0}{\varepsilon}.$$

By this the error between the analytically correct first order term $(p_{bc,\cdot})_1$ and our approximation $p_{1,bc,\cdot}$ tends to zero as $\varepsilon \to 0$:

$$|p_{1,bc,\cdot} - (p_{bc,\cdot})_1| = \left| \frac{p_{bc,\cdot} - p_0}{\varepsilon} - \frac{p_{bc,\cdot} - p_0}{\varepsilon} + \mathcal{O}(\varepsilon) \right| = \mathcal{O}(\varepsilon).$$

[8]For details see Appendix C.2.

**Algorithm 2** (Numerical simulation of AM)**.** *Suppose the numerical solution is known at the step $t^n$. In order to compute the numerical solution at the next time step $t^{n+1}$ the following steps are required:*

1. *compute the time step size $\Delta t^{n+\frac{1}{2}}$ by the CFL condition* (3.24) *and set $t^{n+1} = t^n + \Delta t^{n+\frac{1}{2}}$;*

2. *use the explicit upwind scheme* (3.23) *to compute the numerical solution of the density $\rho^i$ and the ratio of unburnt gas $z^i$ at the time step $t^{n+1}$ for all pipes $(i = 1, \ldots, n_P)$;*

3. *compute all first order pressure values at the vertices by solving the linear system;* (3.30)*;*[9]

4. *use the explicit Euler scheme* (3.25) *to compute the numerical solution of the velocity component $v^i$ for all pipes $(i = 1, \ldots, n_P)$.*

### 3.3.3. Numerical verification of the algorithm for AM

While the presented numerical scheme for model FE is well understood, there are no schemes that were developed particularly for our asymptotic model. Therefore, we want to verify the proposed numerical Algorithm 2. We do not have existence and/or uniqueness theory for the transient asymptotic model. However, in Subsection 3.2.2 we were able to explicitly compute the unique solution to a simplified stationary problem on a network with pipe-to-pipe connection. Hence, we want to validate our numerical transient algorithm for the asymptotic model, by numerically computing a stationary solution and comparing it to the analytical stationary solution given by (3.13) and (3.15).

First, let us explain what we mean by numerically computing a stationary solution.

**Definition 1.** *Consider a transient problem $\mathcal{P}$. Let $y^n \in \mathbb{R}^{J+1}$ be the numerical solution of $\mathcal{P}$ at time step $t^n$ computed by an algorithm for $\mathcal{P}$. Choose a value for $TOL_{stationary} > 0$. We call a solution $y^n$ <u>numerically stationary</u> with respect to the constant $TOL_{stationary}$, if*

$$\max_{j=0,\ldots,J} \left\{ \left| \frac{y_j^n - y_j^{n-1}}{\Delta t^{n+\frac{1}{2}}} \right| \right\} < TOL_{stationary}.$$

[9] Matlab's backslash operator is used for our numerical realization. See `http://www.mathworks.de/de/help/matlab/ref/mldivide.html`

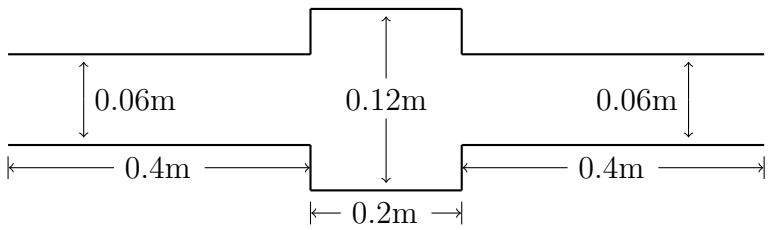


Figure 3.1.: Simple network

Let $y$ be the analytic solution of the simplified stationary problem on a network (3.9), and $y^n \in \mathbb{R}^{J+1}$ the numerically stationary solution of the same simplified, but transient problem[10]. Then, we use the $\infty$-norm to measure the maximal error $E_J$, i.e.,

$$E_J^y := ||y^n - \bar{y}||_\infty = \max_{j=0,\dots,J} \left\{ \left| y_j^n - y(j \cdot \Delta x) \right| \right\},$$

where $\bar{y} \in \mathbb{R}^{J+1}$ is the analytical solution evaluated at every grid point $x_j$ for all $j = 0, \dots, J$. We compute the experimental order of convergence (EOC) by

$$\mathrm{EOC}_J = \log_2 \left( \frac{E_{J/2}}{E_J} \right).$$

### The transient model for the numerical verification

We consider a network (see Figure 3.1) consisting of $n_P = 3$ pipes having the following lengths and radii,

$$\begin{aligned} \tilde{L}^1 &= 0.4\text{m}, & \tilde{L}^2 &= 0.2\text{m}, & \tilde{L}^3 &= 0.4\text{m}, \\ \tilde{r}^1 &= 0.03\text{m}, & \tilde{r}^2 &= 0.06\text{m}, & \tilde{r}^3 &= 0.03\text{m} \end{aligned}$$

with a total length of $\tilde{L} = 1\text{m}$. The governing equations are

$$\begin{aligned} \rho_t^i + v^i \rho_x^i &= 0, \\ v_t^i &= \frac{p_{1,l}^i - p_{1,r}^i}{\int_0^{L^i} \rho^i dx} - C_f^i \frac{v^i |v^i|}{2} \int_0^{L^i} \rho^i dx \end{aligned}$$

on $(0, L^i) \times (0, \infty)$ for all $i \in \{1, 2, 3\}$. Also, we have coupling conditions

$$\rho_r^i = \rho_l^{i+1}, \qquad A^i u_r^i = A^{i+1} u_r^{i+1}, \qquad p_{1,r}^i = p_{1,l}^{i+1}$$

[10] We will state the exact model in the following paragraph.

for all $i \in \{1,2,3\}$, unscaled initial conditions

$$\tilde{\rho}^i(\tilde{x},0) = 1.2\text{kg/m}^3, \qquad \tilde{u}^i(\tilde{x},0) = 0\text{m/s}$$

for all $i \in \{1,2,3\}$ and $\tilde{x} \in (0,\tilde{L}^i)$ and unscaled boundary conditions

$$\begin{aligned} \tilde{\rho}^1(0,\tilde{t}) &= 0.4\text{kg/m}^3 \text{ if } \tilde{u}^1(0,\tilde{t}) > 0\text{m/s}, & \tilde{p}^1(0,\tilde{t}) &= 1.001\text{bar}, \\ \tilde{\rho}^3(\tilde{L}^3,\tilde{t}) &= 1.2\text{kg/m}^3 \text{ if } \tilde{u}^3(\tilde{L}^3,\tilde{t}) < 0\text{m/s}, & \tilde{p}^3(\tilde{L}^3,\tilde{t}) &= 1\text{bar} \end{aligned}$$

for all $\tilde{t} \in [0,\infty)$.

### The analytical stationary solution

In order to compute the analytical stationary solution, we just have to solve the linear system (3.15). We can invert the matrix and obtain

$$\begin{pmatrix} f^1 & e^2 \\ e^2 & f^2 \end{pmatrix}^{-1} = \frac{1}{f^1 f^2 - (e^2)^2} \begin{pmatrix} f^2 & -e^2 \\ -e^2 & f^1 \end{pmatrix}.$$

Hence, the vertex pressures in first order are

$$p^1_{1,V} = \frac{-e^1 f^2 (p_{bc,l})_1 + e^2 e^3 (p_{bc,r})_1}{f^1 f^2 - (e^2)^2}, \qquad p^2_{1,V} = \frac{e^1 e^2 (p_{bc,l})_1 - e^3 f^1 (p_{bc,r})_1}{f^1 f^2 - (e^2)^2}.$$

Plugging this into (3.13) gives us the explicit formulation of the analytic stationary solution.

### Comparison of the stationary results

Figure 3.2 shows the graphs of the unscaled analytical stationary (red) and numerically stationary (blue) solutions. The geometry of the pipe is displayed in the first two graphs by the grey lines. The labelling of the horizontal axis of the bar graph denotes the vertices, where 0 and 3 stand for the outer vertices, i.e., the positions of the boundary conditions for the pressure.

We see, that there is no visible difference between the analytic stationary solution and the numerically stationary solution at a resolution of $J = 512$ spatial grid points. The absolute error measured was $E_{512} = 9.6233e-03$. Now, having three physical variables, i.e., density $\rho$, velocity $u$ and first order pressure $p_1$, the absolute error is defined by

$$E_J := \max\left\{E^\rho_J, E^u_J, \bar{E}^{p_1}_J\right\},$$

where $\bar{E}^{p_1}_J$ is the maximal error measured at the two junctions $i \in \{1,2\}$, and not at every spatial supporting point.

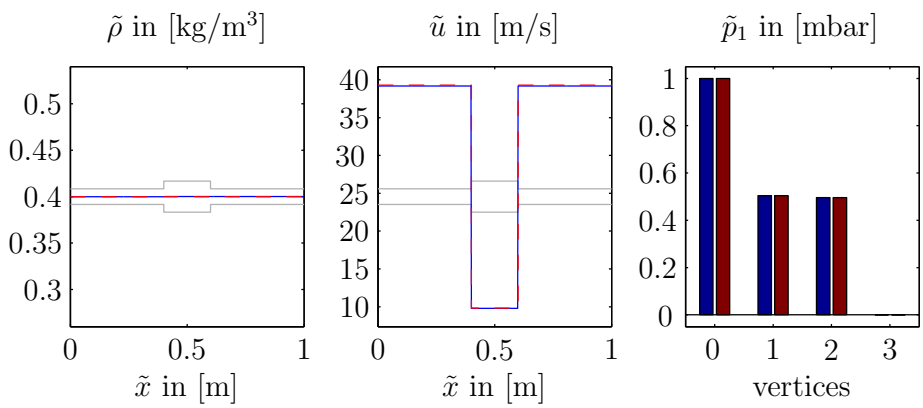


Figure 3.2.: Comparison of analytic stationary (red, dashed) and numerically stationary (blue) solution for $J = 512$ (number of spatial supporting points)

| $J$ | $E_J$ | $\mathrm{EOC}_J$ | $J$ | $E_J$ | $\mathrm{EOC}_J$ |
|---|---|---|---|---|---|
| 8 | 5.2808e-01 | - | 1024 | 4.8201e-03 | 0.9975 |
| 16 | 2.9349e-01 | 0.8474 | 2048 | 2.4152e-03 | 0.9969 |
| 32 | 1.4415e-01 | 1.0257 | 4096 | 1.2082e-03 | 0.9993 |
| 64 | 7.4005e-02 | 0.9619 | 8192 | 6.0404e-04 | 1.0001 |
| 128 | 3.8244e-02 | 0.9524 | 16384 | 3.0205e-04 | 0.9998 |
| 256 | 1.9268e-02 | 0.9890 | 32768 | 1.5105e-04 | 0.9998 |
| 512 | 9.6233e-03 | 1.0016 | 65536 | 7.5527e-05 | 0.9999 |

Table 3.1.: Absolute error $E_J$ and the experimental order of convergence $\mathrm{EOC}_J$ for different numbers of spatial supporting points $J$.

Table 3.1 shows the absolute error for different discretizations, such as the experimental order of convergence. We conclude, that the proposed Algorithm 2 for the transient asymptotic model converges to the analytic stationary solution with order $\mathrm{EOC} = 1$.

## 3.4. Numerical comparison between the hyperbolic and asymptotic model

Both numerical algorithms basically consist of upwind schemes. However, the mathematics and physics behind the computation of the vertex pressure are completely different. In order to determine the pressure at the nodes we have to solve

$n_V = n_P - 1$ linearized Riemann problems in the case of the full Euler model. In the asymptotic model we solve an $n_V \times n_V$ linear system (see (3.30)). So, in terms of numerics we are dealing with $n_V$ local problems in the fully hyperbolic case, whereas in the asymptotic case we have one global problem, with instantaneous influences from all over the network. This is due to the fact that we have a finite speed of propagation in the full Euler model and infinite speed of propagation in the asymptotic model. The infinite speed of propagation in the asymptotic model is a consequence of the small Mach number limit. Determining the vertex pressures in the asymptotic case by solving the linear problem or by solving a fixed point problem in $n_V$ dimensions does not affect the global property. Note, that in the hyperbolic case it is not necessary to compute all the vertex pressures in advance. In order to compute the numerical solution, it would be sufficient to know the vertex pressure at the neighbouring junctions.

### 3.4.1. Numerical costs

Comparing the two CFL conditions for the upwind schemes for the full Euler equations (3.19) and for the asymptotic model (3.24), one can already guess at first sight, that the time step sizes in the full Euler case will be much smaller.

$$\begin{aligned} \text{FE:} \qquad & \lambda_{\max}\frac{\Delta t}{\Delta x} \leq c_N \quad \text{with} \quad \lambda_{\max} := \max|\lambda|, \\ \text{AM:} \qquad & u_{\max}\frac{\Delta t}{\Delta x} \leq c_N \quad \text{with} \quad u_{\max} := \max|u|. \end{aligned}$$

The parameter $c_N$ denotes the Courant number. Assuming we have positive velocities, the maximum eigenvalue for the full Euler equations is $\lambda_{\max} = u_{\max} + c$, where $c$ denotes the speed of sound. Using the same spatial grid and the same Courant number, this would lead to the following relation between the time step size for the asymptotic model ($\Delta t_{AM}$) and the time step size for the full Euler equations ($\Delta t_{FE}$).

$$\boxed{\Delta t_{AM} = \frac{\lambda_{max}}{u_{max}}\Delta t_{FE} = \left(1 + \frac{1}{M}\right)\Delta t_{FE},}$$

where $M = u_{\max}/c$ denotes the Mach number. One can see that the smaller the Mach number is, the more time efficient the algorithm for the asymptotic model is, due to larger step sizes in time.

For further estimates of the numerical costs we can count the *floating point operations* (flops). In order to keep it simple we want to look at just one spatial step of the homogeneous system. For details see Appendix C.5. Keeping in mind, that this is a very rough estimate, we can nevertheless say, that the numerical

costs of a spatial step of Algorithm 1 (for the full Euler model) are higher than the costs of Algorithm 2 (for the asymptotic model). A lower bound for the ratio of numerical work that has to be invested to perform simulations can be given by

$$\frac{\text{work}_{FE}}{\text{work}_{AM}} \geq \frac{\text{flops}_{FE}}{\text{flops}_{AM}} \cdot \frac{\Delta t_{AM}}{\Delta t_{FE}} = \frac{615}{18} \cdot \left(1 + \frac{1}{M}\right).$$

### 3.4.2. Numerical examples

All numerical simulations were performed with a 64-bit version of MATLAB 8.1.0.604 (R2013a) on a personal computer (Intel(R) Core(TM) i7 CPU M620 @ 2.67GHz).

Before we start with the numerical simulation of the whole exhaust pipe, with its complex geometry, we first want to observe the qualitative behaviour of the two different models on one single pipe.

#### A single pipe

In this simplified setting, in which we consider only a single pipe, the cross section area is assumed to be constant and there is no catalytic converter ($\chi = 0$). The pipe we are considering has the length $\tilde{L} = 1$m and the diameter is $\tilde{d} = 0.06$m.

The first example deals with a high pressure difference ($\tilde{p}_l - \tilde{p}_r = 0.01$bar) in the pipe. The detailed input data for this simulation can be found in Table 3.2. The result of the numerical simulation does not change significantly after $\tilde{t}^* = 0.5$s,

| (Numerical) Parameters | | Example 1 | Example 2 |
|---|---|---|---|
| spatial supporting point | $J$ | 100 | |
| simulation time | $\tilde{t}_{\text{end}}$ | 2s | |
| initial density | $\tilde{\rho}_{ic}$ | 1.2 kg/m$^3$ | |
| initial velocity | $\tilde{u}_{ic}$ | 0 m/s | |
| initial pressure | $\tilde{p}_{ic}$ | 1bar | |
| left boundary density | $\tilde{\rho}_{bc,l}$ | 0.4 kg/m$^3$ | |
| right boundary density | $\tilde{\rho}_{bc,r}$ | 1.2 kg/m$^3$ | |
| left boundary pressure | $\tilde{p}_{bc,l}$ | 1.01bar | 1.001bar |
| right boundary pressure | $\tilde{p}_{bc,r}$ | 1bar | |

Table 3.2.: Input data for Example 1 and Example 2. Results are illustrated in Figures 3.3 and 3.4.

therefore we can assume to have reached the stationary state. Figure 3.3 shows the numerical results after this time. The blue curves denote the numerical solution of the asymptotic model (AM), whereas the dashed green curves are those of the full

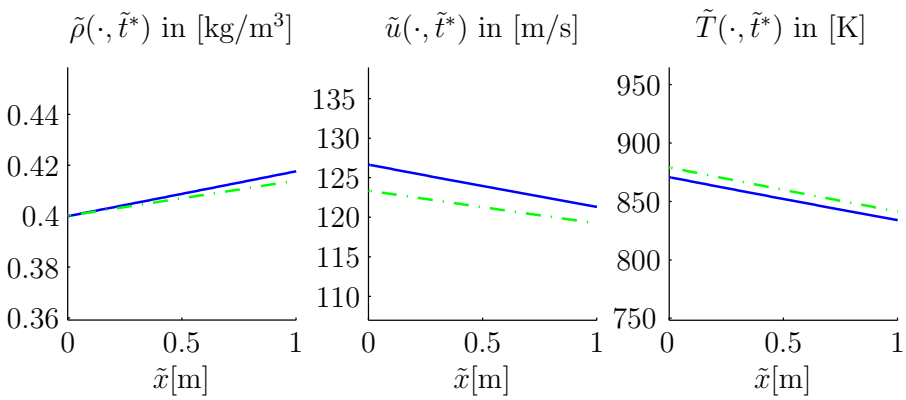


Figure 3.3.: Example 1: Numerical results after $\tilde{t}^* = 0.5$s for the solution of the asymptotic (blue lines) and full Euler model (green, dashed lines).

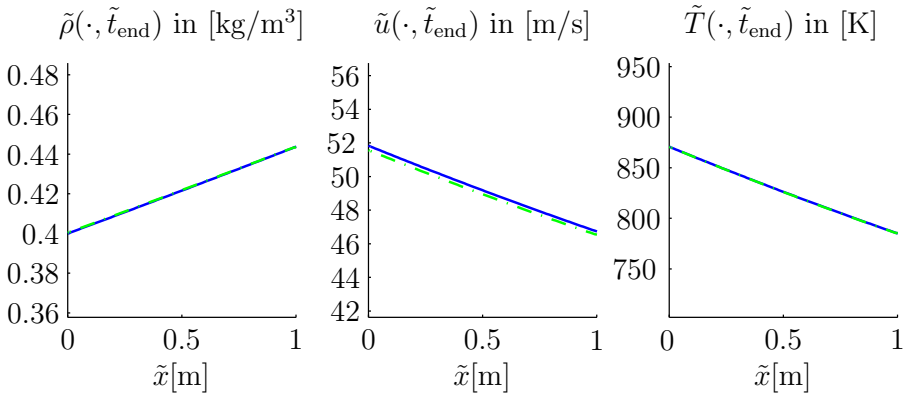


Figure 3.4.: Example 2: Numerical results after $\tilde{t}_{\text{end}} = 2$s for the solution of the asymptotic (blue lines) and full Euler model (green, dashed lines).

Euler model (FE). One can observe that the numerical solutions of both models have the same qualitative behaviour, but are varying in their absolute values.

In the second example we reduce the pressure difference ($\tilde{p}_{bc,l} - \tilde{p}_{bc,r} = 0.001$bar) and see in Figure 3.4 that the difference between the absolute values of the numerical solutions is reduced.

This behaviour is very reasonable, because we lower the Mach number by reducing the pressure difference. Since a low Mach number was the key component of the limit we used for the derivation of the asymptotic model, it is not surprising that the agreement in Example 2 outmatches Example 1.

For further investigations on this behaviour, we consider Figure 3.5. It shows the dependence between the chosen left hand side pressure value $\tilde{p}_{bc,l}$ and the largest, scaled error measured at the state at time $\tilde{t}_{\text{end}} = 2$s. We compute this

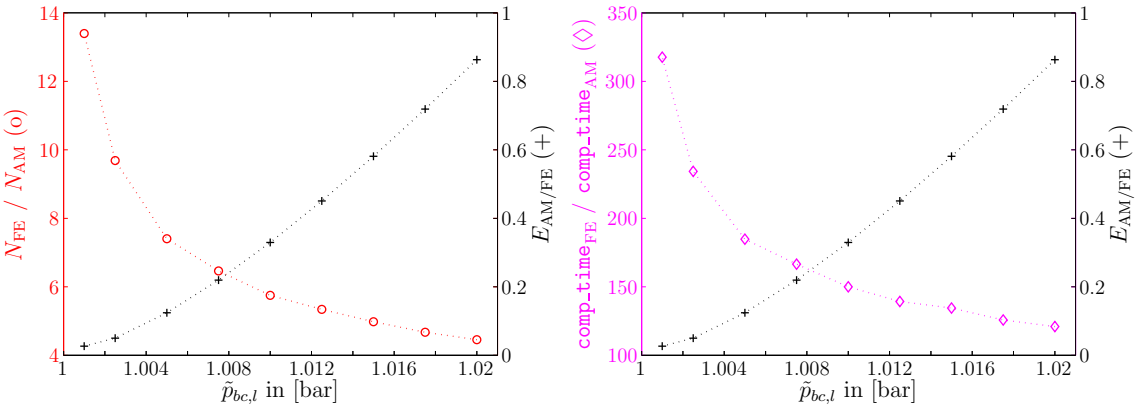


Figure 3.5.: The dependence of the error $E_{\mathrm{AM/FE}}$ (marked with "+") and the efficiency of AM over FE in terms of number of supporting points in time (left plot, marked with "o") and computing time (right plot, marked with "◊") on the boundary condition $\tilde{p}_{bc,l}$.

error $E_{\mathrm{AM/FE}}$ by

$$E_{\mathrm{AM/FE}} = \max_{\tilde{y}\in\{\tilde{\rho},\tilde{u},\tilde{z},\tilde{T}\}} \left\{ \max_{j=0,\ldots,J} \left\{ \left| \frac{\tilde{y}_{\mathrm{AM}}(j\cdot\Delta\tilde{x},\tilde{t}_{\mathrm{end}}) - \tilde{y}_{\mathrm{FE}}(j\cdot\Delta\tilde{x},\tilde{t}_{\mathrm{end}})}{\tilde{y}_{\mathrm{ref}}} \right| \right\} \right\},$$

where $\tilde{y}_{\mathrm{AM}}$ and $\tilde{y}_{\mathrm{FE}}$ are the numerical solution of the state variable $\tilde{y}$ of the asymptotic and full Euler model, respectively. On the one hand we see that the error decays, as the value of the boundary condition for the pressure on the left hand side is reduced (black line, marked with "+"). On the other hand, we can observe an increase of

- the ratio between required supporting points in time of the full Euler ($N_{\mathrm{FE}}$) and the asymptotic ($N_{\mathrm{AM}}$) model (left plot of Figure 3.5, red lines, marked with "o"),
- the ratio between computing times of the full Euler ($\texttt{comp\_time}_{\mathrm{FE}}$) and the asymptotic ($\texttt{comp\_time}_{\mathrm{AM}}$) model (right plot of Figure 3.5, magenta lines, marked with "◊").

A more detailed comparison of the computational effort invested for the numerical results of Example 1 and 2 can be found in Table 3.3. In order to avoid up- and downturns in the computing times, both examples have been simulated 10 times. The displayed computing time in the table is the mean of all simulations. The largest ratio between standard deviation and mean value was less than 1.6%.

| | Example 1 | | Example 2 | |
|---|---|---|---|---|
| | AM | FE | AM | FE |
| time steps $N$ | 24844 | 142853 | 9510 | 127398 |
| last time step size $\Delta\tilde{t}^{N-1/2}$ in [s] | 7.90e-05 | 1.39e-05 | 1.93e-04 | 1.56e-05 |
| $\tilde{u}_{\mathrm{AM}}^{\max}$ vs $\lambda_{\mathrm{FE}}^{\max}$ in [m/s] | 126.66 | 717.79 | 51.84 | 643.15 |
| computing time in [s] | 5.72 | 851.03 | 2.48 | 761.98 |
| $N_{\mathrm{FE}}/N_{\mathrm{AM}}$ | 5.75 | | 13.40 | |
| $\Delta\tilde{t}_{\mathrm{AM}}^{N_{\mathrm{AM}}-1/2}/\Delta\tilde{t}_{\mathrm{FE}}^{N_{\mathrm{FE}}-1/2}$ | 5.67 | | 12.41 | |
| $\lambda_{\mathrm{FE}}^{\max}/\tilde{u}_{\mathrm{AM}}^{\max}$ | 5.67 | | 12.41 | |
| $\mathtt{comp\_time}_{\mathrm{FE}}$ / $\mathtt{comp\_time}_{\mathrm{AM}}$ | 148.88 | | 306.78 | |

Table 3.3.: Output data for Example 1 and Example 2. The computing time, averaged over 10 repetitions, refers to a personal computer (Intel(R) Core(TM) i7 CPU M620 @ 2.67GHz)

We see that the numerical simulations of the asymptotic model are approximately 150 and 300 times faster in the Examples 1 and 2.

Thus, when using the asymptotic model instead of the full Euler model, we have to deal with a difference in the absolute value and a different behaviour in the transient part of the model (infinite vs finite speed of propagation[11]), but significantly reduce computing cost.

### The whole exhaust pipe

Now, having understood the dynamics on one single pipe, we want to consider the whole exhaust pipe, i.e., a simple network of pipes. The geometrical data used for the simulation of the exhaust pipe is the same data which was used in [LN04] and [Pet07] (see Table 2.1 and Figure 2.4). Since we are interested in the time after the engine start, our initial conditions[12] will be (as they also were in the case of the single pipe):

$$\tilde{\rho}_{ic}^{i}(\tilde{x}) = 1.2 \text{ kg/m}^3, \qquad \tilde{u}_{ic}^{i}(\tilde{x}) = 0 \text{ m/s},$$
$$\tilde{p}_{ic}^{i}(\tilde{x}) = 10^5 \text{ kg/(ms}^2), \qquad \tilde{z}_{ic}^{i}(\tilde{x}) = 0$$

for every $i = 1, \ldots, n_P$. We will present again two examples to observe the influence of the pressure difference (and therefore Mach number) on the qualitative and

[11] See Appendix C.6 for more information.

[12] The stated initial conditions for the single and whole pipe fulfil the compatibility condition (2.51) and are therefore applicable for the asymptotic model.

quantitative differences of the two models. Therefore our boundary conditions are:

$$
\begin{aligned}
\tilde{p}_{bc,l}(\tilde{t}) &= \begin{cases} 1.01 \text{ bar}, & \text{Example 3}, \\ 1.001 \text{ bar}, & \text{Example 4}, \end{cases} \\
\tilde{p}_{bc,r}(\tilde{t}) &= 1 \text{ bar}, \\
\left.\begin{aligned} \tilde{\rho}_{bc,l}(\tilde{t}) &= 0.4 \text{ kg/m}^3, \\ \tilde{z}_{bc,l}(\tilde{t}) &= 0.1, \end{aligned}\right\} & \text{ if } \tilde{u}_l^1(\tilde{t}) > 0, \\
\left.\begin{aligned} \tilde{\rho}_{bc,r}(\tilde{t}) &= 1.2 \text{ kg/m}^3, \\ \tilde{z}_{bc,r}(\tilde{t}) &= 0, \end{aligned}\right\} & \text{ if } \tilde{u}_r^{n_P}(\tilde{t}) < 0.
\end{aligned}
$$

Simulations of both models in this section include minor loss terms for angles $\theta = \pi$, i.e., sudden expansions and contractions. The data (parameter values, initial and boundary conditions) were taken from [LN04] and [Pet07] in order to match the simulation with the realistic scenario of a cold start. The numerical solutions, with $J = 360$ spatial supporting points, do not change significantly after $\tilde{t}_{\text{end}} = 3$s and can be considered to be stationary.

Numerical results of Examples 3 and 4 are illustrated in Figures 3.6 and 3.7. All plots show the geometry of the considered exhaust pipe in order to link it to local phenomena, which can be observed in the physical quantities. Furthermore, we show the spatial evaluation of all physical quantities at time $\tilde{t}_{\text{end}}$ in their unscaled version in order to recognize the prescribed boundary conditions more easily.

| | Example 3 | | Example 4 | |
|---|---|---|---|---|
| | AM | FE | AM | FE |
| time steps $N$ | 28764 | 659915 | 4819 | 590619 |
| last time step size $\Delta\tilde{t}^{N-1/2}$ in [s] | 9.83e-05 | 4.52e-06 | 5.41e-04 | 5.04e-06 |
| $\tilde{u}_{\text{AM}}^{\max}$ vs $\lambda_{\text{FE}}^{\max}$ in [m/s] | 30.51 | 663.65 | 5.54 | 594.93 |
| computing time in [s] | 35.62 | 14431.57 | 7.22 | 12898.46 |
| $N_{\text{FE}}/N_{\text{AM}}$ | 22.94 | | 122.56 | |
| $\Delta\tilde{t}_{\text{AM}}^{N_{\text{AM}}-1/2}/\Delta\tilde{t}_{\text{FE}}^{N_{\text{FE}}-1/2}$ | 21.75 | | 107.32 | |
| $\lambda_{\text{FE}}^{\max}/\tilde{u}_{\text{AM}}^{\max}$ | 21.75 | | 107.32 | |
| $\texttt{comp\_time}_{\text{FE}}$ / $\texttt{comp\_time}_{\text{AM}}$ | 405.14 | | 1787.27 | |

Table 3.4.: Output data for Example 3 and Example 4. The computing time, average over 10 repetitions, refers to a personal computer (Intel(R) Core(TM) i7 CPU M620 @ 2.67GHz)

The left bottom plots show the ratio of unburnt gas ($\tilde{z}$). We can see that the

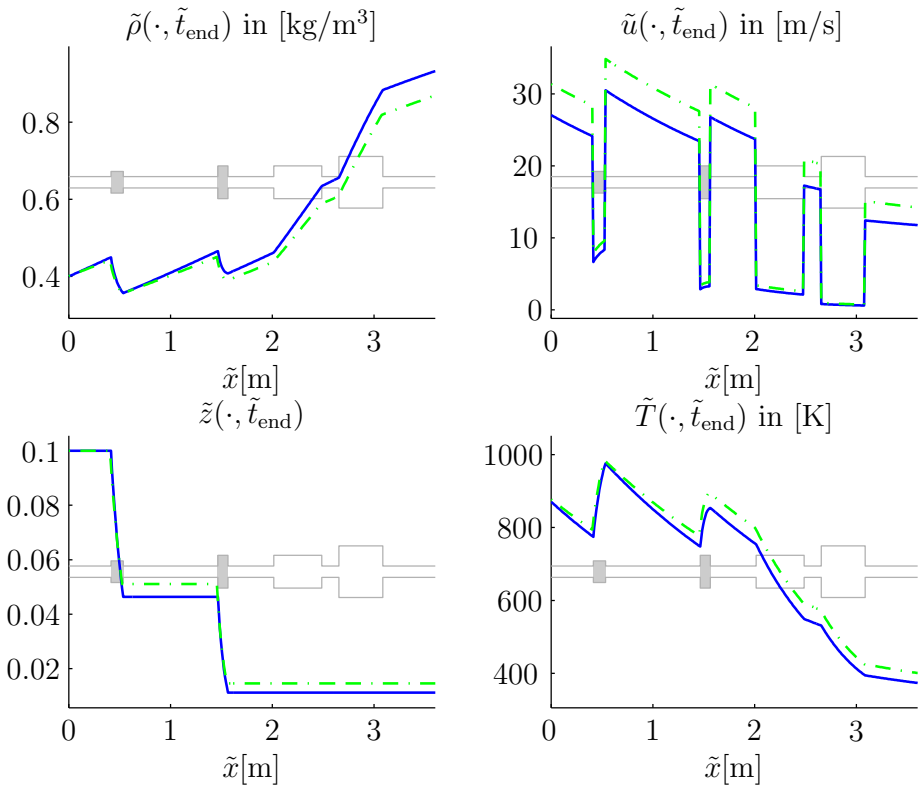


Figure 3.6.: Example 3: Numerical results after $\tilde{t}_{\text{end}} = 3$s for the solution of the asymptotic (blue lines) and full Euler model (green, dashed lines).

unburnt fuel is conserved during the transport outside the catalytic converters, whereas it reacts exothermically inside those.

In the right bottom plots we observe an increase of temperature ($\tilde{T}$) in the catalytic converter. In Example 4 this increase is barely noticeable in the second converter, since the unburnt gas is almost completely consumed in the first catalyst. This high consumption can be explained by the lower pressure difference, and therefore lower velocity. The fluid spends more time in the catalytic converter and can react for a longer period. In pipes without catalytic converters the temperature decreases because of the heat exchange with the colder wall.

Due to the ideal gas law, and a pressure that changes only on a small scale in the full Euler model, the profile of the density ($\tilde{\rho}$), which is shown in the top left plots, can be explained in a similar, but reciprocal way as it was done for the temperature.

The velocity $\tilde{u}$, which is illustrated in the top right plot for both examples, decreases in each pipe as the density increases and vice versa. This corresponds with

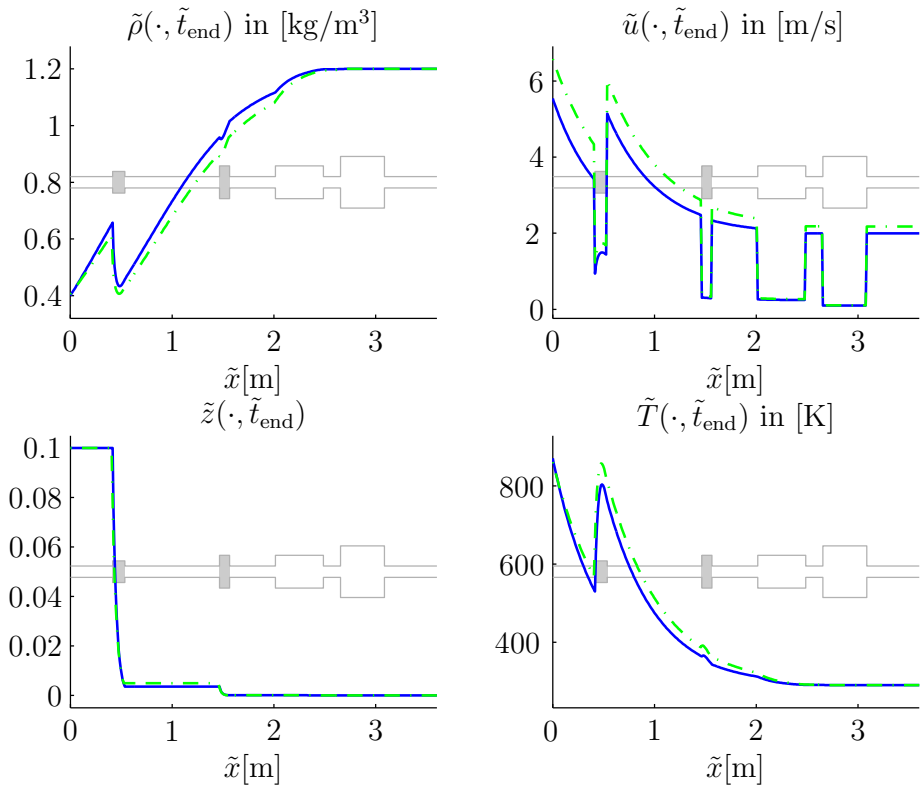


Figure 3.7.: Example 4: Numerical results after $\tilde{t}_{\text{end}} = 3$s for the solution of the asymptotic (blue lines) and full Euler model (green, dashed lines).

the equations, since the product of density and velocity is constant at a steady state. Due to the conservation of mass at the junctions, the velocity has to drop in the pipes with larger diameter.

Although both models describe the same qualitative behaviour we just discussed, there are differences in the absolute values of both solutions. We confirm the observation made in the single pipe settings, and see that those "errors" decrease, in a lower Mach number setting, which we establish by decreasing the difference on the boundary conditions for the pressure. Moreover, we are again able to simulate the asymptotic model much faster. In Example 4 the ratio of computing times of the asymptotic and the full Euler model reaches a value of approximately 2300. A detailed comparison of the numerical output data is listed in Table 3.4. These observations are confirmed by the consideration of Figure 3.8, where we compare the scaled absolute errors as well as the computing efficiencies for different pressure differences.

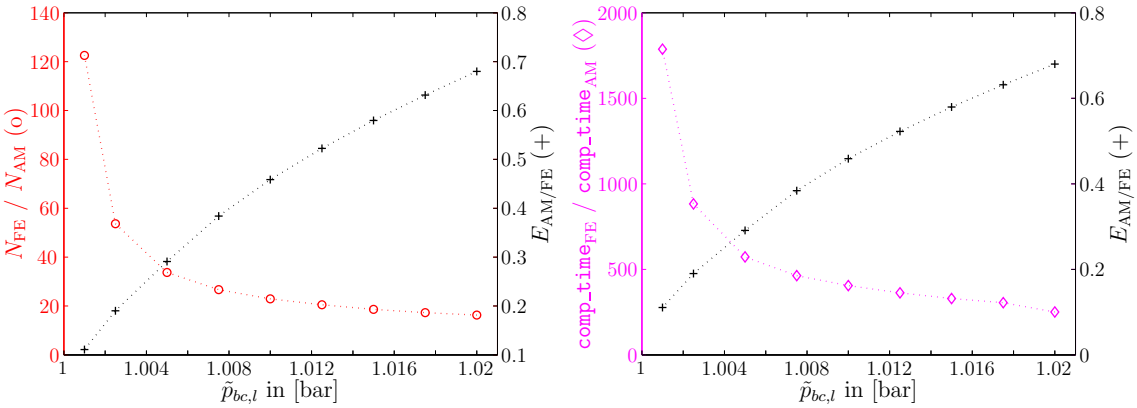


Figure 3.8.: The dependence of the error $E_{\mathrm{AM/FE}}$ (marked with "+") and the efficiency of AM over FE in terms of number of supporting points in time (left plot, marked with "o") and computing time (right plot, marked with "◊") on the boundary condition $\tilde{p}_{bc,l}$.

### Minor loss terms

In this example we want to show the impact of the minor losses at the junctions. Figure 3.9 shows the results for two different simulations. One simulation (blue lines) includes the minor loss term into the coupling condition for the pressure, whereas the other one (red, dashed lines) neglects those (see Subsection 2.4.3 for details). Both simulations were made with the asymptotic model (the full Euler model would give us very similar results) with the same setting as in Example 3. We can observe, that even though the pressure loss terms due to sudden or gradual expansions and contractions are called "minor losses" in the literature, their impact is not "minor" at all in our setting.

## 3.5. Summary

We started this chapter with a short discussion of the problems of providing an existence theory of both transient models, without giving answers to either of them. We studied a simplified stationary problem of the asymptotic model in Section 3.2. We found unique existence of a solution on a network for the case with no heat exchange, whereas we could prove that for the case with heat exchange there exist at least two solutions, one with negative and one with positive flow direction.

In Section 3.3 we presented an easy numerical treatment for the asymptotic and full Euler model. Both algorithms were based on explicit upwind schemes for the purpose of a fair comparison. We verified the proposed algorithm for the

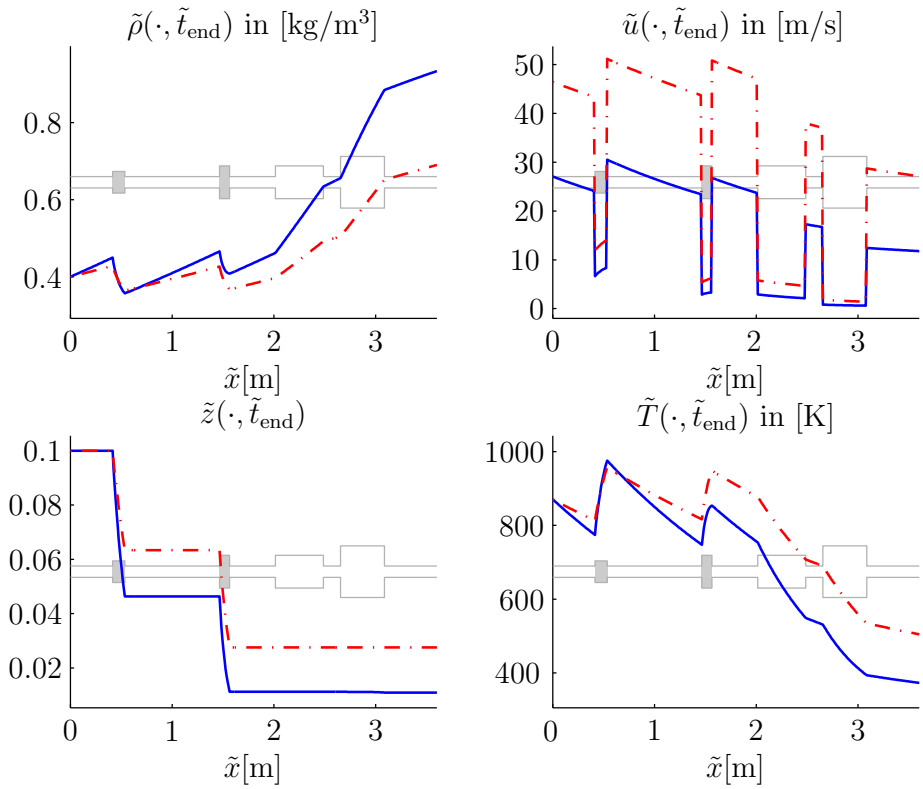


Figure 3.9.: Example 5: Numerical results after $\tilde{t}_{\text{end}} = 3$s for the solution of the asymptotic model with (blue) and without (red, dashed) the inclusion of the minor loss term $\tilde{f}_{ext}$ in the coupling condition for the pressure (see Subsection 2.4.3 for details).

asymptotic model, by showing numerical convergence of the transient numerical solution towards the analytic stationary solution.

We could verify in Subsection 3.4.2 that the new asymptotic model still keeps the main physical features of the application and can compete with the full Euler model, which is well established in the literature. The asymptotic model was computationally much (orders of magnitude) faster than the standard (fully compressible) model, which we could also verify analytically by comparing the CFL condition and flops of both numerical algorithms (see Subsection 3.4.1).

Furthermore, we showed that the impact of the minor loss terms on the numerical solution is significant in the application's setting. Therefore, it should not be neglected, as it is done in various literature.

Lastly, we want to comment on the difference in absolute values of the asymptotic and full Euler model, which we could observe in the examples. Although

the difference is not negligible (at least in Example 1 (Figure 3.3) and Example 3 (Figure 3.6)), we should keep in mind, that neither of the considered models was tested with experimental data. Both models agree in the physical quality of the steady state solutions. Since one-dimensional hyperbolic "FE-like" models were successfully fitted to experimental data in the literature (see e.g., [DFO00, LN04, LTW09, MSZH11]), we assume that this is also possible for the asymptotic model. Then, one would have a model which describes the physics in a qualitatively and quantitatively correct way, and is computationally much faster.

# 4. Optimal control

In this chapter we want to consider the optimization task mentioned in the introduction, namely how to optimally control the inflow of ratio of unburnt gas in order to heat up the catalytic converter after a cold start. Therefore, we first extend our asymptotic model AM by an equation for the temperature of the catalytic converter (Section 4.1). In Section 4.2 we then formulate the optimization task. Clearly, it strongly depends on the structure of the cost functional. Subsequently, we formally derive a set of first order optimality conditions (Sections 4.3 - 4.5) by differentiating the Lagrangian functional with respect to the control, state and adjoint variables. Then, we are able to compute a descent direction by a projected gradient algorithm. Lastly, we discuss discretization issues in Section 4.6 and show some numerical examples in Section 4.7.

The whole content of this chapter has been published in [GRW14b][1]. The Sections 4.3, 4.4 and D.3 as well as the Subsections 4.6.2. 4.6.3 and 4.6.4 are mostly taken word by word from the article [GRW14b].

## 4.1. Modelling the temperature of the catalytic converter

Since the temperature of the catalytic converter is not considered in the equations of the asymptotic model (2.57), we will have to augment it. We model the temperature evolution of the catalytic converter $t \mapsto T_c^i(t)$ as a result of the heat exchange between catalyst (temperature $T_c^i$) and gas (averaged temperature $T_{\text{Gas}}^i$) in the $i$-th pipe.

$$T_{\text{Gas}}^i(t) := \frac{1}{L^i} \int_0^{L^i} T^i(x,t)dx. \tag{4.1}$$

[1]Using the published content in this thesis is in agreement with the copy rights of the publisher: `http://www.elsevier.com/journal-authors/author-rights-and-responsibilities`.

We choose the following ordinary differential equation with the (scaled[2]) heat exchange coefficient $h_c$ to model this relation:

$$(T_c^i(t))_t = -h_c(T_c^i(t) - T_{\text{Gas}}^i(t)) \tag{4.2}$$

for all times $t \in (0, t_{\text{end}})$ and for all pipes $i \in I_{cc}$, where $I_{cc}$ is the index set that contains all pipes with a catalytic converter, i.e.,

$$I_{cc} := \left\{ i \in \{1, \dots, n_P\} \mid \chi^i = 1 \right\}. \tag{4.3}$$

Since this heat exchange works both ways, we have to adjust the energy gain and loss term $q$, which is defined in Equation (2.46). Now taking also the heat difference of the gas temperature and the temperature of the catalytic converter into account, the energy balance $q^i$ for the $i$-th pipe becomes

$$q^i[\rho^i, z^i, T_c^i] := \frac{1}{\gamma p_0} \left[ -h^i(T^i - T_{\text{Wall}}^i) + \chi^i \left( -h_c(T^i(t) - T_c^i(t)) + q_0 \rho^i z^i K(T^i) \right) \right].$$

This also has an impact on $Q^i$, since it is the potential of $q^i$. For a shorter notation we introduce

$$\begin{aligned} (R^i(x))(t) &:= \int_x^{L^i} \rho^i(y,t)dy, \\ \Phi^i[\rho^i, z^i, v^i] &:= p_{1,l}^i - p_{1,r}^i - \int_0^{L^i} \rho^i Q_t^i dx - \int_0^{L^i} \rho^i (v^i + Q^i) q^i dx \\ &\quad - C_f \int_0^{L^i} \rho^i \frac{(v^i + Q^i)|v^i + Q^i|}{2} dx - \chi^i C_c \int_0^{L^i} \rho^i (v^i + Q^i)\, dx. \end{aligned} \tag{4.4}$$

Thus, the asymptotic model with the additional ODE for $T_c^i$ consists of the following **system**

$$\begin{aligned} \rho_t^i + (v^i + Q^i)\rho_x^i &= -q^i \rho^i, \\ z_t^i + (v^i + Q^i) z_x^i &= -\chi^i z^i K(T^i), \\ v_t^i &= \Phi^i / R^i(0), \\ (T_c^j)_t &= -h_c(T_c^j - T_{\text{Gas}}^j) \end{aligned} \tag{4.5}$$

for all pipes $i = 1, \dots, n_P$, $j \in I_{cc}$ and $(x,t) \in (0, L^i) \times (0, t_{\text{end}})$, with **closing relation**

$$\rho^i(x,t) T^i(x,t) = p_0 \tag{4.6}$$

[2]Information about the unscaled heat exchange can be found in the Appendix D.1.

for all pipes $i = 1, \ldots, n_P$ and $(x,t) \in [0, L^i] \times [0, t_{\text{end}}]$, **initial conditions**

$$\rho^i(x,0) = \rho^i_{ic}(x), \qquad z^i(x,0) = z^i_{ic}(x), \qquad v^i(0) = v^i_{ic}, \qquad T^j_c(0) = T^j_{c,ic} \tag{4.7}$$

for all pipes $i = 1, \ldots, n_P$, $j \in I_{cc}$ and $x \in [0, L^i]$, **boundary conditions**

$$\rho^1(0,t) = \rho_{bc,l}(t), \qquad z^1(0,t) = z_{bc,l}(t) \tag{4.8}$$

for all times $t \in [0, t_{\text{end}}]$ and **coupling conditions**

$$\rho^{i-1}(L^{i-1},t) = \rho^i(0,t), \qquad z^{i-1}(L^{i-1},t) = z^i(0,t) \tag{4.9}$$

for all pipes $i = 2, \ldots, n_P$.

**Remark 6.**

1. *The boundary conditions* (4.8) *already imply a positive flow direction, which will be stated in Assumption 3. Otherwise we would have to prescribe inflow boundary conditions like in* (2.59) *and* (2.60).

2. *As we know from Chapter 2 and 3, there are of course additional physical boundary conditions we need to prescribe, i.e., the pressure value at the exhaust pipe's left end right end:*

$$p^1_1(0,t) = p^1_{1,l}(t) = (p_{bc,l})_1(t), \qquad p^{n_P}_1(L^{n_P},t) = p^{n_P}_{1,r}(t) = (p_{bc,r})_1(t).$$

   *However, for the mathematical model* (4.5) *these are just parameters (which appear in* $\Phi^i$*, see* (4.4)*). Therefore, and for similarity to the yet underived adjoint system, we do not mention those boundary conditions in the model description.*

## 4.2. The optimization problem

As we know, the desired reactions in the catalyst, which reduce the exhaust gas pollution, take place best if a certain temperature is achieved. More precisely, the catalyst does not function if the temperature is below a certain threshold ("light off temperature" $\tilde{T}_{lo} \approx 550 - 600\text{K}$). However, it may be damaged if a certain critical temperature is exceeded.

As we can deduce from the numerical examples in Subsection 3.4.2, the exothermic reaction has a significant impact on the gas temperature in the catalytic converters. Therefore, the unburnt fuel is used to heat up the converters after a cold start.

Hence, it is natural to consider an optimization problem to reach a desired temperature $T_{opt}$ by controlling the inflow of unburnt gas $z_{bc,l}$. We will neglect the natural constraints induced by avoiding damage (e.g., possible reduction of the reaction rate of the exothermic reaction).

In order to formulate this optimization task, we first need a cost functional. On the one hand we want to reach the light off temperature $\tilde{T}_{lo}$ in the catalyst as soon as possible. On the other hand we do not want to use too much fuel. We express this objective by the following cost functional.

$$\mathcal{J}\left(\left\{T_c^i\right\}_{i\in I_{cc}}, z_{bc,l}\right) := \frac{1}{2}\sum_{i\in I_{cc}}\int_0^{t_{\text{end}}}(T_c^i(t)-T_{opt})^2dt + \sigma\int_0^{t_{\text{end}}} z_{bc,l}(t)dt \tag{4.10}$$

with the cost of control $\sigma \in \mathbb{R}_+$. Additionally, we have upper and lower bounds for the inflow of unburnt gas $z_{bc,l}$

$$0 \leq z_{bc,l}(t) \leq z_{bc,l}^{\max} \quad \forall t \in [0, t_{\text{end}}].$$

The choice of an $L_1$-type term for the unburnt gas is physically well motivated by the linear costs associated with the amount of fuel used.

As mentioned above, exceeding of the optimal temperature is not wanted either. Therefore, a penalization in both directions is meaningful. Besides this, there is no physical or chemical motivation for our choice of the tracking type term for the temperature. Measuring the costs by an $L_2$-type term is rather arbitrary and could be replaced by other functionals on the temperature.

We assume[3] that for any non-negative function $z_{bc,l} \in L_1(0, t_{\text{end}})$ there is a unique temperature $T_c^i = T_c^i(z_{bc,l}) \in L_2(0, t_{\text{end}})$ given by the model (4.5) - (4.9). This gives rise to the reduced problem of finding an inflow distribution $z_{bc,l}$ solving

$$\min_{z_{bc,l}\in Z_{ad}} j(z_{bc,l}) := \mathcal{J}\left(\left\{T_c^i(z_{bc,l})\right\}_{i\in I_{cc}}, z_{bc,l}\right), \tag{4.11}$$

with the space of admissible controls

$$Z_{ad} = \{z_{bc,l} \in L_1(0, t_{\text{end}}) \mid 0 \leq z_{bc,l}(t) \leq z_{bc,l}^{\max}\}.$$

### 4.2.1. The strategy to solve the optimal problem

When it comes to numerical optimization with PDE constraints, there is always one question concerning the approach one has to answer:

*"First discretize, then optimize"* or *"First optimize, then discretize"*?

[3] This will also be stated in Assumption 3 on Page 79.

There is a lot of literature dealing with this issue (e.g., [Gun02] and [HPUU09]). In the following calculations, we follow the first-optimize-then-discretize approach, meaning that we will derive the necessary optimality conditions for the continuous problem and then discretize the optimality conditions to obtain a discrete problem. We will discuss this aspect in Section 4.6.

For the numerical realization of the optimal control task, we apply a projected gradient method in this reduced setting, see Section 4.6 for details. Before we can do so, we need to calculate the derivatives of the reduced cost functional which is done in the following two sections.

## 4.3. The optimality system and its derivation

As already discussed in Section 3.1 developing an existence theory for the (expanded) asymptotic model was beyond the scope of this thesis. In order to proceed formally, we have to assume the existence of a unique solution and differentiability of this solution with respect to the control variable (inflow of unburnt gas).

For the following computation we also need to assume, that the velocity $u^i = v^i + Q^i$ is non-negative. Then $|v^i + Q^i| = v^i + Q^i$ in the term $\Phi$ (compare (4.4)). This assumption is in correspondence with the application, and under certain conditions also with the theory as the results on the quality of stationary solutions indicate (see Section 3.2 for details).

We sum this up in the following

**Assumption 3.**

*(A4)* *For any $z_{bc,l} \in Z_{ad}$ there exists a unique solution of the problem* (4.5) - (4.9). *Moreover, we assume the variables $\rho, z, v, T_c$ and their Lagrangian multipliers $\xi_\rho, \xi_z, \xi_v, \xi_{T_c}$ to be smooth enough for the required formal operations, such as partial integration.*

*(A5)* *The reduced cost functional is differentiable with respect to $z_{bc,l} \in L_1(0, t_{end})$.*

*(A6)* *The velocity $u^i(x,t) = v^i(t) + Q^i(x,t)$ is non-negative for all $(x,t) \in [0, L^i] \times [0, t_{end}]$ in all pipes $i = 1, \ldots, n_P$.*

Since we want to determine the gradient of our cost functional $\mathcal{J}$ by an adjoint-based method, we need to calculate the adjoint. To do so, we formulate a Lagrangian functional. Let $W := (w^1, \ldots, w^{n_P})$ be the vector of all state variables, i.e., $w^i := (\rho^i, z^i, v^i, T_c^i)$ and $\Lambda := (\lambda^1, \ldots, \lambda^{n_P})$ the vector of all adjoint variables, i.e., $\lambda^i := (\xi_\rho^i, \xi_z^i, \xi_v^i, \xi_{T_c}^i, \eta_\rho, \eta_z, \nu_\rho^i, \nu_z^i, \nu_v^i, \nu_{T_c}^i, \zeta_\rho^i, \zeta_z^i)$. Then the Lagrangian functional

is

$$\mathcal{L}(W, z_{bc,l}, \Lambda) = \sum_{i \in I_{cc}} \int_0^{t_{\text{end}}} (T_c^i(t) - T_{opt})^2 dt + \sigma \int_0^{t_{\text{end}}} z_{bc,l}(t) dt \tag{4.12}$$

$$- \sum_{i=1}^{n_P} \int_0^{t_{\text{end}}} \int_0^{L^i} \xi_\rho^i (\rho_t^i + (v^i + Q^i)\rho_x^i + q^i \rho^i) dx dt \tag{4.13}$$

$$- \sum_{i=1}^{n_P} \int_0^{t_{\text{end}}} \int_0^{L^i} \xi_z^i (z_t^i + (v^i + Q^i) z_x^i + \chi^i z^i K(T^i)) dx dt \tag{4.14}$$

$$- \sum_{i=1}^{n_P} \int_0^{t_{\text{end}}} \xi_v^i \left( v_t^i - \frac{\Phi^i}{R^i(0)} \right) dt \tag{4.15}$$

$$- \sum_{i \in I_{cc}} \int_0^{t_{\text{end}}} \xi_{T_c}^i ((T_c^i)_t + h_c (T_c^i - T_{\text{Gas}}^i)) dt \tag{4.16}$$

$$- \int_0^{t_{\text{end}}} \eta_\rho (\rho^1(0,t) - \rho_{bc,l}(t)) dt - \int_0^{t_{\text{end}}} \eta_z (z^1(0,t) - z_{bc,l}(t)) dt \tag{4.17}$$

$$- \sum_{i=1}^{n_P} \int_0^{L^i} \nu_\rho^i (\rho^i(x,0) - \rho_{ic}^i(x)) dx - \sum_{i=1}^{n_P} \int_0^{L^i} \nu_z^i (z^i(x,0) - z_{ic}^i(x)) dx \tag{4.18}$$

$$- \sum_{i=1}^{n_P} \nu_v^i (v^i(0) - v_{ic}^i) - \sum_{i \in I_{cc}} \nu_{T_c}^i (T_c^i(0) - T_{c\,ic}^i) \tag{4.19}$$

$$- \sum_{i=2}^{n_P} \int_0^{t_{\text{end}}} \zeta_\rho^i \left( \rho^{i-1}(L^{i-1}, t) - \rho^i(0,t) \right) dt \tag{4.20}$$

$$- \sum_{i=2}^{n_P} \int_0^{t_{\text{end}}} \zeta_z^i \left( z^{i-1}(L^{i-1}, t) - z^i(0,t) \right) dt. \tag{4.21}$$

Before starting with the computation, let us have a quick look at the lines of this large term. Line (4.12) represents the cost functional. Lines (4.13) - (4.16) are the four state equations multiplied with *Lagrangian multipliers* $\xi_*^i$, integrated over space and time and summed up over all pipes of the network. The last four lines are the boundary conditions multiplied with their Lagrangian multipliers $\eta_*^i$ and integrated over time (4.17), the initial conditions multiplied with their Lagrangian multipliers $\nu_*^i$ integrated over space (4.18) - (4.19) and the coupling conditions multiplied with their Lagrangian multipliers $\zeta_*^i$ and integrated over time (4.20) - (4.21).

We derive the optimality system by computing the first variation with respect to Lagrangian multipliers, state variables, and the control quantity. Then, the

stationarity requirement yields the following set of first order optimality conditions

$$\begin{aligned}
\frac{\partial \mathcal{L}}{\partial \lambda_j^i} &= 0 && \Rightarrow \quad \text{constraints or state equations,} \\
\frac{\partial \mathcal{L}}{\partial w_j^i} &= 0 && \Rightarrow \quad \text{adjoint or co-state equations,} \\
\frac{\partial \mathcal{L}}{\partial z_{bc,l}}(z_{bc,l}^* - z_{bc,l}) &\geq 0 \; \forall \, z_{bc,l}^* \in [0, z_{bc,l}^{\max}] && \Rightarrow \quad \text{reduced optimality condition.}
\end{aligned} \tag{4.22}$$

### 4.3.1. Derivation of the reduced optimality condition

Let us start with the derivation of the optimality condition. This computation is the easiest, since $z_{bc,l}$ only appears in the terms (4.12) and (4.17). Let $\delta z_{bc,l}$ be an arbitrarily chosen $L_1$-function, such that $0 \leq z_{bc,l} + \epsilon \delta z_{bc,l} \leq z_{bc,l}^{\max}$, for sufficiently small $\epsilon > 0$. Then the first variation of the Lagrangian $\mathcal{L}$ with respect to the control $z_{bc,l}$ in direction $\delta z_{bc,l}$ is

$$\frac{\partial \mathcal{L}(W, z_{bc,l}, \Lambda)}{\partial z_{bc,l}}(\delta z_{bc,l}) = \int_0^{t_{\text{end}}} \delta z_{bc,l}(\sigma + \eta_z) dt.$$

Given that (4.22) holds for all feasible test-functions we assert that the inequality in the reduced optimality condition holds pointwisely almost everywhere in $[0, t_{\text{end}}]$ due to the fundamental lemma of calculus of variation (see, e.g., the textbook of Tröltzsch [Trö10, Lemma 2.26]). This yields

$$\boxed{(\sigma + \eta_z)(z_{bc,l}^* - z_{bc,l}) \geq 0 \;\; \forall \; 0 \leq z_{bc,l}^* \leq z_{bc,l}^{\max},}$$

which in turn is equivalent to

$$\sigma + \eta_z \begin{cases} \geq 0, & \text{if } z_{bc,l} = 0, \\ = 0, & \text{if } 0 < z_{bc,l} < z_{bc,l}^{\max}, \\ \leq 0, & \text{if } z_{bc,l} = z_{bc,l}^{\max}. \end{cases}$$

### 4.3.2. Derivation of the constraints or state equations

In order to obtain the state equations, we have to compute the first variation of the Lagrangian functional $\mathcal{L}$ with respect to the Lagrangian multipliers. The computation works just like in the above case. We then obtain the state system consisting of our differential equations (4.5) as well as our initial (4.7), boundary (4.8) and coupling conditions (4.9).

### 4.3.3. Derivation of the adjoint or co-state equations

Since this part is very long and technical, it will get its own section, namely the following Section 4.4.

## 4.4. Derivation of the adjoint or co-state equations

In this section, we cease to write superscripts, but compute the first variations for a single pipe of length $L = 1$ with a catalytic converter ($\chi = 1$). The computation of the adjoint equations for a pipe without a catalyst is just a special case (no equation for $T_c$ and $\chi = 0$).

Note, that in the case of a single pipe no coupling conditions are required. We will deal with this problem in Subsection 4.4.3. The following part is the most complicated one when it comes to computation of the first variation. This is the case, because all state variables except $v$ appear in the functional $Q = Q[\rho, z, T_c]$.

We compute the first variation with respect to the space-independent velocity component $v$ and the density $\rho$ in this section. The first variation of $\mathcal{L}$ with respect to the density involves most of the terms in the Lagrangian and includes all techniques that are required for the computation of the variations with respect to the other two variables $z$ and $T_c$. However, we refer to the Appendix D.3 for the remaining calculations.

We start with $\partial\mathcal{L}/\partial v$, since this is the easier one of the two cases.

### 4.4.1. First variation of $\mathcal{L}$ with respect to $v$

The space independent velocity component $v$ appears in the Lagrangian $\mathcal{L}$ in the density PDE (4.13), the ratio of unburnt gas PDE (4.14) and its own ODE (4.15) as well as its initial condition (4.19). One has to keep in mind, that the functional $\Phi$ (4.4) also depends on $v$. So before computing the first variation of $\mathcal{L}$ with respect to $v$, let us have a closer look at the functional $\Phi$.

$$\begin{aligned}
\Phi[\rho, z, v + \epsilon\delta v, T_c] - \Phi[\rho, z, v, T_c] \\
&= -\epsilon\delta v \int_0^1 \left( \rho q + C_f \rho \left( (v + Q) + \frac{\epsilon\delta v}{2} \right) + \chi C_c \rho \right) dx \\
&= -\epsilon\delta v \int_0^1 \left( \rho q + C_f \rho (v + Q) + \chi C_c \rho \right) dx - \frac{\epsilon^2 \delta v^2}{2} \int_0^1 C_f \rho dx.
\end{aligned}$$

We have already isolated the term of order $\epsilon^2$, since it is of higher order and will vanish in the limit $\epsilon \to 0$.

$$\begin{aligned}\frac{\partial \mathcal{L}(W, z_{bc,l}, \Lambda)}{\partial v}(\delta v) \\ &= \lim_{\epsilon \to 0} \frac{1}{\epsilon} \Bigg[ - \int_0^{t_{\text{end}}} \int_0^1 \epsilon \delta v (\xi_\rho \rho_x + \xi_z z_x) dx dt - \nu_v \epsilon \delta v|_{t=0} \\ &\qquad - \int_0^{t_{\text{end}}} \xi_v \left( \epsilon \delta v_t + \epsilon \delta v S(0) \right) + o(\epsilon) \Bigg]\end{aligned}$$

with

$$S(x) := \frac{1}{R(0)} \int_x^1 \left( \rho q + C_f \rho (v + Q) + C_c \rho \right) dy. \tag{4.23}$$

Using integration by parts, we shift the time derivative of $\delta v$ to the co-state $\xi_v$. This also leads to an evaluation at the boundaries.

$$- \int_0^{t_{\text{end}}} \xi_v \delta v_t dt = \int_0^{t_{\text{end}}} (\xi_v)_t \delta v dt - \Big[ \xi_v \delta v \Big]_{t=0}^{t=t_{\text{end}}}.$$

The limit $\epsilon \to 0$ gives

$$\begin{aligned}\frac{\partial \mathcal{L}(W, z_{bc,l}, \Lambda)}{\partial v}(\delta v) = &\int_0^{t_{\text{end}}} \delta v \left[ (\xi_v)_t - \int_0^1 \xi_\rho \rho_x + \xi_z z_x dx - \xi_v S(0) \right] dt \\ &- \Big[ \xi_v \delta v \Big]_{t=0}^{t=t_{\text{end}}} - \nu_v \delta v(0).\end{aligned}$$

Now, we assume (referring to the optimality system (4.22)) the derivative of the Lagrangian with respect to $v$, in the direction $\delta v$, to vanish. Since the variation $\delta v$ is arbitrary, we choose a variation that vanishes at the boundaries, i.e., at $t = 0$ and $t = t_{\text{end}}$. Then we deduce, by the fundamental theorem of variational calculus, that

$$\boxed{-(\xi_v)_t = -\xi_v S(0) - \int_0^1 \xi_\rho \rho_x + \xi_z z_x dx.} \tag{4.24}$$

By choosing a variation that vanishes only at one of the end points $t = 0$, $t = t_{\text{end}}$, we obtain, with the knowledge that (4.24) holds,

$$\boxed{\xi_v = 0 \quad \text{for } t = t_{\text{end}}.} \tag{4.25}$$

### 4.4.2. First variation of $\mathcal{L}$ with respect to $\rho$

We have to compute the first variation of $\mathcal{L}$ with respect to $\rho$, i.e., $\partial\mathcal{L}/\partial\rho$. Since the density appears in many terms in the Lagrangian, this computation is very long and technical. Therefore, we divide this task into several subtasks, i.e., computation of the first variation of

a) the integral (4.13) with test function $\xi_\rho$,

b) the integral (4.14) with test function $\xi_z$,

c) the integral (4.15) with test function $\xi_v$,

d) the integral (4.14) with test function $\xi_{T_c}$.

The remaining integrals depend linearly on $\rho$, hence the first variation is trivial to calculate. In the end, we will put all results of the subtasks back together and finalize with $\partial\mathcal{L}/\partial\rho$.

Before we start the computation of the derivative, let us focus on the dependence of $q$ and $Q$ upon the density $\rho$. We assume $\rho \geq c > 0$, which is in correspondence with the physics.

$$q[\rho+\epsilon\delta\rho, z, T_c] = \frac{1}{\gamma p_0}\Bigg[-h\left(\frac{p_0}{\rho+\epsilon\delta\rho} - T_{\text{Wall}}\right) - \chi h_c\left(\frac{p_0}{\rho+\epsilon\delta\rho} - T_c\right) + \chi q_0(\rho+\epsilon\delta\rho) z K_\rho(\rho+\epsilon\delta\rho)\Bigg]$$

with a density-dependent reaction rate function[4]

$$K_\rho(\rho^i) := \frac{\tilde{K}_0\tilde{x}_{\text{ref}}}{\tilde{u}_{\text{ref}}}\exp\left(-\frac{\tilde{T}^+}{\tilde{T}_{\text{ref}}p_0}\rho^i\right).$$

We observe that the density variable and its variation do not appear in a linear way, but as the denominator of a friction and the argument of an exponential function. In order to subtract the evaluation of $q$ at $\rho+\epsilon\delta\rho$, we have to get rid of these terms. We do this by Taylor expansion:

$$\frac{1}{\rho+\epsilon\delta\rho} = \frac{1}{\rho} - \epsilon\delta\rho\frac{1}{\rho^2} + o(\epsilon),$$
$$K_\rho(\rho+\epsilon\delta\rho) = K_\rho(\rho) + \epsilon\delta\rho K'_\rho(\rho) + o(\epsilon).$$

[4]Due to the asymptotic ideal gas law (2.39) we have a reciprocal dependence of gas density and gas temperature. Therefore, this formulation of the reaction rate function is equivalent to the original (2.7).

In order to shorten the expressions, we define the following abbreviations for the computation of $\partial\mathcal{L}/\partial\rho$:

$$q := q[\rho, z, T_c], \quad q_\epsilon := q[\rho + \epsilon\delta\rho, z, T_c], \quad Q := Q[\rho, z, T_c], \quad Q_\epsilon := Q[\rho + \epsilon\delta\rho, z, T_c].$$

By replacing non-linear density-dependent terms by their Taylor expansions, we obtain

$$q_\epsilon - q = \epsilon\delta\rho\frac{1}{\gamma p_0}\left[\frac{p_0(h+\chi h_c)}{\rho^2} + \chi q_0 z(\rho K'_\rho(\rho) + K_\rho(\rho))\right] + o(\epsilon).$$

By definition of $Q$, this yields

$$Q_\epsilon - Q = \int_0^x \epsilon\delta\rho q_\rho dy + o(\epsilon),$$

where

$$q_\rho := \frac{1}{\gamma p_0}\left(\frac{p_0(h+\chi h_c)}{\rho^2} + \chi q_0 z(\rho K'_\rho(\rho) + K_\rho(\rho))\right). \tag{4.26}$$

**a) The $\xi_\rho$-integral** (4.13)

$$\begin{aligned}
&-\int_0^{t_{\text{end}}}\int_0^1 \xi_\rho\big((\rho+\epsilon\delta\rho)_t + (v+Q_\epsilon)(\rho+\epsilon\delta\rho)_x + q_\epsilon(\rho+\epsilon\delta\rho)\big)dxdt \\
&\qquad + \int_0^{t_{\text{end}}}\int_0^1 \xi_\rho\big(\rho_t + (v+Q)\rho_x + q\rho\big)dxdt \\
&\qquad = -\int_0^{t_{\text{end}}}\int_0^1 \xi_\rho\Bigg(\epsilon\delta\rho_t + (v+Q)\epsilon\delta\rho_x + q\epsilon\delta\rho \\
&\qquad\qquad + \rho q_\rho\epsilon\delta\rho + \rho_x\int_0^x \epsilon\delta\rho q_\rho dy\Bigg)dxdt + o(\epsilon) \\
&\qquad =: \mathcal{I}_{\xi_\rho}.
\end{aligned} \tag{4.27}$$

Our aim is to isolate the variation $\delta\rho$, such that we can apply the fundamental lemma of variational calculus again. Therefore we need to integrate by parts twice (once with respect to the spatial and once with respect to the time component). Furthermore, we need to use the following identity

$$\int_0^1 f(x)\left(\int_0^x g(y)dy\right)dx = \int_0^1 g(x)\left(\int_x^1 f(y)dy\right)dx,$$

which is a consequence of Fubini's theorem[5]. With this we manipulate (4.27), integrate by parts and using $(v+Q)_x = q$ obtain

$$\begin{aligned}\mathcal{I}_{\xi_\rho} = &\int_0^{t_{\text{end}}}\int_0^1 \epsilon\delta\rho\left((\xi_\rho)_t + (v+Q)(\xi_\rho)_x - q_\rho\left[\rho\xi_\rho + \int_x^1 \xi_\rho\rho_x dy\right]\right)dxdt \\ &- \left[\int_0^{t_{\text{end}}} \epsilon\delta\rho(v+Q)\xi_\rho dt\right]_{x=0}^{x=1} - \left[\int_0^1 \epsilon\delta\rho\xi_\rho dx\right]_{t=0}^{t=t_{\text{end}}} + o(\epsilon).\end{aligned} \tag{4.28}$$

**b) The $\xi_z$-integral** (4.14)

Analog calculations give

$$\begin{aligned}&-\int_0^{t_{\text{end}}}\int_0^1 \xi_z\big(z_t + (v+Q_\epsilon)z_x + \chi z K_\rho(\rho+\epsilon\delta\rho)\big)dxdt \\ &+\int_0^{t_{\text{end}}}\int_0^1 \xi_z\big(z_t + (v+Q)z_x + \chi z K_\rho(\rho)\big)dxdt \\ &\qquad = -\int_0^{t_{\text{end}}}\int_0^1 \xi_z\left(z_x\int_0^x \epsilon\delta\rho q_\rho dy + \chi\epsilon\delta\rho z K'_\rho(\rho)\right)dxdt + o(\epsilon) \\ &\qquad = -\int_0^{t_{\text{end}}}\int_0^1 \epsilon\delta\rho\left(q_\rho\int_x^1 \xi_z z_x dy + \chi\xi_z z K'_\rho(\rho)\right)dxdt + o(\epsilon).\end{aligned} \tag{4.29}$$

**c) The $\xi_v$-integral** (4.15)

This is the most technical subtask, since $\rho$ appears in this term so often. Let us develop this step by step. First, we have a look at the density integral in the denominator. By Taylor expansion we obtain:

$$\begin{aligned}\frac{1}{\int_0^1 \rho + \epsilon\delta\rho dx} &= \frac{1}{\int_0^1 \rho dx} - \int_0^1 \epsilon\delta\rho dx \frac{1}{\left(\int_0^1 \rho dx\right)^2} + o(\epsilon) \\ &= \frac{1}{R(0)} - \frac{1}{R(0)^2}\int_0^1 \epsilon\delta\rho dx + o(\epsilon).\end{aligned}$$

The term $\Phi$ evaluated at $\rho + \epsilon\delta\rho$, will have the following form:

$$\Phi[\rho+\epsilon\delta\rho, z, v, T_c] = \Phi[\rho, z, v, T_c] + \epsilon\Phi_\rho[\delta\rho; \rho, z, v, T_c] + o(\epsilon).$$

To shorten the integrals, we introduce the following abbreviations:

$$\Phi := \Phi[\rho, z, v, T_c], \qquad \Phi_\epsilon := \Phi[\rho+\epsilon\delta\rho, z, v, T_c].$$

[5]Details and proof can be found in the Appendix D.2.

Please note the different meaning of $\Phi_\epsilon$ and the derivative $\Phi_\rho$. We will compute $\Phi_\rho$ in detail later. Let us first have a look at the whole integral containing $\xi_v$.

$$\begin{aligned}
-\int_0^{t_{\text{end}}} \xi_v \left( v_t - \frac{1}{\int_0^1 \rho + \epsilon\delta\rho dx} \Phi_\epsilon \right) dt + \int_0^{t_{\text{end}}} \xi_v \left( v_t - \frac{1}{\int_0^1 \rho dx} \Phi \right) dt \\
= \int_0^{t_{\text{end}}} \xi_v \left( \frac{1}{R(0)} \epsilon \Phi_\rho - \frac{1}{R(0)^2} \int_0^1 \epsilon\delta\rho dx \ \Phi \right) dt + o(\epsilon) =: I_{\xi_v}.
\end{aligned} \tag{4.30}$$

The term $\epsilon\Phi_\rho$ consists of all the terms in which $\epsilon$ appears linearly, when evaluating $\Phi$ at $\rho + \epsilon\delta\rho$. We will now compute those terms. Therefore, we split $\Phi$ into several parts.

$$\begin{aligned}
\Phi[\rho, z, v, T_c] = \ & p_{1,l} - p_{1,r} - \overbrace{\int_0^1 \rho Q_t dx}^{=:\Phi_1[\rho,z,T_c]} - \overbrace{\int_0^1 \rho(v+Q) q dx}^{=:\Phi_2[\rho,z,v,T_c]} \\
& - \underbrace{C_f \int_0^1 \rho \frac{(v+Q)^2}{2} dx}_{=:\Phi_3[\rho,z,v,T_c]} - \underbrace{\chi C_c \int_0^1 \rho(v+Q) dx}_{=:\Phi_4[\rho,z,v,T_c]}.
\end{aligned}$$

We compute the difference $-\Phi_i[\rho + \epsilon\delta\rho, z, v, T_c] + \Phi_i[\rho, z, v, T_c] =: -\Phi_{i;\epsilon} + \Phi_i$:

$$\begin{aligned}
-\Phi_{1;\epsilon} + \Phi_1 &= -\int_0^1 (\rho + \epsilon\delta\rho)(Q_\epsilon)_t dx + \int_0^1 \rho Q_t dx \\
&= -\int_0^1 \epsilon\delta\rho Q_t + [\epsilon\delta\rho q_\rho]_t R(x) dx + o(\epsilon).
\end{aligned} \tag{4.31}$$

For the remaining terms, we obtain in a similar fashion

$$\begin{aligned}
-\Phi_{2;\epsilon} + \Phi_2 &= -\int_0^1 \epsilon\delta\rho \left( (v+Q)q + \rho(v+Q)q_\rho + q_\rho \int_x^1 \rho q dy \right) dx + o(\epsilon), \\
-\Phi_{3;\epsilon} + \Phi_3 &= -C_f \int_0^1 \epsilon\delta\rho \left( \frac{(v+Q)^2}{2} + q_\rho \int_x^1 \rho(v+Q) dy \right) dx + o(\epsilon), \\
-\Phi_{4;\epsilon} + \Phi_4 &= -\chi C_c \int_0^1 \epsilon\delta\rho \left( (v+Q) + q_\rho \int_x^1 \rho dy \right) dx + o(\epsilon).
\end{aligned}$$

Then, the directional derivative $\Phi_\rho$ is given as

$$\begin{aligned}
\Phi_\rho[\delta\rho; \rho, z, v, T_c] = & -\int_0^1 \delta\rho \left( \rho(v+Q)q_\rho + q_\rho R(0) S(x) - \frac{\phi}{\rho} \right) dx \\
& - \int_0^1 R(x) [\delta\rho \ q_\rho]_t dx
\end{aligned}$$

with

$$\phi[\rho, z, v, T_c] := -\left(\rho Q_t + \rho(v+Q)q + C_f\rho\frac{(v+Q)^2}{2} + \chi C_c\rho(v+Q)\right). \tag{4.32}$$

Before finalizing the $\xi_v$-integral, we have to integrate by parts in order to get rid of the time derivative of the perturbation $\delta\rho$ in the term (4.31). This yields

$$\begin{aligned}
&-\int_0^{t_{\text{end}}}\int_0^1 \xi_v\frac{R(x)}{R(0)}[\epsilon\delta\rho\ q_\rho]_t dxdt + \left[\xi_v\frac{1}{R(0)}\int_0^1 \epsilon\delta\rho\ q_\rho R(x)dx\right]_{t=0}^{t=t_{\text{end}}}\\
&= \int_0^{t_{\text{end}}}\int_0^1 \epsilon\delta\rho\ q_\rho\left[\xi_v\frac{R(x)}{R(0)}\right]_t dxdt\\
&= \int_0^{t_{\text{end}}}\int_0^1 \epsilon\delta\rho\ q_\rho\left[(\xi_v)_t\frac{R(x)}{R(0)} + \xi_v\frac{R_t(x)}{R(0)} - \xi_v\frac{R_t(0)R(x)}{R(0)^2}\right]dxdt\\
&= \int_0^{t_{\text{end}}}\int_0^1 \epsilon\delta\rho\ q_\rho\left[\left(\xi_v S(0) + \int_0^1 \xi_\rho\rho_x + \xi_z z_x dx\right)\frac{R(x)}{R(0)}\right.\\
&\qquad\qquad\left. + \xi_v\frac{R_t(x)}{R(0)} - \xi_v\frac{R_t(0)R(x)}{R(0)^2}\right]dxdt\\
&= \int_0^{t_{\text{end}}}\int_0^1 \epsilon\delta\rho q_\rho\left[\frac{R(x)}{R(0)}\int_0^1 \xi_\rho\rho_x + \xi_z z_x dx\right.\\
&\qquad\qquad\left. + \xi_v\frac{1}{R(0)}\left(R(x)S(0) + R_t(x) - \frac{R_t(0)R(x)}{R(0)}\right)\right]dx.
\end{aligned}$$

Thus, our $\xi_v$-integral (4.30) equals

$$\begin{aligned}
I_{\xi_v} = &\int_0^{t_{\text{end}}}\int_0^1 \epsilon\delta\rho q_\rho\left[\xi_v\frac{1}{R(0)}\left(-\rho(v+Q) - R(0)S(x) + R(x)S(0) + R_t(x)\right.\right.\\
&\qquad\left.\left. - \frac{R_t(0)R(x)}{R(0)}\right) + \frac{R(x)}{R(0)}\int_0^1 \xi_\rho\rho_x + \xi_z z_x dx\right]dxdt\\
&-\int_0^{t_{\text{end}}}\int_0^1 \epsilon\delta\rho\ \xi_v\frac{1}{R(0)}\left(\frac{\Phi}{R(0)} - \frac{\phi}{\rho}\right)dxdt\\
&-\left[\xi_v\frac{1}{R(0)}\int_0^1 \epsilon\delta\rho\ q_\rho R(x)dx\right]_{t=0}^{t=t_{\text{end}}} + o(\epsilon).
\end{aligned} \tag{4.33}$$

**d) The $\xi_{T_c}$-integral** (4.16)

Although the considered pipe's length is $L = 1$ in this section, we now write $L$. The reason for this is, that the pipe's length appears as a factor in the definition of $T^i_{\text{Gas}}$ (see (4.1)). We want to emphasize the appearance of the factor $L$ here, since in the network case the pipes lengths are never 1, but vary between 0 and 1. Applying the ideal gas law (4.6), we obtain

$$\begin{aligned} &-\int_0^{t_{\text{end}}} \xi_{T_c}\left[(T_c)_t + h_c\left(T_c - \frac{1}{L}\int_0^L \frac{p_0}{\rho+\epsilon\delta\rho}dx\right)\right]dt \\ &+\int_0^{t_{\text{end}}} \xi_{T_c}\left[(T_c)_t + h_c\left(T_c - \frac{1}{L}\int_0^L \frac{p_0}{\rho}dx\right)\right]dt \\ &= -\int_0^{t_{\text{end}}}\int_0^L \epsilon\delta\rho\,\frac{p_0 h_c}{\rho^2 L}\,\xi_{T_c}\,dxdt + o(\epsilon). \end{aligned} \tag{4.34}$$

**e) The summary of the first variation of $\mathcal{L}$ with respect to $\rho$**

Everything is prepared and we can conclude the calculations. Using the terms (4.28),(4.29),(4.33), (4.34), and the derivatives for the equations (4.17) and (4.18), we obtain:

$$\begin{aligned} \frac{\partial\mathcal{L}(W, z_{bc,l}, \Lambda)}{\partial\rho}(\delta\rho) = \lim_{\epsilon\to 0}\frac{1}{\epsilon}\Bigg[&\int_0^{t_{\text{end}}}\int_0^1 \epsilon\delta\rho\left((\xi_\rho)_t + (v+Q)(\xi_\rho)_x - q_\rho F\right)dxdt \\ &+\int_0^{t_{\text{end}}}\int_0^1 \epsilon\delta\rho\left(-\xi_v\frac{1}{R(0)}\left(\frac{\Phi}{R(0)} - \frac{\phi}{\rho}\right)\right. \\ &\qquad\left. - \chi z K'_\rho(\rho)\xi_z - \chi\frac{p_0 h_c}{\rho^2 L}\xi_{T_c}\right)dxdt \\ &-\left[\int_0^{t_{\text{end}}} \epsilon\delta\rho(v+Q)\xi_\rho dt\right]_{x=0}^{x=1} \\ &-\left[\xi_v\frac{1}{R(0)}\int_0^1 \epsilon\delta\rho\; q_\rho R(x)dx + \int_0^1 \epsilon\delta\rho\xi_\rho dx\right]_{t=0}^{t=t_{\text{end}}} \\ &-\int_0^{t_{\text{end}}} \epsilon\delta\rho(0,t)\eta_\rho dt - \int_0^1 \epsilon\delta\rho(x,0)\nu_\rho dx + o(\epsilon)\Bigg], \end{aligned}$$

where $F$ is defined as

$$\begin{aligned} F[\rho, z, v, T_c, \xi_\rho, \xi_z, \xi_v] := \xi_\rho\rho + \int_x^1 \xi_\rho\rho_x + \xi_z z_x dy - \frac{R(x)}{R(0)}\int_0^1 \xi_\rho\rho_x + \xi_z z_x dx \\ +\xi_v\frac{1}{R(0)}\left(\rho(v+Q) + R(0)S(x) - R(x)S(0) - R_t(x) + \frac{R_t(0)R(x)}{R(0)}\right). \end{aligned} \tag{4.35}$$

Using that $\delta\rho$ is arbitrary, we end up with

$$\boxed{-(\xi_\rho)_t - (v+Q)(\xi_\rho)_x = -q_\rho F - \xi_v \frac{1}{R(0)}\left(\frac{\Phi}{R(0)} - \frac{\phi}{\rho}\right) - \chi z K'_\rho(\rho)\xi_z - \chi \frac{p_0 h_c}{\rho^2 L}\xi_{T_c},} \tag{4.36}$$

the terminal condition

$$\boxed{\xi_\rho = 0 \quad \text{for} \quad t = t_{\text{end}}} \tag{4.37}$$

and the boundary condition

$$\boxed{\xi_\rho(v+Q) = 0 \quad \text{for} \quad x = 1.} \tag{4.38}$$

**Remark 7.** *Note that we will have a problem evaluating the boundary condition for $x = 1$, if the velocity $u = v + Q$ at $x = 1$ vanishes at some time. We therefore have to assume positive velocities at $x = 1$ for all times $t \in (0, t_{end}]$. The only exception will be at $t = 0$, where we will have $u(x, 0) = 0$ in the case of an engine start. The boundary condition for $\xi_\rho$ at time $t = 0$ is then given by continuation.*

### 4.4.3. Coupling conditions for the adjoint equations

Now, let us discuss the derivation of coupling conditions for the adjoint equations. The above derivation was valid for a single pipe, not connected to any other pipe, i.e., we neglected the coupling conditions in the Lagrangian (4.20). Let us consider the first variation of the Lagrangian for the whole network (4.12) - (4.21) with respect to the density in an inner pipe $i$. Similarly, as outlined in Subsection 4.4.2, we would deduce (4.36) and (4.37). Since $i \in \{2, \dots, n_P - 1\}$ we have to neglect the boundary condition for the density (4.17). Finally, we would be left only with the following integrals:

$$\begin{aligned} 0 \overset{!}{=} \frac{\partial \mathcal{L}(W, z_{bc,l}, \Lambda)}{\partial \rho^i}(\delta\rho) = &- \int_0^{t_{\text{end}}} \delta\rho^i(L^i, t)\left((v^i(t) + Q^i(L^i, t))\xi^i_\rho(L^i, t) + \zeta^{i+1}_\rho(t)\right) dt \\ &+ \int_0^{t_{\text{end}}} \delta\rho^i(0, t)\left((v^i(t) + Q^i(0, t))\xi^i_\rho(0, t) + \zeta^i_\rho(t)\right) dt. \end{aligned}$$

Using the fact that $\delta\rho^i$ is arbitrary, we obtain

$$(v^i(t) + Q^i(L^i, t))\xi^i_\rho(L^i, t) = -\zeta^{i+1}_\rho(t) \tag{4.39}$$

and

$$(v^i(t) + Q^i(0, t))\xi^i_\rho(0, t) = -\zeta^i_\rho(t). \tag{4.40}$$

So increasing the indices of all terms in (4.40), we can write together with (4.39):

$$\boxed{(v^i(t) + Q^i(L^i, t))\xi^i_\rho(L^i, t) = -\zeta^{i+1}_\rho(t) = (v^{i+1}(t) + Q^{i+1}(0, t))\xi^{i+1}_\rho(0, t).}$$

## 4.5. Summary of the adjoint calculus - The optimality system

We want to summarize the results of all computations in this section. Our optimality system now consists of *(a) constraints or state equations*, *(b) adjoint or co-state equations* and *(c) the optimality condition.*

*(a) Constraints or state equations*

The constraints consist of the governing system of equations (4.5), the closing relation (ideal gas law) (4.6) and the initial, boundary and coupling conditions (4.7), (4.8) (4.9).

*(b) Adjoint or co-state equations*[6]

The adjoint problem consists of the **system**

$$\boxed{\begin{aligned}
-(\xi^i_\rho)_t - (v^i + Q^i)(\xi^i_\rho)_x =& - q^i_\rho F^i - \chi^i \left( z^i K'_\rho(\rho^i)\xi^i_z + \frac{p_0 h_c}{(\rho^i)^2 L^i}\xi^i_{T_c} \right) \\
& - \xi^i_v \frac{1}{R^i(0)} \left( \frac{\Phi^i}{R^i(0)} - \frac{\phi^i}{\rho^i} \right), \\
-(\xi^i_z)_t - (v^i + Q^i)(\xi^i_z)_x =& - q^i_z F^i - \xi^i_z \left( \chi^i K(T^i) - q^i \right), \\
-(\xi^i_v)_t =& - \xi^i_v S^i(0) - \int_0^{L^i} \xi^i_\rho \rho^i_x + \xi^i_z z^i_x dx, \\
-(\xi^j_{T_c})_t =& - \int_0^{L^j} q^j_{T_c} F^j dx - h_c \xi^j_{T_c} + (T^j_c - T_{opt})
\end{aligned}} \tag{4.41}$$

for all pipes $i = 1, \ldots, n_P, j \in I_{cc}$ and $(x,t) \in (0, L^i) \times (0, t_{\text{end}})$, with **terminal conditions**

$$\boxed{\xi^i_\rho(x, t_{\text{end}}) = 0, \quad \xi^i_z(x, t_{\text{end}}) = 0, \quad \xi^i_v(t_{\text{end}}) = 0, \quad \xi^j_{T_c}(t_{\text{end}}) = 0}$$

for all pipes $i = 1, \ldots, n_P, j \in I_{cc}$ and $x \in [0, L^i]$, **boundary conditions**[7]

$$\boxed{\begin{aligned}
&\xi^{n_P}_\rho(L^{n_P}, t)(v^{n_P}(t) + Q^{n_P}(L^{n_P}, t)) = 0, \\
&\xi^{n_P}_z(L^{n_P}, t)(v^{n_P}(t) + Q^{n_P}(L^{n_P}, t)) = 0
\end{aligned}}$$

[6]See D.3 for the derivation of equations for $\xi^i_z$ and $\xi^i_{T_c}$.
[7]The boundary condition for $\xi^{n_P}_z$ is derived in D.3.2.

for all times $t \in [0, t_{\text{end}}]$ as well as **coupling conditions**[8]

$$\boxed{\begin{aligned}(v^i(t) + Q^i(L^i, t))\xi^i_\rho(L^i, t) &= (v^{i+1}(t) + Q^{i+1}(0, t))\xi^{i+1}_\rho(0, t),\\ (v^i(t) + Q^i(L^i, t))\xi^i_z(L^i, t) &= (v^{i+1}(t) + Q^{i+1}(0, t))\xi^{i+1}_z(0, t)\end{aligned}}$$

for all pipes $i = 1, \ldots, n_P$ and times $t \in [0, t_{\text{end}}]$. The variables $q^i_\rho, q^i_z, q^i_{T_c}, \phi^i, S^i$ and $F^i$ are defined in (4.26), (D.8), (D.1), (4.32), (4.23) and (4.35), respectively. Furthermore, as $\eta_z$ appears in the optimality condition, we are interested in this quantity. It is given by the relation[9]

$$\boxed{\xi^1_z(0, t)(v^1(t) + Q^1(0, t)) = \eta_z(t)} \tag{4.42}$$

for all $t \in [0, t_{\text{end}}]$.

*(c) reduced optimality condition*

$$\boxed{(\sigma + \eta_z)(z^*_{bc,l} - z_{bc,l}) \geq 0 \quad \forall\, 0 \leq z^*_{bc,l} \leq z^{\max}_{bc,l}} \tag{4.43}$$

for all $t \in [0, t_{\text{end}}]$.

## 4.6. Discretization

As already mentioned in Subsection 4.2.1, the question in which order one prefers to discretize and optimize is a delicate task. We shortly discuss this issue on the basis of [Gun02, Section 2.9].

1. **First discretize, then optimize.**
   First, we could consider any discretization of the state equation (4.5) - (4.9), the control $z_{bc,l}$, and the cost functional (4.10) to obtain a finite dimensional optimization problem. For this problem one can derive optimality conditions, using adjoint calculus, similar to the continuous case above, but doing all calculations for the discrete equation.

2. **First optimize, then discretize.**
   The second approach is to formally derive the optimality system (as this has been done in Sections 4.3 and 4.4) consisting of state (4.5) - (4.9) and adjoint equations (4.41) - (4.42) as well as the representation of the gradient (4.43). Then, one considers any discretion of the state equations, adjoint equations and gradient.

[8] See D.3.3 for the derivation of the coupling condition for $\xi^i_z$.
[9] See D.3.2 and equation (D.15) for the derivation.

One way to deal with the discrepancy of the two approaches is the construction of adjoint consistent schemes, i.e., discretization methods that ensure that both approaches yield the same adjoints. Such a reformulation is analyzed, for instance in [Hag00] for Runge-Kutta schemes applied to optimal control with ODEs. In the context of PDEs, such reformulations may become more involved, since spatial irregularities may influence the choice of the temporal discretization, see, e.g., [GRW11]. However, for a strongly simplified example consistency of both approaches is shown in the Appendix D.4.

Both approaches are well established in the literature, and therefore it is not surprising that there are advantages and disadvantages on both sides, whereas an advantage of one approach automatically induces a disadvantage of the other.

- **Advantage of the first-discretize-then-optimize approach**.
  1. When following this approach, we have, by construction, consistency of the gradient with the discrete cost functional, whereas in the case of the other approach, we do not have any consistency in general - neither with the discrete nor the continuous cost functional.
  2. In a discrete optimization problem, it is possible to shift the technical computations to an automatic differentiation software. But although using such software can simplify the technical calculations (like Sections 4.3, 4.4 and D.3), it requires more storage and CPU-time than corresponding handwritten codes.
- **Advantage of the first-optimize-then-discretize approach**.
  1. The derivation of the continuous optimality system is independent of the discretization. Therefore, once the gradient and the adjoint equations have been derived, one can change the discretization easily. This would demand a new derivation of the discrete optimality conditions in the first-discretize-then-optimize approach.
  2. Furthermore, the derivation of a discrete optimality system with an underlying sophisticated discretization for the state equation could be even more technical than the computation for the continuous approach.
  3. Lastly, although we are not making any use of it, the first-optimize-then-discretize approach gives the freedom of using different numerical meshes for the state and adjoint system.

Hence, the main weakness of the second approach is the inconsistency of the gradient, since the induced approximated gradients are in general not the exact gradients of any functional. However, they are approximations to the gradients of both the continuous and discrete cost functional. So, if the approximations

are sufficiently accurate, the approximated gradient should converge to the exact gradient of the functional as the grid size tends to zero.

Thus, we decided to follow the first-optimize-then-discretize approach to numerically calculate a solution to the necessary optimality conditions, consisting of state equations, adjoint equations and the optimality condition.

From the discussion above, we already know, that we only have an approximation to the discrete derivatives. If this approximation is not good enough, the calculated approximate negative gradient direction need not be a "descent direction" and thus fail to give descent for the discretized functional. However, if this happens any further iteration on the given discretization is misleading anyway, since discretization errors become dominant so that a refinement of the discretization is warranted. Hence failure of convergence without nearly satisfied optimality conditions serves us as a cheap estimate for the accuracy of the applied discretization; for more details see Table 4.2 and the discussion in Subsection 4.6.3.

### 4.6.1. Discretization of the state and adjoint system

For the discretization of the state equation (4.5) an explicit upwind scheme for the spatial differential operator and explicit Euler for the time derivative is used (see Subsection 3.3.2 for details). Since the adjoint system (4.41) is posed backwards in space and time, we first substitute the time and space variables by $\hat{t} := t_{\text{end}} - t$ and $\hat{x} = L^i - x$. Then the same numerical scheme (Algorithm 2) that we use for solving the state system is applied (see Appendix D.4.2 for details).

By the operation "$\cdot$" between two elements of $\mathbb{R}^M$, we denote the weighted scalar product, which is an approximation for the $L_2$ scalar product, i.e., for two mappings $\varphi, \psi : [0,1] \to \mathbb{R}$ and their discretizations $\varphi_h, \psi_h \in \mathbb{R}^M$ we have

$$\varphi_h \cdot \psi_h = \frac{1}{M} \sum_{m=1}^{M} (\varphi_h)_m (\psi_h)_m \approx (\varphi, \psi)_{L_2} = \int_0^1 \varphi \psi dy,$$

noting that we have uniform step sizes.

In order to avoid too many subscripts, we do not discriminate between the continuous and discrete state, adjoint and control variables, as we always work with the discrete quantities in this section. Discretization of functionals, such as $j : L_1 \to \mathbb{R}$, will be denoted by the subscript $h$, i.e., $j \approx j_h$.

### 4.6.2. Algorithm: Projected gradient method

As already mentioned in Subsection 4.2.1 we use a projected gradient method (see e.g., [Trö10, Section 2.12.2]). Before we present it in detail, we will first define two stopping criteria.

(S1) `STOP` if the optimality condition $\|P(j')\| \approx \frac{1}{N}||P(j'_h)||_2 < TOL_{opt}$ with a tolerance $TOL_{opt} > 0$ and $P(j'_h)$ the discretized projected gradient, i.e.,

$$
\begin{aligned}
(P(j'_h))_n &= (P(\sigma(1,\dots,1)^T + \eta_z))_n \\
&= \begin{cases} \sigma + (\eta_z)_n, & \text{if } 0 < (z_{bc,l})_n < z_{bc,l}^{\max}, \\ \min(0, \sigma + (\eta_z)_n), & \text{if } (z_{bc,l})_n = 0, \\ \max(0, \sigma + (\eta_z)_n), & \text{if } (z_{bc,l})_n = z_{bc,l}^{\max}. \end{cases}
\end{aligned}
$$

(S2) `STOP` if the value of the cost functional does not change anymore, i.e., $|j_h(z_{bc,l}^k) - j_h(z_{bc,l}^{k+1})| < TOL_{\text{diff}}$, with a tolerance $TOL_{\text{diff}} > 0$.

The first criterion is related to almost satisfied optimality conditions. The second criterion, however, can occur whenever the step size $z_{bc,l}^{(k)} - z_{bc,l}^{(k+1)}$ tends to zero. This is the case, in particular, when the computed continuous gradient and the discrete gradient are too far apart. Thus if the algorithm stops due to the second criteria a refinement of the discretization is reasonable to assert convergence of the gradient used to determine the search direction.

**Algorithm 3.**
*Pick an initial control $z_{bc,l}^{(0)} \in \mathbb{R}^N$, where $N$ is the number of grid points in time. For $k = 0, 1, 2, \dots$ repeat the following steps until one of the above stopping criteria is fulfilled:*

1. *solve the constraints with control $z_{bc,l}^{(k)}$ to obtain the corresponding state variables $\rho^{(k)} = \rho(z_{bc,l}^{(k)})$, $z^{(k)} = z(z_{bc,l}^{(k)})$, $v^{(k)} = v(z_{bc,l}^{(k)})$, and $T_c^{(k)} = T_c(z_{bc,l}^{(k)})$;*

2. *solve the adjoint system with state variables $\rho^{(k)}, z^{(k)}, v^{(k)}, T_c^{(k)}$ to obtain the adjoint variables $\xi_\rho^{(k)}$, $\xi_z^{(k)}$, $\xi_v^{(k)}$, $\xi_{T_c}^{(k)}$, $\eta_z^{(k)}$;*

3. *use $\eta_z^{(k)}$ to compute the reduced gradient[10] $j'_h(z_{bc,l}^{(k)}) = \sigma + \eta_z^{(k)} \in \mathbb{R}^N$;*

4. *compute step length $\alpha$ via projected line search (Armijo rule[11] applied to $j_h(z_{bc,l})$);*

5. *set $z_{bc,l}^{(k+1)} = \min\left(z_{bc,l}^{\max}, \max\left(0, z_{bc,l}^{(k)} - \alpha j'_h(z_{bc,l}^{(k)})\right)\right)$ pointwise.*

[10] If the state and co-state variables fulfil the state and co-state equations respectively, then the gradient of the reduced cost functional and the optimality condition coincide.

[11] Details about the parameters choice for the line serach algorithm can be found in the Appendix D.5.

| | $\sigma = 0.01$ | | | $\sigma = 10$ | | |
|---|---|---|---|---|---|---|
| $N$ | $DQ_h$ | $j_h'(z_{bc,l}) \cdot \delta z_{bc,l}$ | $E_\epsilon$ | $DQ_h$ | $j_h'(z_{bc,l}) \cdot \delta z_{bc,l}$ | $E_\epsilon$ |
| 50 | -85.3 | -2052.5 | 1967.1 | 1579.7 | -387.4 | 1967.1 |
| 100 | -91.8 | -1964.9 | 1873.1 | 1573.2 | -299.9 | 1873.1 |
| 200 | -93.9 | -1876.2 | 1782.3 | 1571.1 | -211.2 | 1782.3 |
| 400 | -94.9 | -1835.9 | 1741.1 | 1570.1 | -170.9 | 1741.1 |
| 800 | -95.4 | -1810.9 | 1715.5 | 1569.6 | -145.9 | 1715.5 |
| 1600 | -95.7 | -1798.5 | 1702.7 | 1569.3 | -133.5 | 1702.7 |

Table 4.1.: Difference quotient ($DQ_h$) and discretized analytic gradient ($j_h'(z_{bc,l}) \cdot \delta z_{bc,l}$) for $\epsilon = 1$ and $z_{bc,l} = 0.1$.

It is easy to see that the algorithm is always terminating on any given fixed mesh, since $j_h$ is bounded from below, and by construction $j_h$ is non increasing. Thus after finitely many iterations stopping criterion (S2) must be satisfied. Once the mesh is refined, we can restart the algorithm on the new mesh. To avoid stopping of the algorithm due to the slope of the cost functional being to small, it is advisable to pick $TOL_{\text{diff}} = o(1)$ as $N \to \infty$, where $N$ is the number of temporal grid points.

### 4.6.3. Numerical test: Continuous vs. discrete gradient

In a first step, we test whether our implementation is correct. In particular, we test the implementation of the derivatives of $j_h$, as we use them as stopping criteria in our algorithm. To do so, we compare directional derivatives with difference approximations ($DQ_h$), i.e., we check

$$E_\epsilon = |DQ_h - j_h'(z_{bc,l}) \cdot \delta z_{bc,l}| = \left| \frac{j_h(z_{bc,l} + \epsilon \delta z_{bc,l}) - j_h(z_{bc,l})}{\epsilon} - j_h'(z_{bc,l}) \cdot \delta z_{bc,l} \right| \to 0$$

for various values of $\epsilon$. Before this, we first need to check the influence of the chosen discretization on $E_\epsilon$.

In Table 4.1, we calculated $DQ_h, j_h'(z_{bc,l}) \cdot \delta z_{bc,l}$ and $E_\epsilon$ for the values $(\delta z_{bc,l})_n = 1$ for all $n = 1, \ldots, N$ (unscaled $(\delta \tilde{z}_{bc,l})_n = 0.1$) for various values of spatial grid points $J$. Due to the CFL condition, this also leads to a refinement of the time mesh, i.e., $N = \mathcal{O}(J)$, where $N$ is the number of time grid points. As we can see, in Table 4.1, the difference quotient for $\epsilon = 1$ is relatively stable with respect to the mesh size. However, the calculated derivatives are still sensitive to mesh

refinement. This implies that even at $J = 1600$, we will have to expect effects of unresolved derivatives in our optimization algorithms. On the other hand, by comparing the subtables for $\sigma = 0.01$ and $\sigma = 10$, it is clear, that any numerical test for the correct implementation of the derivative will require a much more refined mesh in space and time.

**Remark 8.** *The reason why the error $E_\epsilon$ in Table 4.1 is constant for different values of $\sigma$, is that for all $\epsilon > 0$ we have*

$$\begin{aligned}
\epsilon E_\epsilon &= |j_h(z_{bc,l} + \epsilon\delta z_{bc,l}) - j_h(z_{bc,l}) - \epsilon j_h'(z_{bc,l}) \cdot \delta z_{bc,l}| \\
&= \left| j_h^{T_c}(z_{bc,l} + \epsilon\delta z_{bc,l}) - j_h^{T_c}(z_{bc,l}) + \sigma\frac{\epsilon}{N}\sum_{n=1}^{N}(\delta z_{bc,l})_n - \frac{\epsilon}{N}\sum_{n=1}^{N}(\sigma + (\eta_z)_n)(\delta z_{bc,l})_n \right| \\
&= \left| j_h^{T_c}(z_{bc,l} + \delta z_{bc,l}) - j_h^{T_c}(z_{bc,l}) - \frac{\epsilon}{N}\sum_{n=1}^{N}(\eta_z)_n(\delta z_{bc,l})_n \right|
\end{aligned}$$

*and thus, $E_\epsilon$ is independent of $\sigma$. Above, we denoted*

$$j_h^{T_c}(z_{bc,l}) := \sum_{i\in I_{cc}}\left(\frac{1}{2N}\sum_{n=1}^{N}\left((T_c^i)_n - T_{opt}\right)^2\right) \approx \sum_{i\in I_{cc}}\frac{1}{2}\int_0^{t_{end}}(T_c^i - T_{opt})^2 dt.$$

To avoid large influence of the discretization onto $E_\epsilon$ we note that the discretization error gets smaller if the end time $t_{\text{end}}$ is chosen smaller. Now, we have to look at the behavior of $E_\epsilon$ where $\tilde{t}_{\text{end}}$ is chosen between 1s and 2s.

In Figure 4.1, we see the behavior of the error between directional derivatives and difference quotients for various choices of simulation times $t_{\text{end}}$. As it is to be expected, the error $E_\epsilon = \mathcal{O}(\epsilon)$ for all values of $t_{\text{end}}$ as $\epsilon$ decreases. As standard numerical analysis reveals, at some point round-off errors become dominant, leading to a behavior $E_\epsilon = \mathcal{O}(\epsilon^{-1})$ as it can be seen in the graphic. We can see clearly that the point where round-off errors become dominate travels to larger $\epsilon$ as $t_{\text{end}}$ grows. However, at small final times, we can see that the error is small. Since the only change in the program is switching the value for the final time we conclude that our implementation yields correct values for the derivatives.

### 4.6.4. Numerical test: Convergence failure, refinement

As a next test, we come back to our statement at the beginning of Section 4.6. Namely, we investigate the effect of the inconsistent discretization on the behavior of the gradient projection algorithm. To this end, we consider the behavior of Algorithm 3 with the same initial value $z_{bc,l}^{(0)} = 0$ and $\sigma = 0.01$ for two different spatial (and thus also temporal) refinements. As we can see from Table 4.2, already

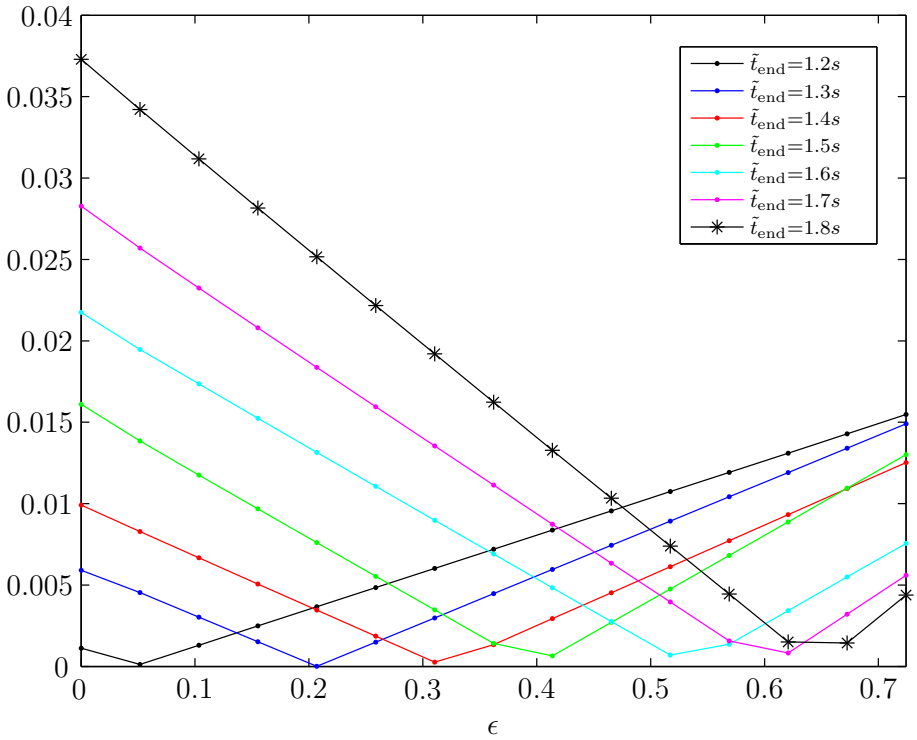


Figure 4.1.: Error $E_\epsilon$ between gradient and difference quotient

in the first iteration differences in the value of the cost functional are visible, this has to be expected from what we have seen in the previous test case, as the discretization error on the interval $(0, t_{\text{end}})$ is again significant. More importantly for the stopping criterion, the norm of the projected gradient differs significantly between the two meshes.

As predicted the algorithm becomes stagnant once the error in the calculated gradient approximation becomes too large, since we do not calculate the discrete derivatives. Already after the third iteration the value of the cost functional is almost unchanged during the application of Algorithm 3 for $J = 50$. However, the projected gradient is still large, i.e., $\frac{1}{N}\|P(j_h')\|_2 \geq 5 \cdot 10^{-3}$. On the other hand when $J = 1600$ we can continue until $\frac{1}{N}\|P(j_h')\|_2 \approx 5 \cdot 10^{-4}$ with significantly lower value of $j$ before the cost functional is again stagnant. This confirms our expectation on the convergence of the algorithm and the possible cure for a lack of convergence by means of refinement.

| | $J = 50$ | | $J = 1600$ | |
|---|---|---|---|---|
| iteration | $j_h$ | $\frac{1}{N}\|\|P(j_h')\|\|_2$ | $j_h$ | $\frac{1}{N}\|\|P(j_h')\|\|_2$ |
| 0 | 198.2154 | 0.0613 | 169.9120 | 0.0093 |
| 1 | 109.9411 | 0.0241 | 98.0908 | 0.0035 |
| 2 | 39.3864 | 0.0063 | 28.5489 | 0.0005 |
| 3 | 39.2464 | 0.0060 | 26.8061 | 0.0012 |
| 4 | 39.2349 | 0.0057 | 26.1496 | 0.0003 |
| 5 | 39.2349 | 0.0057 | 25.8218 | 0.0014 |
| 6 | - | - | 24.2810 | 0.0009 |
| 7 | - | - | 23.8705 | 0.0006 |
| 8 | - | - | 23.8574 | 0.0004 |
| 9 | - | - | 23.8574 | 0.0004 |

Table 4.2.: Results of the optimization algorithm for different numbers of spatial grid points $J$ (rounded to four digits)

## 4.7. Numerical examples

For all simulations, that will be presented in this section, we consider the same geometry of the exhaust pipe, which is illustrated in Figure 2.4. Furthermore, we still keep the same parameters as in the numerical simulations in Subsection 3.4.2. However, since we have to consider an additional equation for the temperature of the catalytic converter (recall Section 4.1) as well as a cost functional, we have four new model parameters in comparison to the previous chapter which are listed in Table 4.3.

| | **description** | **unit** | **value** |
|---|---|---|---|
| $\tilde{h}_c$ | heat exchange coefficient between gas and cat. converter | $\frac{\text{kg}}{\text{Kms}^3}$ | 100 |
| $\tilde{T}_{opt}$ | optimal temperature for the catalytic converter | K | 800 |
| $\tilde{t}_{\text{end}}$ | time horizon for optimal control | s | 60 |
| $\tilde{z}_{bc,l}^{\max}$ | upper bound for the control variable $\tilde{z}_{bc,l}$ | - | 0.5 |
| $\sigma$ | cost of the control variable | - | - |

Table 4.3.: Parameters that additionally appear in the context of the optimal control task

The initial conditions correspond to an engine start. For all pipes $i = 1, \ldots, 9$ and for all $\tilde{x} \in (0, \tilde{L}^i)$

$$\tilde{\rho}^i_{ic}(\tilde{x}) = 1.2\frac{\text{kg}}{\text{m}^3}, \quad \tilde{z}^i_{ic}(\tilde{x}) = 0, \quad \tilde{u}^i_{ic}(\tilde{x}) = 0\frac{\text{m}}{\text{s}}, \quad \tilde{T^i_{c,ic}} = 290.28\text{K}. \tag{4.44}$$

Recall, that these are the physical and not mathematical initial conditions for this problem. For our mathematical model (4.5), we need an initial condition for $\tilde{v}^i$. From the above conditions we can derive it by integration (see Equation (2.50)).

The boundary condition for the density for all $\tilde{t} \in [0, \tilde{t}_{\text{end}}]$ is given by

$$\tilde{\rho}_{bc,l}(\tilde{t}) = 0.4\frac{\text{kg}}{\text{m}^3}.$$

The pressure boundary conditions $\tilde{p}_{bc,l}$ and $\tilde{p}_{bc,r}$ are only physical boundary conditions. For the mathematical model (4.5) they are only parameters. However, for the sake of completeness we also state them here:

$$\tilde{p}_{bc,l}(\tilde{t}) = 1.01\text{bar} \qquad \text{and} \qquad \tilde{p}_{bc,r}(\tilde{t}) = 1\text{bar} \qquad \forall \tilde{t} \in [0, \tilde{t}_{\text{end}}].$$

The boundary condition for the ratio of unburnt gas will be declared in the next subsection, since it is used as the control variable.

We want to show results of two optimization problems we have simulated:

1. **Setting:** High cost of control, high starting control.
   **Expectation:** A decrease of ratio of unburnt gas $z_{bc,l}$ is more important than achieving an optimal temperature in the catalysts.

2. **Setting:** Low cost of control, low starting control.
   **Expectation:** The control variable $z_{bc,l}$ should be increased in order to reach optimal temperature in the catalysts.

### 4.7.1. Example 1: High cost of control, high starting control

The cost of control $\sigma$ and the value for the first guess of the control variable $z_{bc,l}$ (the boundary condition for the ratio of unburnt gas) for this simulation are

$$\sigma = 20, \qquad \tilde{z}_{bc,l}(\tilde{t}) = 0.15 \;\; \forall \tilde{t} \in [0, \tilde{t}_{\text{end}}].$$

The results of the simulation are illustrated in Table 4.4 and Figure 4.2. The first figure shows the mapping $\tilde{t} \mapsto \tilde{z}_{bc,l}(\tilde{t})$. The two other mappings show the temperature development over time in the two catalytic converters (pipe 2 and 4).

The table shows the evaluation of the cost functional for the iterations done by the algorithm. We split the cost functional as follows

$$j_h = \sigma j_h^z + \sum_{l \in I_{cc}} j_h^{T_c^l},$$

$$j_h^z := \frac{t_{\text{end}}}{M} \sum_{m=1}^{M} (z_{bc,l})_m \approx \int_0^{t_{\text{end}}} z_{bc,l}(t)dt,$$

$$j_h^{T_c^i} := \frac{t_{\text{end}}}{2M} \sum_{m=1}^{M} ((T_c^i)_m - T_{opt})^2 \approx \frac{1}{2} \int_0^{t_{\text{end}}} (T_c^i(t) - T_{opt})^2 dt.$$

Since the unscaled values are quite large and therefore demand a lot of space, we display only the scaled quantities in the tables. The key quantities like relation between initial and final cost and the optimality conditions, will retain their informative value, despite scaling.

| iteration | $j_h$ | $j_h^z$ | $j_h^{T_c^2}$ | $j_h^{T_c^4}$ | $\frac{1}{M}\|\|P(j_h')\|\|$ |
|---|---|---|---|---|---|
| **0** | **5042.791** | **250** | **17.842** | **24.948** | **0.01698** |
| **1** | **169.912** | **0** | **36.764** | **133.149** | **0** |

Table 4.4.: Example 1: Evaluation of the scaled cost functional (rounded to three decimal places) and optimality condition (rounded to five decimal places) for different control variables $\tilde{z}_{bc,l}$, computed by the optimization algorithm. (Compare Figure 4.2 for corresponding control)

We observe that after one iteration the optimization algorithm stops, since the optimality condition is fulfilled. Due to the high cost of the control, the optimal solution is $\tilde{z}_{bc,l}(\tilde{t}) = 0$ for all $\tilde{t} \in [0, \tilde{t}_{\text{end}}]$. This means for our application, that one should use at least the stoichiometric amount of air in the combustion chamber of the engine, i.e., enough air for a complete combustion of the fuel, such that no unburnt gas enters the pipe. In other words, fuel is so expensive, it should not be used for heating up the catalytic converters.

In Figure 4.3, we can see the steady state solutions of the state variables for the initial control (black dotted lines) and the optimal control (green dashed lines). The grey lines show the geometry of the exhaust pipe and the filled rectangles illustrate the catalysts.

The first two plots of Figure 4.3 show the velocity and ratio of unburnt gas in the exhaust pipe at the end time $\tilde{t}_{\text{end}}$, respectively. In the first iteration (black dotted line), we have a concentration of 0.15 at the boundary condition for the unscaled ratio of unburnt gas, which decreases in both catalytic converters during

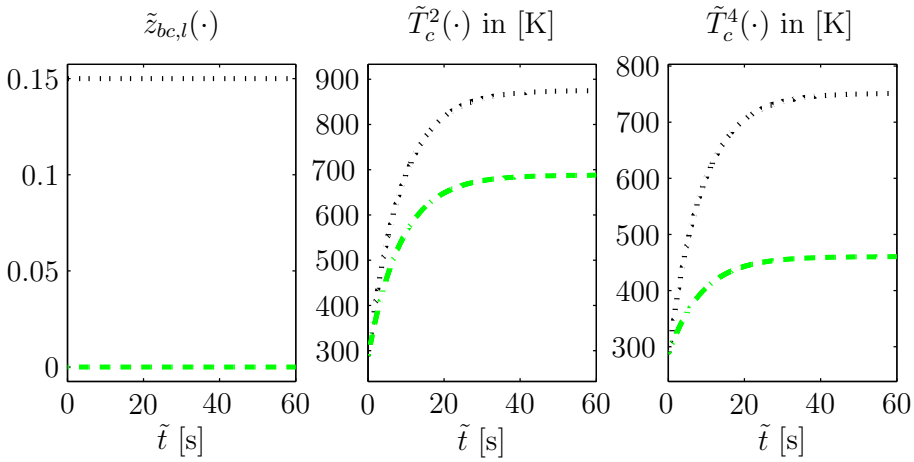


Figure 4.2.: Example 1: Boundary condition for ratio of unburnt gas $\tilde{z}$ and temperatures in the catalytic converters $\tilde{T}_c^i$ in [K] for some iterations (Compare Table 4.4 for corresponding evaluation of the cost functional)

the exothermic reaction. The temperature (third plot) increases in the catalytic converters, in the case in which we have a positive concentration of unburnt gas, and decreases over the whole exhaust pipe due to the heat exchange with the (colder) wall.

### 4.7.2. Example 2: Low cost of control, low starting control

The cost of control $\sigma$ and the value for the first guess of the control variable $\tilde{z}_{bc,l}$ (the boundary condition for the ratio of unburnt gas) for this simulation are

$$\sigma = 0.01, \qquad \tilde{z}_{bc,l}(\tilde{t}) = 0 \;\; \forall \tilde{t} \in [0, \tilde{t}_{\text{end}}].$$

The results of the simulation are illustrated in the Table 4.5 and Figure 4.4. In this scenario (fuel is cheap), the optimization algorithm suggests to use more of fuel. After 9 iterations this yields our "optimal" control, although the stopping criterion which led to the abortion of the algorithm, was the second criterion (S2) (no change of the cost functional due to 20 line search attempts, $TOL_{\text{diff}} = 10^{-5}$). Nevertheless, the obtained control leads to a fast heating to a temperature close to the optimal $\tilde{T}_{opt} = 800K$ in both catalytic converters, i.e., from the application's point of view: a satisfying result.

With simple programming techniques, a further refinement is not applicable on the used PC[12]. The number of spatial ($J = 1,600$) and temporal ($N = 1,677,244$) unknowns is close to the limit of the storage capacity. Another refinement would exceed those limitations.

[12] We used Matlab 8.1.0.604 on an Intel(R) Core(TM) i5 CPU @2.67 GHz with 8 GB of RAM.

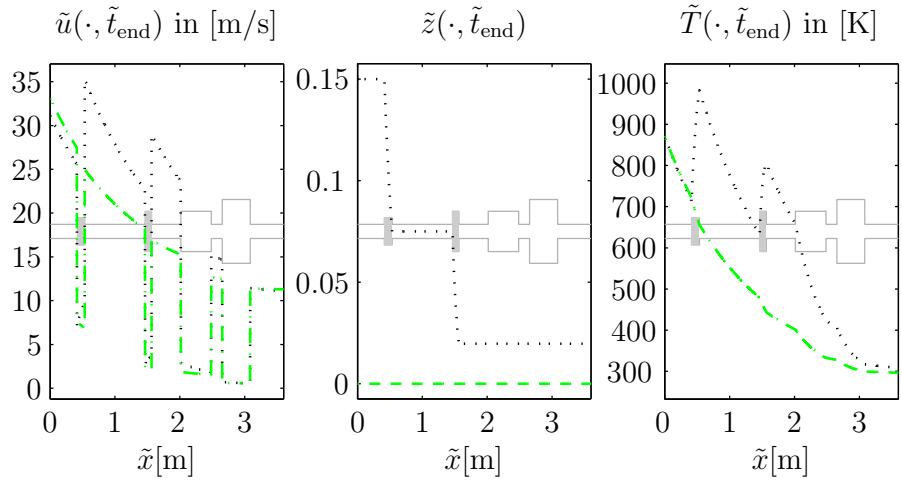


Figure 4.3.: Example 1: Results of numerical simulation of the state variables velocity $\tilde{u}$ in $[\frac{\text{m}}{\text{s}}]$, ratio of unburnt gas $\tilde{z}$ and gas temperature $\tilde{T}$ in [K] at time $\tilde{t}_{\text{end}} = 60s$ (compare colors given in Table 4.4)

## 4.8. Summary

In this chapter, we were able to answer the question, how to ensure reaching an optimal temperature in a catalytic converter of an exhaust pipe after the engine start by controlling the ratio of unburnt gas in the gas mixture.

After the introduction of an additional ODE to model the temperature evolution in the catalytic converter (Section 4.1) and the formulation of the optimal control problem (Section 4.2), we followed the first-optimize-then-discretize approach and derived the necessary first order optimality conditions. Undeniably, this is a major effort and spreads out on several pages (also in the appendix). However, once having done this we were able to produce convincing numerical results in the context of the application (see Subsection 4.7.2).

From the mathematical point of view we faced some issues, such as stagnation of the projected gradient algorithm due to insufficient resolution of the differential equations, which can thus be healed by refinement of the discretization (see Subsection 4.6.4). On the other hand, from the application's point of view, the results are physically very meaningful and give an answer how to improve the heating process of the catalytic converts after the engine start.

Of course, a delicate task would be to determine the parameter $\sigma$ which represents the cost of control. We comment on this issue in the following Chapter Summary and Outlook.

| iteration | $j_h$ | $j_h^z$ | $j_h^{T_c^2}$ | $j_h^{T_c^4}$ | $\frac{1}{M}\|\|P(j_h')\|\|$ |
|---|---|---|---|---|---|
| **0** | **169.912** | **0** | **36.765** | **133.148** | **0.00933** |
| **1** | **98.091** | **482.276** | **51.327** | **41.941** | **0.00347** |
| **2** | **28.549** | **317.238** | **15.390** | **9.986** | **0.00058** |
| 3 | 26.806 | 282.716 | 10.502 | 13.477 | 0.00130 |
| **4** | **26.150** | **333.782** | **14.747** | **8.065** | **0.00035** |
| **5** | **25.822** | **266.863** | **8.843** | **14.310** | **0.00139** |
| **6** | **24.281** | **283.835** | **9.858** | **11.584** | **0.00091** |
| **7** | **23.870** | **295.016** | **10.702** | **10.219** | **0.00061** |
| 8 | 23.857 | 302.555 | 11.346 | 9.486 | 0.00042 |
| **9** | **23.857** | **302.555** | **11.346** | **9.486** | **0.00042** |

Table 4.5.: Example 2: Evaluation of the scaled cost functional (rounded to three decimal places) and optimality condition (rounded to five decimal places) for different control variables $z_{bc,l}$, computed by the optimization algorithm. (Compare figure 4.4 for corresponding control)

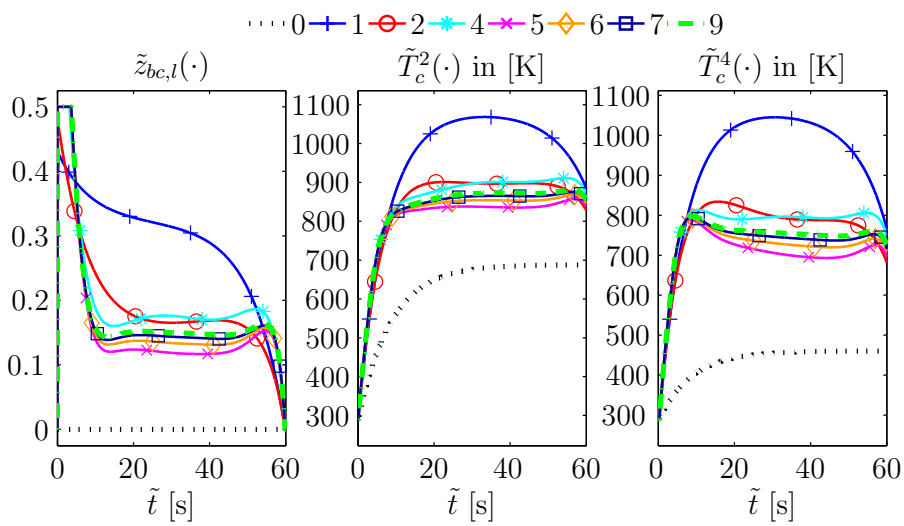


Figure 4.4.: Example 2: Boundary condition for ratio of unburnt gas $\tilde{z}$ and temperatures in the catalytic converters $\tilde{T}_c^i$ in [K] for some iterations (Compare Table 4.5 for corresponding evaluation of the cost functional)

# 5. Summary and outlook

In this thesis we proposed a new asymptotic model (AM) to describe the transient gas dynamics in a car's exhaust pipe. We verified it by numerical experiments and used it to solve an optimal control task related to exhaust gas flow.

Each major chapter, dealing with modelling, numerical simulations and optimization, ended with a summary. However, we give here a short overview of the content of each chapter anyway:

In Chapter 2 we began with the presentation of a promising hyperbolic model, which was derived by Lacoste and Natalini in [LN04] and is based on the reactive Euler equations of gas dynamics. We discussed its drawbacks, which resulted in large computing times. Those were a space dependent cross section function and the fact that the model includes information about the propagation of sound waves, which are, depending on the type of application, not necessarily relevant. The key steps of the derivation of our new asymptotic models were a network approach and a low Mach number limit. Due to the first step describing the pipe's geometry with a space dependent function became unnecessary, whereas the limit process ruled out sound waves.

In Chapter 3 we were able to construct the unique solution of a simplified stationary problem, which originated from our newly derived asymptotic model. We used this result to numerically verify the correctness of the proposed algorithm for AM. We also compared the results of our asymptotic model with the established hyperbolic model FE on a network. In particular we saw that the numerical results of both models are close to each other if the Mach number is small. Furthermore, we could confirm numerically and analytically that neglecting sound waves gave the asymptotic model a huge advantage with respect to computing times.

Lastly, we considered an optimization task in Chapter 4. The aim was to optimally control the inflow boundary condition for the ratio of unburnt gas, such that the catalytic converter heats up as fast as possible. In order to apply a projected gradient method for the numerical realization, we derived the gradient via adjoint calculus. Although there were issues concerning the discretization, we were able to obtain reasonable results from this approach.

In the end, this thesis can be seen as a prototype example of how to derive a numerically efficient model for fluid flow in a low Mach number regime on a network of pipes and use it to solve optimization tasks. Hence, this "modelling, simulation and optimization" framework could be applied to several related real

world problems, e.g., the propagation of fire in tunnels, flow in an energy tower, etc.

Clearly, there are a lot of open problems for future research:

**Inclusion of secondary air and mufflers (Modelling).** The intake of secondary air[1] is not described in our model. This could be modeled by a source term in the mass equation. Moreover, the mufflers were not considered in the description of the exhaust gas flow, either. We could include their physical influence, at least in the case of damping material in the mufflers, by an additional local friction term. However, the inclusion of such terms would demand to determine the corresponding parameters. Therefore, experimental data would be needed.

**Extension of the results on the existence and uniqueness of stationary solution (Theory).** The existence of stationary solutions is only shown for a simple setting. On a network we proved unique existence without considering heat exchange, minor loss terms and catalytic converters.

**Stability in the case of non-uniqueness of stationary solutions (Theory).** The inclusion of the heat exchange in the study of the stationary problem led to non-unique solutions (see Subsection 3.2.1). One could try to investigate the transient stability of the two different stationary solution. Maybe, this study could give a meaning to the less intuitive solution where we have a negative flow direction despite a positive pressure difference. Stability of stationary solutions in the related tunnel fire setting was studied in [GS06a].

**Parameter identification with the help of data from real experiments (Optimal control).** If, for instance, one would expand the model by inclusion of a source term that models the inflow of secondary air and/or a friction term that describes the flow dynamics in the mufflers, one would have to identify parameters, such as a friction coefficient. Having real experimental data, one could identify such model parameters by solving an inverse problem with similar techniques as those presented in Chapter 4.

**The determination of the parameter $\sigma$, which represents the cost of control in the cost functional** (4.10) **(Modelling).** One would have to investigate the cost of fuel consumption and relate it the cost caused non-optimal temperature conditions in the catalytic converters. Whereas the first task should be feasible, the determination of the related penalization factor for the tracking-type functional is everything, but trivial. The influence of the temperature on the emission of harmful gases, such as the connected environmental damage caused by it, would have to be expressed by a scalar "financial" value in the cost functional.

[1] Recall Section 2.1.

# Bibliography


[BGH11] Brouwer, J., Gasser, I., and Herty, M.: *Gas pipeline models revisited: Model hierarchies, nonisothermal models, and simulations of networks.* Multiscale Modeling and Simulation, 9:601–623, 2011.

[BHK06] Banda, M.K., Herty, M., and Klar, A.: *Coupling conditions for gas networks governed by the isothermal euler equations.* Networks and Heterogeneous Media, 1:295–314, 2006.

[BHT+] Braun, J., Hauber, T., Többen, H., Windmann, J., Zacke, P., Chatterjee, D., Correa, C., Deutschmann, O., Maier, L., Tischer, S., and Warnatz, J.: *Three-dimensional simulation of the transient behavior of a three-way catalytic converter.* 2002 Society of Automotive Engineers, Inc.

[BK14] Borsche, R. and Klar, A.: *Flooding in urban drainage systems: Coupling hyperbolic conservation laws for sewer systems and surface flow.* ArXiv e-prints, 1402.4254, 2014.

[CCDD03] Chakravarthy, V.K., Conklin, J.C., Daw, C.S., and D'Azevedo, E.F.: *Multidimensional simulation of cold-startet transient in a catalytic converter under steady inflow conditions.* Applied Catalysis A, 241:289–306, 2003.

[CF01] Cumberbatch, E. and Fitt, A.: *Mathematical Modeling - Case Studies from Industry.* Cambridge University Press, 2001.

[CH99] Chan, S.H. and Hoang, D.L.: *Heat transfer and chemical reactions in exhaust system of a cold-start engine.* International Journal of Heat and Mass Transfer, 42:4165–4183, 1999.

[CIR52] Courant, R, Isaacson, E., and Rees, M.: *On the solution of nonlinear hyperbolic differential equations by finite differences.* Communications on Pure and Applied Mathematics, 5:243–255, 1952.

[CP09] Codina, R. and Principe, J.: *Mathematical models for thermally coupled low speed flows.* Advances in Theoretical and Applied Mechanics, 2:93 – 112, 2009.

[Cra82] Crane Company: *Flow of Fluids Through Valves, Fittings, and Pipe - Technical Paper No. 410.* Crane Valves, 1982.

[CS08] Chauhan, S. and Srivastava, V.K.: *Modeling exhaust gas pollution abatement: Part I - single hydrocarbon propylene.* Computers & Mathematics with Applications, 55:319–330, 2008.

[DFO00] D'Errico, G., Ferrari, G., and Onorati, A.: *Numerical modeling of unsteady reacting flows in the exhaust system of a s.i. engine including the catalytic converter.* In *Seoul 2000 FISITA World Automotive Congress*, 2000.

[FKP10] Frank, M., Klar, A., and Pinnau, R.: *Optimal control of glass cooling using simplified $P_N$ theory.* Transport Theory and Statistical Physics, 39:282–311, 2010.

[FL94] Friedman, A. and Littman, W.: *Industrial Mathematics - A course in Solving Real-World Problems.* Society for Industrial and Applied Mathematics, 1994.

[For84] Forster, O.: *Analysis 3.* Vieweg, 1984.

[FW66] Fickett, W. and Wood, W.W.: *Flow calculus for pulsating one dimensional detonation.* Physics of Fluids, 9:903–916, 1966.

[GB12] Gasser, I. and Bauer, M.: *Modeling, asymptotic analysis, and simulation of an energy tower.* SIAM Journal of Applied Mathematics, 72:362–381, 2012.

[GF13] Gasser, I. and Felaco, E.: *Modelling, asymptotic analysis and simulation of the gas dynamics in a chimney.* Journal of Mathematics in Industry, 3:3, 2013.

[GHH10] Geringer, B., Hofmann, P., and Holub, R.: *Verbesserung des Hochlaufs und des Emissionsverhaltens im Kaltstart und Warmlauf bei Ottomotoren.* MTZ - Motortechnische Zeitschrift, 71:368 – 372, 2010.

[GHKL05] Gugat, M., Herty, M., Klar, A., and Leugering, G.: *Optimal control for traffic flow networks.* Journal of Optimization Theory and Applications, 126:589–616, 2005.

[GK99] Geiger, C. and Kanzow, C.: *Numerische Verfahren zur Lösung unrestringierter Optimierungsaufgaben.* Springer, 1999.

[GK08] Gasser, I. and Kraft, M.: *Modelling and simulation of fires in tunnels.* Networks and Heterogeneous Media, 3:691–707, 2008.

[GR13] Gasser, I. and Rybicki, M.: *Modelling and simulation of gas dynamics in an exhaust pipe.* Applied Mathematical Modelling, 37:2747–2764, 2013.

[GRS07] Großmann, C., Roos, H. G., and Stynes, M.: *Numerical Treatment of Partial Differential Equations.* Springer, 2007.

[GRW11] Goll, C., Rannacher, R., and Wollner, W.: *The damped Crank-Nicolson time-marching scheme for the adaptive solution of the Black-Scholes equation.* accepted in Journal of Computational Finance, 2011.

[GRW14a] Gasser, I., Rybicki, M., and Wollner, W.: *Modelling, simulation and optimization of gas dynamics in an exhaust pipe.* In *Hyperbolic Problems: Theory, Numerics, Applications (Proceedings of the 14th International Conference on Hyperbolic Problems held in Padova, June 25–29, 2012)*, 8:907–914, 2014.

[GRW14b] Gasser, I., Rybicki, M., and Wollner, W.: *Optimal control of the temperature in a catalytic converter.* Computers & Mathematics with Applications, 67:1521–1544, 2014.

[GS02] Gasser, I. and Struckmeier, J.: *An asymptotic-induced one-dimensional model to describe fires in tunnels.* Mathematical methods in the applied sciences, 25:1231–1249, 2002.

[GS06a] Gasser, I. and Steinrück, H.: *An asymptotic one-dimensional model to describe fires in tunnels III.* SIAM Journal of Applied Mathematics, 66:2187–2203, 2006.

[GS06b] Gasser, I. and Steinrück, H.: *On the existence of transient solutions of a tunnel fire model.* Communications in Mathematical Sciences, 4:609–619, 2006.

[Gun02] Gunzburger, M.: *Perspectives in Flow Control and Optimization.* SIAM, 2002.

[GV99] Guillarda, H. and Viozata, C.: *On the behaviour of upwind schemes in the low Mach number limit.* Computers & Fluids, 28:63 – 86, 1999.

[Hag00] Hager, W. W.: *Runge-kutta methods in optimal control and the transformed adjoint system.* Numerische Mathematik, 87:247–282, 2000.

[HDRD11] Hornikx, M., De Roeck, W., and Desmet, W.: *Flow and geometrical effects on radiated noise from exhausts computed by a hybrid extended Fourier PSTD method.* In *17th AIAA/CEAS Aeroacoustics Conference (32nd AIAA Aeroacoustics Conference)*, 2011.

[HPUU09] Hinze, M., Pinnau, R., Ulbrich, M., and Ulbrich, S.: *Optimization with PDE Contraints.* Springer, 2009.

[HS07] Herty, M. and Sachers, V.: *Adjoint calculus for optimization of gas networks.* Networks and Heterogeneous Media, 2:733–750, 2007.

[JW98] Jakubauskas, V.F. and Weaver, D.S.: *Transverse vibrations of bellows expansion joints - Part I and II.* Journal of fluid and structures, 12:445–473, 1998.

[KM82] Klainerman, S. and Majda, A.: *Compressible and incompressible fluids.* Communications on Pure and Applied Mathematics, 35:629–651, 1982.

[KSGF09] Kwatra, N., Su, J., Grétarsson, J. T., and Fedkiw, R.: *A method for avoiding the acoustic time step restriction in compressible flow.* Journal of Computational Physics, 228:4146 – 4161, 2009.

[LeV92] LeVeque, R. J.: *Numerical methods for conservation laws.* Birkhäuser, 1992.

[LeV02] LeVeque, R. J.: *Finite Volume Methods for Hyperbolic Problems.* Cambridge Texts in Applied Mathematics, 2002.

[Lin94] Ling, S. F.: *Vibration isolation of exhaust pipe under vehicle chassis.* International Journal of Vehicle Design, 15:131–142, 1994.

[Lio98] Lions, P. L.: *Mathematical Topics in Fluid Dynamics, Volume 2. Compressible Models.* Oxford University Press, 1998.

[Liu82] Liu, T. P.: *Transonic gas flow in a duct of varying area.* Archive for Rational Mechanics and Analysis, 80:1–18, 1982.

[LN04] Lacoste, L. and Natalini, R.: *Mathematical modeling of chemical processes in exhaust pipe.* Technical report, IAC Rome, 2004.

[LT11] Lianga, S. M. and Taib, S. M.: *Analysis and prediction of shock-induced near-field acoustics from an exhaust pipe.* Computers & Fluids, 45:222–232, 2011.

[LTW09] Liang, S. M., Tsai, S. J., and Wang, S. F.: *An effective approach for calculation of exhaust pipe flows.* Journal of Mechanics, 25:177–188, 2009.

[Mei99] Meister, A.: *Asymptotic single and multiple scale expansions in the low Mach number limit.* SIAM Journal of Applied Mathematics, 60:256–271, 1999.

[MSZH11] Menina, R., Saurel, R., Zereg, M., and Houas, L.: *Modelling gas dynamics in 1D ducts with abrupt area change.* Shock Waves, 21:451–466, 2011.

[Mul04] Mulley, R.: *Flow of Industrial Fluids - Theory and Equations.* CRC Press, 2004.

[NW06] Nocedal, J. and Wright, S. J.: *Numerical Optimization.* Springer, 2006.

[Pet07] Petrucci, R.: *Un modello matematico di combustione dei gas di scarico in marmitte catalitiche.* Master's thesis, Roma Tre - Universit delgi studi, 2007.

[Rja95] Rjasanow, S.: *Heat transfer in an insulated exhaust pipe.* Journal of Engineering Mathematics, 29:33–49, 1995.

[Rog14] Roggensack, A.: *Low Mach number equations with a heat source on networks - Modelling and analysis.* PhD thesis, University of Hamburg, 2014.

[SK11] Schwarz, H. R. and Köckler, N.: *Numerische Mathematik.* Vieweg, 2011.

[SMT93] Sesterhenn, J., Müller, B., and Thomann, H.: *Flux-vector splitting for compressible low Mach number flow.* Computers & Fluids, 22:441–451, 1993.

[SMT99] Sesterhenn, J., Müller, B., and Thomann, H.: *On the cancellation problem in calculating compressible low Mach number flows.* Journal of Computational Physics, 151:597–615, 1999.

[SW81] Steger, J. L. and Warming, R. F.: *Flux vector splitting of the inviscid gas dynamics equations with application to finite-difference methods.* Journal of Computational Physics, 40:263–293, 1981.

[Tor09] Toro, E. F.: *Riemann Solvers and Numerical Methods for Fluid Dynamics: A Practical Introduction.* Springer, 2009.

[Trö10] Tröltzsch, F.: *Optimal Control of Partial Differential Equations: Theory, Methods, and Applications.* Graduate Studies in Mathematics. American Mathematical Society, 2010.

[vBS05] Basshuysen, R. van and Schäfer, F.: *Handbuch Verbrennungsmotor.* Vieweg, 2005.

[Whi74] Whitham, G.B.: *Linear and Nonlinear Waves (Pure and Applied Mathematics).* Wiley-Interscience, 1974.

[Whi79] White, F.M.: *Fluid Mechanics.* Mcgraw-Hill College, 1979.

# A. Nomenclature

| Reference values | | | |
|---|---|---|---|
| **quantity** | **unit** | **reference quantity** | **reference value** |
| $\tilde{t}$ | s | $\tilde{t}_{\text{ref}} = \tilde{x}_{\text{ref}}/\tilde{u}_{\text{ref}}$ | 0.36 |
| $\tilde{x}$ | m | $\tilde{x}_{\text{ref}} = \tilde{L}$ | 3.6 |
| $\tilde{\rho}$ | kg/m$^3$ | $\tilde{\rho}_{\text{ref}}$ | 1.2 |
| $\tilde{u}$ | m/s | $\tilde{u}_{\text{ref}}$ | 10 |
| $\tilde{p}$ | kg/(ms$^2$) | $\tilde{p}_{\text{ref}}$ | $10^5$ |
| $\tilde{T}$ | K | $\tilde{T}_{\text{ref}} = \tilde{p}_{\text{ref}}/(R\tilde{\rho}_{\text{ref}})$ | 290.28 |
| $\tilde{z}$ | - | $\tilde{z}_{\text{ref}}$ | 0.1 |

| | |
|---|---|
| $\tilde{y}$ | unscaled variable (see Section 2.5.1 for details on scaling) |
| $y$ | scaled variable (see Section 2.5.1 for details on scaling) |
| $y^i$ | variable in the $i$-th pipe |
| $y_l, y_r$ | left and right spatial evaluation of the variable |
| $y_{ic}$ | initial condition for the variable $y$ |
| $y_{bc,l}, y_{bc,r}$ | left and right boundary condition for the variable $y$ |
| $y_0, y_1$ | zeroth or first order term of variable's $y$ asymptotic expansion (2.37) |
| $y_h$ | discretization of the continuous variable $y$ |

Dimensionless parameters and index set $I_{cc}$:

$$C_f^i := \frac{\xi \tilde{x}_{\text{ref}}}{\tilde{d}^i}, \qquad C_c := \frac{\tilde{C}_c \tilde{x}_{\text{ref}}}{\tilde{u}_{\text{ref}}}, \qquad \gamma - 1 = \frac{\tilde{R}}{\tilde{c}_v},$$

$$h^i := \frac{4\tilde{h}\tilde{x}_{\text{ref}}}{\tilde{d}^i \tilde{\rho}_{\text{ref}} \tilde{u}_{\text{ref}} c_v}, \quad q_0 := \frac{\tilde{\rho}_{\text{ref}} \tilde{z}_{\text{ref}} \tilde{q}_0 R}{\tilde{p}_{\text{ref}} c_v}, \qquad K(T) := \frac{\tilde{x}_{\text{ref}}}{\tilde{u}_{\text{ref}}} \tilde{K}(\tilde{T}_{\text{ref}} T),$$

$$h_c := \frac{\tilde{h}_c \tilde{x}_{\text{ref}}}{\tilde{\rho}_{\text{ref}} \tilde{u}_{\text{ref}} c_v}, \qquad I_{cc} := \left\{ i \in \{1, \ldots, n_P\} \mid \chi^i = 1 \right\}.$$

| Variables and Functions | | | |
|---|---|---|---|
| | **description** | **unit** | **ref.** |
| $\tilde{x}$ | spatial coordinate | m | - |
| $\tilde{t}$ | time coordinate | s | - |
| $\tilde{A}(\tilde{x})$ | pipe's cross section area at point $\tilde{x}$ | $m^2$ | (2.4) |
| $\tilde{r}(\tilde{x})$ | pipe's radius at point $\tilde{x}$ | m | (2.5) |
| $\tilde{d}(\tilde{x})$ | pipe's diameter at point $\tilde{x}$ | m | (2.4) |
| $\tilde{\chi}_f(\tilde{x})$ | indicator function, denotes whether $\tilde{x}$ is inside or outside catalytic converter | - | (2.8) |
| $\tilde{\chi}^i$ | indicator mapping, denotes whether pipe $i$ has a converter | - | (2.1) |
| $\tilde{\rho}(\tilde{x},\tilde{t})$ | density of the exhaust gas | $kg/m^3$ | - |
| $\tilde{u}(\tilde{x},\tilde{t})$ | velocity of the exhaust gas | m/s | - |
| $\tilde{p}(\tilde{x},\tilde{t})$ | pressure of the exhaust gas | $kg/(ms^2)$ | - |
| $\tilde{T}(\tilde{x},\tilde{t})$ | temperature of the exhaust gas | K | - |
| $\tilde{z}(\tilde{x},\tilde{t})$ | ratio of unburnt gas in the exhaust gas | - | - |
| $\tilde{T}_c(\tilde{t})$ | temperature of the catalytic converter | K | - |
| $\tilde{T}_{\text{Wall}}(\tilde{x},\tilde{t})$ | pipe's wall temperature | K | (2.11) |
| $\tilde{T}_{\text{Gas}}(\tilde{t})$ | spatial average of the gas temperature | K | (4.1) |
| $\tilde{K}(\tilde{T}(\tilde{x},\tilde{t}))$ | temperature depending reaction rate, modelled by *Arrhenius'* law | $s^{-1}$ | (2.7) |
| $P, \text{sgn}$ | maps that describe geometrical relations of pipes in a network | - | (2.17) |
| | | - | (2.18) |
| $\tilde{f}^j_{ext}(t)$ | pressure loss term at junction $j$ | $kg/(ms^2)$ | (2.31) |
| $p_1(x,t)$ | mechanical pressure component | - | - |
| $q(x,t), Q(x,t)$ | (aggregated) energy gain and loss term | - | (2.46) |
| $v(t)$ | space-independent velocity component | - | (2.47) |

| Parameters | | | |
|---|---|---|---|
| | **description** | **unit** | **value** |
| $\tilde{C}_c$ | friction coefficient in the catalytic converters | 1/s | 800 |
| $\tilde{c}_v$ | specific heat at constant volume of the exhaust gas | $m^2/(Ks^2)$ | 717.7 |
| $\tilde{h}$ | heat exchange coefficient between gas and pipe's wall | $m^2/(Ks^2)$ | 100 |
| $\tilde{h}_c$ | heat exchange coefficient between gas and catalytic converter | $m^2/(Kms^2)$ | 100 |
| $\tilde{K}_0$ | pre-exponential factor in *Arrhenius'* law | 1/s | 100 |
| $\tilde{L}$ | length of the whole exhaust pipe | m | 3.6 |
| $M$ | Mach number of the fluid | - | - |
| $n_P$ | number of pipes with constant cross section | - | 9 |
| $n_V$ | number of junctions between pipes | - | 8 |
| $\tilde{p}_0$ | thermodynamic pressure component | $kg/(ms^2)$ | $10^5$ |
| $\tilde{q}_0$ | specific heat release coefficient of the exothermic reaction in the catalysts | $m^2/s^2$ | $5 \cdot 10^6$ |
| $\tilde{R}$ | ideal gas constant | $m^2/(Ks^2)$ | 287.08 |
| $\tilde{T}^+$ | activation temperature of the exothermic reaction in catalyst | K | 600 |
| $\tilde{T}_{opt}$ | optimal temperature of a catalytic converter | K | 800 |
| $\tilde{T}_{out}$ | outside temperature | K | 290.28 |
| $\tilde{z}_{bc,l}^{\max}$ | upper bound for the control variable $\tilde{z}_{bc,l}$ | - | 0.15 |
| $\gamma$ | adiabatic exponent of the exhaust gas | - | 1.4 |
| $\xi$ | wall friction coefficient | - | 0.0241 |

# B. Modelling

## B.1. The influence of the term $A_x p$

Let us assume the momentum equation has the following shape

$$(\tilde{A}\tilde{\rho}\tilde{u})_{\tilde{t}} + (\tilde{A}\tilde{\rho}\tilde{u}^2)_{\tilde{x}} + (\tilde{A}\tilde{p})_{\tilde{x}} = 0.$$

The integral of the third term $(\tilde{A}\tilde{p})_{\tilde{x}}$ over an arbitrary interval $[\tilde{x}_1, \tilde{x}_2] \subset [0, \tilde{L}]$ would represent the surface pressure $\tilde{F}_s$.

$$\tilde{F}_s = \int_{\tilde{x}_1}^{\tilde{x}_2} \left( \tilde{A}(\tilde{x})\tilde{p}(\tilde{x}, \tilde{t}) \right)_{\tilde{x}} d\tilde{x}.$$

Assuming the pressure is constant in space and time, we would deduce with the Fundamental Theorem of Calculus

$$\tilde{F}_s = \tilde{p}_{const} \left( \tilde{A}(\tilde{x}_2) - \tilde{A}(\tilde{x}_1) \right).$$

Hence, if the pipe's cross section area is not constant, the surface force would not vanish, even though the pressure is constant. This would imply a non-physical mass flow.

Therefore, we need a correction term, that makes the surface pressure forces vanish, if the pressure is constant. This corrective force is the one that acts on the fluid in case of contraction or expansions of the considered pipe and is modeled by

$$\tilde{F}_{s,\text{correction}} = -\int_{\tilde{x}_1}^{\tilde{x}_2} \tilde{A}_{\tilde{x}}(\tilde{x})\tilde{p}(\tilde{x}, \tilde{t}) d\tilde{x}.$$

Then our corrected surface pressure force is

$$\tilde{F}_{s,\text{corrected}} = \tilde{F}_s + \tilde{F}_{s,\text{correction}} = \int_{\tilde{x}_1}^{\tilde{x}_2} \tilde{A}(\tilde{x})\tilde{p}_{\tilde{x}}(\tilde{x}, \tilde{t}) d\tilde{x}.$$

If the pressure is constant now, the surface pressure force vanishes, and we describe the right physical behaviour with our equation.

## B.2. Different formulations of the model of Lacoste and Natalini

This section is just relevant, if you want to study the scientific report by Lacoste and Natalini from 2004. The notation of the system (2.14) does not correspond to the one on [LN04]. We explain the differences:

The model in [LN04] on Page 31 is (besides the $\sim$ on top of the variables) the following:

$$\begin{aligned}
\tilde{\rho}_{\tilde{t}} + (\tilde{\rho}\tilde{u})_{\tilde{x}} &= -\frac{\tilde{A}_x}{\tilde{A}}\tilde{\rho}\tilde{u}, \\
(\tilde{\rho}\tilde{u})_{\tilde{t}} + (\tilde{\rho}\tilde{u}^2 + \tilde{p})_{\tilde{x}} &= -\frac{\tilde{A}_x}{\tilde{A}}\tilde{\rho}\tilde{u}^2 - C_f\tilde{w}\tilde{\rho}\frac{\tilde{u}^2}{2\tilde{A}} - \tilde{C}\tilde{\rho}\tilde{u}, \\
(\tilde{\rho}\tilde{e})_{\tilde{t}} + (\tilde{u}(\tilde{\rho}\tilde{e} + \tilde{p}))_{\tilde{x}} &= -\frac{\tilde{A}_x}{\tilde{A}}\tilde{u}(\tilde{\rho}\tilde{e} + \tilde{p}) - \frac{1}{\tilde{A}}\tilde{w}\tilde{h}(\tilde{T} - \tilde{T}_{\text{Wall}}), \\
(\tilde{\rho}\tilde{z})_{\tilde{t}} + (\tilde{\rho}\tilde{u}\tilde{z})_{\tilde{x}} &= -\frac{\tilde{A}_x}{\tilde{A}}\tilde{\rho}\tilde{u}\tilde{z} - \frac{1}{\tilde{A}}\tilde{\rho}\tilde{z}\tilde{K}
\end{aligned}$$

with the ideal gas law $\tilde{p} = \tilde{R}\tilde{\rho}\tilde{T}$.

First let us note, that the cross section function $A$ is shifted to the right hand sides of the equations in this formulation. In order to have a better comparison with our formulation (2.14), we rewrite the model, such that the cross section function can be found only on the left hand side:

$$(\tilde{A}\tilde{\rho})_{\tilde{t}} + (\tilde{A}\tilde{\rho}\tilde{u})_{\tilde{x}} = 0, \tag{B.1}$$

$$(\tilde{A}\tilde{\rho}\tilde{u})_{\tilde{t}} + (\tilde{A}\tilde{\rho}\tilde{u}^2)_{\tilde{x}} + \tilde{A}\tilde{p}_{\tilde{x}} = -C_f\tilde{w}\tilde{\rho}\frac{\tilde{u}^2}{2} - \tilde{C}\tilde{A}\tilde{\rho}\tilde{u}, \tag{B.2}$$

$$(\tilde{A}\tilde{\rho}\tilde{e})_{\tilde{t}} + (\tilde{A}\tilde{u}(\tilde{\rho}\tilde{e} + \tilde{p}))_{\tilde{x}} = -\tilde{w}\tilde{h}(\tilde{T} - \tilde{T}_{\text{Wall}}), \tag{B.3}$$

$$(\tilde{A}\tilde{\rho}\tilde{z})_{\tilde{t}} + (\tilde{A}\tilde{\rho}\tilde{u}\tilde{z})_{\tilde{x}} = -\tilde{\rho}\tilde{z}\tilde{K}. \tag{B.4}$$

To the end of an easier comparision, we restate our formulation of the model (2.14) here:

$$(\tilde{A}\tilde{\rho})_{\tilde{t}} + (\tilde{A}\tilde{\rho}\tilde{u})_{\tilde{x}} = 0, \tag{B.5}$$

$$(\tilde{A}\tilde{\rho}\tilde{u})_{\tilde{t}} + (\tilde{A}\tilde{\rho}\tilde{u}^2)_{\tilde{x}} + \tilde{A}\tilde{p}_{\tilde{x}} = -\frac{\xi}{4}\pi\tilde{d}\tilde{\rho}\frac{\tilde{u}|\tilde{u}|}{2} - \tilde{\chi}_f\tilde{C}_c\tilde{A}\tilde{\rho}\tilde{u}, \tag{B.6}$$

$$(\tilde{A}\tilde{\rho}\tilde{E})_{\tilde{t}} + (\tilde{A}\tilde{\rho}\tilde{u}\tilde{E} + \tilde{A}\tilde{u}\tilde{p})_{\tilde{x}} = -\tilde{h}\pi\tilde{d}(\tilde{T} - \tilde{T}_{\text{Wall}}) + \tilde{\chi}_f\tilde{q}_0\tilde{A}\tilde{\rho}\tilde{z}\tilde{K}(\tilde{T}), \tag{B.7}$$

$$(\tilde{A}\tilde{\rho}\tilde{z})_{\tilde{t}} + (\tilde{A}\tilde{\rho}\tilde{z}\tilde{u})_{\tilde{x}} = -\tilde{\chi}_f\tilde{A}\tilde{\rho}\tilde{z}\tilde{K}(\tilde{T}). \tag{B.8}$$

We study the differences equation-wise:

- **Conservation of mass**: The equations (B.1) and (B.5) are identical.

- **Momentum balance**: The left hand sides of the equations (B.2) and (B.6) are also identical. The first term on the right hand side is the wall friction. The friction coefficients are just differently named.

$$C_f = \frac{\xi}{4}.$$

The function $\tilde{x} \to \tilde{w}(\tilde{x})$ denotes the pipe's perimeter at point $\tilde{x}$, which equals the product of diameter $\tilde{x} \to \tilde{d}(\tilde{x})$ and $\pi$, i.e.,

$$\tilde{w} = \pi \tilde{d}.$$

In the original formulation of the model, the flow velocity $\tilde{u}$ is assumed to be positive. This physical meaningful assumption implies

$$\tilde{u}^2 = \tilde{u}|\tilde{u}|.$$

The second term is the local friction in the catalytic converter. First, the friction coefficients are differently named. Whereas we denote it by $\tilde{C}_c$, it is denoted by $\tilde{C}$ in (B.2). Second, the locality is not denoted by any indicator function, as it is done in our formulation with $\tilde{\chi}_f$. However, the friction coefficient in the model of Lacoste and Natalini is space dependent and contains an indicator function in its definition, i.e.,

$$\tilde{C}(\tilde{x}) = \begin{cases} \tilde{C} = \tilde{C}_c, & \text{if } \tilde{x} \text{ in catalyst,} \\ 0, & \text{otherwise.} \end{cases}$$

- **Energy balance**: The total energy density are differently defined in the equations (B.2) and (B.6). Whereas the energy density in our formulation $\tilde{\rho}\tilde{E}$ consists of the internal and kinetic energy, the energy density in the original formulation $\tilde{\rho}\tilde{e}$ contains additionally the chemical energy, i.e.,

$$\tilde{e} = \tilde{c}_v \tilde{T} + \frac{\tilde{u}^2}{2} + \tilde{q}_0 \tilde{z}, \qquad \tilde{E} = \tilde{c}_v \tilde{T} + \frac{\tilde{u}^2}{2}.$$

Thus, $\tilde{e} - \tilde{E} = \tilde{q}_0 \tilde{z}$. Plugging this into (B.3) and using the reaction equation, leads to the second term on the right hand side of (B.7), which describes the energy gain due to the exothermic reaction in the catalytic converter. Hence, by the assumption of smoothness of the unknowns, both formulations are equivalent.

- **Reaction equation**: The left hand sides of the equations (B.4) and (B.8) are identical. On the right hand side, we note two differences. First, there is no indicator function in the original formulation, since $\tilde{K}$ is defined as follows:

$$\tilde{K} = \begin{cases} \tilde{K}(\tilde{T}), & \text{if } \tilde{x} \text{ in catalyst,} \\ 0, & \text{otherwise.} \end{cases}$$

  Second, the source term in the reaction equation differs by the factor $\tilde{A}$. Since the exothermic reaction takes place on the catalyst surface, this source should depend on the cross section of the catalyst. Therefore, the combustion term in the original formulation $-\tilde{\rho}\tilde{z}\tilde{K}$ was replaced by $-\tilde{\chi}_f\tilde{A}\tilde{\rho}\tilde{z}\tilde{K}(\tilde{T})$. This has an impact on the reaction rate coefficient $\tilde{K}_0$. Let $\tilde{K}_0^{\mathrm{LN}}$ and $\tilde{K}_0$ be the reaction rate coefficient of the original formulation of Lacoste and Natalini in [LN04] and the one from (2.14), respectively. Then

$$\tilde{K}_0^{\mathrm{LN}} = \frac{\tilde{K}_0}{\tilde{A}_{cc}},$$

  where $\tilde{A}_{cc} = (\tilde{A}^2 + \tilde{A}^4)/2$, i.e., the average cross section area of the considered catalytic converters.

- **Boundary conditions**: Since the pipe flow direction is assumed to be known in the original formulation, there is no need to prescribe inflow boundary conditions. Furthermore, instead of a boundary condition for the pressure at the pipes exit, a boundary conditions for the velocity was given at $\tilde{x} = 0$ in [LN04]. These are not the right boundary conditions for this application, since it is not possible (or at least very difficult) to measure the gas velocity at the junction of combustion chamber and exhaust pipe. On the other hand, it is easy to measure the pressure at the exhaust pipe's exit, since it is equal to the outside pressure.

# C. Numerical simulations

## C.1. Separation method in proof of Proposition 2

We use the separation method to find the solution.

$$\begin{aligned}
\frac{d\rho}{dx} &= \frac{h}{2\gamma p_0 m}\rho(p_0 - \rho \cdot T_{out}) \\
\frac{2\gamma p_0 m}{h}\int_{\rho_{bc}}^{\rho} \frac{1}{r(p_0 - r \cdot T_{out})} dr &= \int_0^x d\xi \\
\frac{2\gamma p_0 m}{h}\left[\int_{\rho_{bc}}^{\rho} \frac{1}{p_0 r} dr + \int_{\rho_{bc}}^{\rho} \frac{T_{out}}{{p_0}^2 - r \cdot p_0 T_{out})} dr\right] &= \int_0^x d\xi \\
\frac{2\gamma m}{h}\left[\ln(r) - \ln(p_0 - r \cdot T_{out})\right]_{\rho_{bc}}^{\rho} &= x \\
\frac{2\gamma m}{h}\left[\ln\left(\frac{r}{p_0 - r \cdot T_{out}}\right)\right]_{\rho_{bc}}^{\rho} &= x \\
\frac{2\gamma m}{h}\left[\ln\left(\frac{\rho}{p_0 - \rho \cdot T_{out}}\right) - \ln\left(\frac{\rho_{bc}}{p_0 - \rho_{bc} \cdot T_{out}}\right)\right] &= x
\end{aligned}$$

Now, the aim is to isolate $\rho$.

$$\begin{aligned}
\frac{\rho}{p_0 - \rho \cdot T_{out}} &= \frac{\rho_{bc}}{p_0 - \rho_{bc} \cdot T_{out}} \exp\left(\frac{h}{2\gamma m} x\right) \\
\rho &= (p_0 - \rho \cdot T_{out}) \frac{\rho_{bc}}{p_0 - \rho_{bc} \cdot T_{out}} \exp\left(\frac{h}{2\gamma m} x\right) \\
\rho &= \frac{p_0 \frac{\rho_{bc}}{p_0 - \rho_{bc} \cdot T_{out}} \exp\left(\frac{h}{2\gamma m} x\right)}{1 + T_{out} \frac{\rho_{bc}}{p_0 - \rho_{bc} \cdot T_{out}} \exp\left(\frac{h}{2\gamma m} x\right)} \\
\rho &= \frac{p_0}{(p_0/\rho_{bc} - T_{out}) \exp\left(-\frac{h}{2\gamma m} x\right) + T_{out}}
\end{aligned}$$

## C.2. Regularity of the tridiagonal matrix A

We recall the matrix $\mathbf{A}$ from (3.15):

$$\mathbf{A} = \begin{pmatrix} f^1 & e^2 & & \\ e^2 & \ddots & \ddots & \\ & \ddots & \ddots & e^{n_V} \\ & & e^{n_V} & f^{n_V} \end{pmatrix}, \qquad e^i = \frac{(A^i)^2}{C_f^i}, \qquad f^i = -e^i - e^{i+1}.$$

First, we explain what we mean by *weak diagonal dominance* and *irreducibility*. Both definitions are taken from [SK11].

**Definition 2.** *A matrix* $\mathbf{A} \in \mathbb{R}^{n\times n}$ *is called* <u>*weakly diagonally dominant*</u>*, if*

$$|a_{ii}| \geq \sum_{k=1,k\neq i}^{n} |a_{ik}| \qquad \forall i = 1, \ldots, n,$$

*where the strict inequality has to hold for at least one index* $i_0 \in \{1, \ldots, n\}$.

**Definition 3.** *A matrix* $\mathbf{A} \in \mathbb{R}^{n\times n}$ *is called* <u>*irreducible*</u>*, if for every pair of indices* $i$ *and* $j$*, with* $i, j \in \{1, \ldots, n\}$*, either* $a_{ij} \neq 0$ *or a finite sequence of indices* $k_1, k_2, \ldots, k_s$ *exists, such that*

$$a_{ik_1} \cdot a_{k_1k_2} \cdot a_{k_2k_3} \cdot \ldots \cdot a_{k_sj} \neq 0 \tag{C.1}$$

*holds.*

It is obvious that our considered matrix $\mathbf{A}$ is weakly diagonally dominant.

**Proposition 6.** *Any tridiagonal matrix with non-vanishing elements on the secondary diagonals is irreducible.*

*Proof.* We pick an arbitrary element $a_{ij}$, with $a_{ij} = 0$.

1. If $i < j$, then $i+1, i+2, \ldots, j-2, j-1$ is a sequence of indices satisfying (C.1).
2. If $i > j$, then $i-1, i-2. \ldots, j-2, j-1$ is a sequence of indices satisfying (C.1).
3. If $i = j$, then $i-1$ or $i+1$ is such a sequence, consisting of a single index.

□

The following lemma (also taken from [SK11]) states that those two conditions are sufficient to guarantee regularity of $\mathbf{A}$.

**Lemma 1.** *A irreducible and weakly diagonally dominant matrix $A \in \mathbb{C}^{n\times n}$ is regular and has non-vanishing elements on the diagonal.*

See [SK11, Page 498] for the proof.

## C.3. The Riemann problem at the boundaries

Let us assume a non-negative flow direction for this observation, i.e., $\tilde{u}(0,\tilde{t}) \geq 0$ for all times $\tilde{t} \in [0,\infty)$. Otherwise, one just have to switch the consideration for the left and right boundary.

Suppose we prescribe the unscaled physical boundary conditions (2.54) and (2.55) for the problem (3.20), i.e.,

$$\begin{aligned} \tilde{p}^1(0,\tilde{t}) &= \tilde{p}_{bc,l}(\tilde{t}), & \tilde{p}^{n_P}(\tilde{L}^{n_P},\tilde{t}) &= \tilde{p}_{bc,r}(\tilde{t}), \\ \tilde{\rho}(0,\tilde{t}) &= \tilde{\rho}_{bc,l}(\tilde{t}), & \tilde{z}(0,\tilde{t}) &= \tilde{z}_{bc,l}(\tilde{t}). \end{aligned}$$

Since we need the left eigenvalues (from (3.21)) for solving the linearized Riemann problems, we restate them here:

$$\begin{aligned} l_1 &= \left( \frac{\tilde{u}}{2\tilde{c}} + \frac{\tilde{u}^2}{2(2\tilde{H}-\tilde{u}^2)}, \quad -\frac{\tilde{u}}{2\tilde{H}-\tilde{u}^2} - \frac{1}{2\tilde{c}}, \quad \frac{1}{2\tilde{H}-\tilde{u}^2}, \quad 0 \right), \\ l_2 &= \left( 2 - \frac{2\tilde{H}}{2\tilde{H}-\tilde{u}^2}, \quad \frac{2\tilde{u}}{2\tilde{H}-\tilde{u}^2}, \quad -\frac{2}{2\tilde{H}-\tilde{u}^2}, \quad 0 \right), \\ l_3 &= \left( -\frac{\tilde{u}^2\tilde{z}}{2\tilde{H}-\tilde{u}^2}, \quad \frac{2\tilde{u}\tilde{z}}{2\tilde{H}-\tilde{u}^2}, \quad -\frac{2\tilde{z}}{2\tilde{H}-\tilde{u}^2}, \quad 1 \right), \\ l_4 &= \left( \frac{\tilde{u}^2}{2(2\tilde{H}-\tilde{u}^2)} - \frac{\tilde{u}}{2\tilde{c}}, \quad \frac{1}{2\tilde{c}} - \frac{\tilde{u}}{2\tilde{H}-\tilde{u}^2}, \quad \frac{1}{2\tilde{H}-\tilde{u}^2}, \quad 0 \right). \end{aligned}$$

### C.3.1. Left boundary

Figure C.1 illustrates the Riemann problem at the left boundary. In order to find the unknown component $\tilde{u}_l$ of the state $U_l$ we have to solve

$$U_l + a_2 r_2(U_+) + a_3 r_3(U_+) + a_4 r_4(U_l) = U_+$$

with unknowns $a_i$. This condition is equivalent to

$$(0, a_2, a_3, a_4)^T = L(U_+)(U_+ - U_l). \tag{C.2}$$

The first equation of (C.2) gives us the unknown component of $U_l$:

$$l_1(U_+)(U_+ - U_l) = 0. \tag{C.3}$$

Multiplying (C.3) with $2\tilde{H}_+ - \tilde{u}_+^2 = 2\tilde{c}_+^2/(\gamma - 1)$ simplifies the equation to a quadratic one for $\tilde{u}_l$, i.e.,

$$\tilde{u}_l^2 + \tilde{\alpha}_1 \tilde{u}_l + \tilde{\alpha}_2 = 0 \tag{C.4}$$

with

$$\tilde{\alpha}_1 := -2\tilde{u}_+ - \frac{2\tilde{c}_+}{\gamma - 1}, \qquad \tilde{\alpha}_2 := \frac{2\tilde{c}_+\tilde{u}_+}{\gamma - 1} + \tilde{u}_+^2 + \frac{2(\tilde{p}_l - \tilde{p}_+)}{\tilde{\rho}_l(\gamma - 1)}.$$

The roots of the quadratic equation (C.4) are

$$(\tilde{u}_l)_{1/2} = -\frac{\tilde{\alpha}_1}{2} \pm \sqrt{\left(\frac{\tilde{\alpha}_1}{2}\right)^2 - \tilde{\alpha}_2}.$$

Taking the positive root would imply, leaving the subsonic (low Mach number) regime and dealing with velocities larger than $\tilde{u} + \tilde{c}/\gamma{-}1$. This would be of course non-physical, if the neighbouring velocity $\tilde{u}_+$ is in a low Mach number regime.

Therefore, we have to take the negative root, i.e.,

$$\tilde{u}_l = -\frac{\tilde{\alpha}_1}{2} - \sqrt{\left(\frac{\tilde{\alpha}_1}{2}\right)^2 - \tilde{\alpha}_2}.$$

Since we already assumed a positive velocity $\tilde{u}_+ \geq 0$, the only physical meaningful relation between the pressure values is $\tilde{p}_l > \tilde{p}_+$. Then we know that $\tilde{\alpha}_2$ is positive, and therefore

$$-\frac{\tilde{\alpha}_1}{2} > \sqrt{\left(\frac{\tilde{\alpha}_1}{2}\right)^2 - \tilde{\alpha}_2}.$$

This relation guarantees us, that the determined velocity $\tilde{u}_l$ is positive, and also in a low Mach number regime. By plugging the definitions of $\tilde{\alpha}_1$ and $\tilde{\alpha}_2$ into the solution for $\tilde{u}_l$, we deduce

$$\tilde{u}_l = \tilde{u}_+ + \frac{\tilde{c}_+}{\gamma - 1} - \sqrt{\left(\frac{\tilde{c}_+}{\gamma - 1}\right)^2 - \frac{2(\tilde{p}_l - \tilde{p}_+)}{\tilde{\rho}_l(\gamma - 1)}}.$$

Hence, if the pressure values $\tilde{p}_+$ and $\tilde{p}_l$ would coincide, we would also have coinciding velocities. This would not be the case, if we had chosen the positive root.

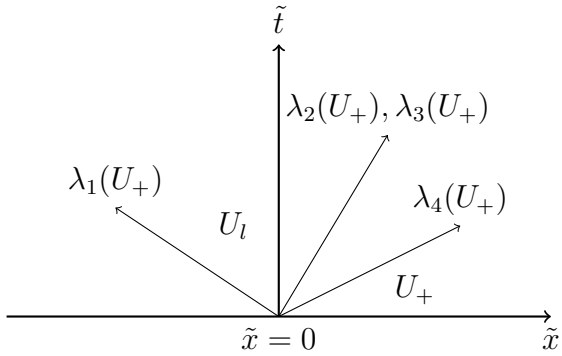


Figure C.1.: Linearized Riemann problem at the left boundary

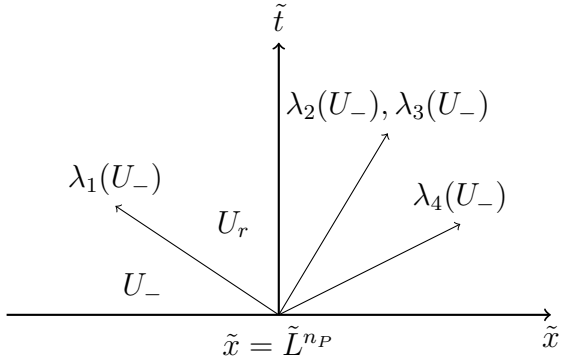


Figure C.2.: Linearized Riemann problem at the right boundary

## C.3.2. Right boundary

Figure C.2 illustrates the Riemann problem at the right boundary. In order to find the unknown components $\tilde{\rho}_r, \tilde{u}_r$ and $\tilde{z}_r$ of $U_r$ we have to solve

$$U_- + a_1 r_1(U_-) = U_r \Leftrightarrow (a_1, 0, 0, 0)^T = L(U_-)(U_r - U_-) \tag{C.5}$$

with the unknown $a_1$. See Figure C.2 for the illustration. The last three equations of (C.5) give us the unknown components of $U_r$. Hence, we have to solve a non-linear $3 \times 3$ system.

1. We start by multiplying $-\tilde{z}_-$ to the second equation and adding the result to the third equation.

   $$0 = (-\tilde{z}_- l_2(U_-) + l_3(U_-))(U_r - U_-) = (-\tilde{z}_-, 0, 0, 1)\,(U_r - U_-).$$

   Simplifying this equation leads us to

   $$-\tilde{z}_-(\tilde{\rho}_r - \tilde{\rho}_-) + (\tilde{\rho}_r \tilde{z}_r - \tilde{\rho}_- \tilde{z}_-) = 0 \qquad \Leftrightarrow \qquad \tilde{\rho}_r(\tilde{z}_r - \tilde{z}_-) = 0.$$

   Under the physically meaningful assumption on non-vacuum states, i.e., $\tilde{\rho}_r \neq 0$, we end up with

   $$\boxed{\tilde{z}_r = \tilde{z}_-.} \tag{C.6}$$

2. We continue by multiplying the fourth equation by 2, adding it to the second equation and multiplying the result with the speed of sound $c_-$.

   $$\begin{aligned} & 0 = c_-(2l_4(U_-) + l_2(U_-))(U_r - U_-) \\ \Leftrightarrow \quad & 0 = (\tilde{c}_- - \tilde{u}_-, 1, 0, 0)\,(U_r - U_-). \end{aligned}$$

After some manipulations we come up with

$$u_r = u_- + \tilde{c}_- \left( \frac{\tilde{\rho}_-}{\tilde{\rho}_r} - 1 \right). \tag{C.7}$$

In the next step, we want to determine another relation between $\tilde{u}_r$ and $\tilde{\rho}_r$ and plug it into (C.7) afterwards.

3. We multiply the seconds equation by $2\tilde{H} - \tilde{u}^2 = 2\tilde{c}^2/(\gamma - 1)$ and divide it by two. We obtain:

$$0 = \frac{1}{2}(2\tilde{H}_- - \tilde{u}_-^2) l_2(U_-)(U_r - U_-) = \left( \frac{\tilde{c}_-^2}{\gamma - 1} - \frac{\tilde{u}_-^2}{2}, \tilde{u}_-, -1, 0 \right)(U_r - U_-).$$

Isolating this equation with respect to the unknown density $\tilde{\rho}_r$ leads to the following relation to the unknown velocity $\tilde{u}_r$:

$$\tilde{\rho}_r = \frac{\tilde{p}_r + (\gamma - 1)\tilde{p}_-}{c_-^2 - \frac{\gamma-1}{2}(\tilde{u}_- - \tilde{u}_r)^2}. \tag{C.8}$$

4. We plug (C.8) into (C.7) and obtain the following quadratic equation

$$\tilde{u}_r^2 + \tilde{\beta}_1 \tilde{u}_r + \tilde{\beta}_2 = 0$$

with

$$\tilde{\beta}_1 := -2\tilde{u}_- + \frac{2(\tilde{p}_r + (\gamma - 1)\tilde{p}_-)}{\tilde{c}_- \tilde{\rho}_- (\gamma - 1)},$$
$$\tilde{\beta}_2 := \tilde{u}_-^2 + \frac{2\tilde{c}_-(\tilde{p}_r - \tilde{p}_-) - 2\tilde{u}_-(\tilde{p}_r + (\gamma - 1)\tilde{p}_-)}{\tilde{c}_- \tilde{\rho}_- (\gamma - 1)}.$$

The two solutions of this quadratic problem are

$$(\tilde{u}_r)_{1/2} = \tilde{u}_- - \frac{\tilde{p}_r + (\gamma - 1)\tilde{p}_-}{\tilde{c}_- \tilde{\rho}_- (\gamma - 1)} \pm \sqrt{\left( \frac{\tilde{p}_r + (\gamma - 1)\tilde{p}_-}{\tilde{c}_- \tilde{\rho}_- (\gamma - 1)} \right)^2 - \frac{2(\tilde{p}_r - \tilde{p}_-)}{\tilde{\rho}_- (\gamma - 1)}}.$$

It is obvious, that only one root, namely the positive one, is physically meaningful. In the case of coinciding pressure values $\tilde{p}_r$ and $\tilde{p}_-$ the velocity must stay conserved. Therefore, we have the unique solution for the velocity $\tilde{u}_r$:

$$\boxed{\tilde{u}_r = \tilde{u}_- - \frac{\tilde{p}_r + (\gamma - 1)\tilde{p}_-}{\tilde{c}_- \tilde{\rho}_- (\gamma - 1)} + \sqrt{\left( \frac{\tilde{p}_r + (\gamma - 1)\tilde{p}_-}{\tilde{c}_- \tilde{\rho}_- (\gamma - 1)} \right)^2 - \frac{2(\tilde{p}_r - \tilde{p}_-)}{\tilde{\rho}_- (\gamma - 1)}}.} \tag{C.9}$$

5. Plugging the solution for $\tilde{u}_r$ (C.9) into the forumla for $\tilde{\rho}_r$ (C.8) gives us the solution for $\tilde{\rho}_r$, which depends upon the known pressure values $\tilde{p}_r, \tilde{p}_-$ and the known density $\tilde{\rho}_-$.

## C.4. Riemann problem at the vertices

The linearized Riemann problem at a junction $i$ (connecting pipe $i$ and $i+1$) is illustrated in Figure C.3. The variables' affiliations to pipes is obvious in this consideration[1]. Therefore, we cease to write superscripts to the end of a easier readability.

In order to determine the unknown states $U_r$ and $U_l$ at the junction $i$, we need to solve

$$U_- + a_1 r_1(U_-) = U_r, \tag{C.10}$$

$$U_+ - a_2 r_2(U_+) - a_3 r_3(U_+) - a_4 r_4(U_+) = U_l, \tag{C.11}$$

subject to the coupling conditions (2.56). If these coupling conditions were linear for the state variable $U$, the solution would be very simple. However, they are not linear, and we have to solve a non-linear problem to determine the unknowns $U_r$ and $U_l$. The idea is the following:

1. As we learned from the Riemann problem at the right boundary (Section C.3), we can determine $U_r$, if we know $\tilde{p}_r$, i.e., $U_r = U_r(\tilde{p}_r)$.

2. With the help of the coupling conditions, we can express the state $U_l$ with the components of $U_r$. Therefore, $U_l$ depends only upon $\tilde{p}_r$, i.e., $U_l = U_l(\tilde{p}_r)$.

3. We solve (C.11) numerically with Newton's method (see e.g., [BK14]) and obtain a solution for $\tilde{p}_r$.

The first task was already fulfilled in Subsection C.3.2. We have the functions $\tilde{u}_r = \tilde{u}_r(\tilde{p}_r)$, $\tilde{\rho}_r = \tilde{\rho}_r(\tilde{u}_r)$ and $\tilde{z}_r = \tilde{z}_-$ given by (C.9), (C.8) and (C.6), repectively. Therefore, we start with the second task. By using the coupling conditions (2.56) we can deduce

$$U_l = \begin{pmatrix} \tilde{\rho}_l \\ \tilde{\rho}_l \tilde{u}_l \\ \tilde{\rho}_l \dfrac{(\tilde{u}_l)^2}{2} + \dfrac{\tilde{p}_l}{\gamma - 1} \\ \tilde{\rho}_l \tilde{z}_l \end{pmatrix} = \begin{pmatrix} \dfrac{\tilde{p}_r - \tilde{f}_{ext}}{\tilde{p}_r} \tilde{\rho}_r \\ \dfrac{\tilde{A}_r}{\tilde{A}_l} \tilde{\rho}_r \tilde{u}_r \\ \left(\dfrac{\tilde{A}_r}{\tilde{A}_l}\right)^2 \dfrac{\tilde{p}_r}{\tilde{p}_r - \tilde{f}_{ext}} \tilde{\rho}_r \dfrac{(\tilde{u}_r)^2}{2} + \dfrac{\tilde{p}_r - \tilde{f}_{ext}}{\gamma - 1} \\ \dfrac{\tilde{p}_r - \tilde{f}_{ext}}{\tilde{p}_r} \tilde{\rho}_r \tilde{z}_r \end{pmatrix},$$

[1] Clearly, $y_-$ and $y_r$ belong to pipe $i$, whereas $y_+$ and $y_l$ belong to pipe $i+1$ (see Figure C.3).

where the pressure loss term, which depends on density and velocity, is evaluated either at the states $\tilde{\rho}_-, \tilde{u}_-$ or $\tilde{\rho}_+, \tilde{u}_+$[2]. We now proceed with the third step in the same way, we did in the case of the Riemann problem at the left boundary (see Subsection C.3.1), i.e., we first rearrange equation C.11 such that we use the left eigenvectors, consider only the first (homogeneous) equation and multiply it by $2\tilde{H}_+ - \tilde{u}_+^2$. We obtain an equation for the unknown $\tilde{p}_r$:

$$\begin{aligned}
0 &= (2\tilde{H}_+ - \tilde{u}_+^2) l_1(U_+)(U_+ - U_l(\tilde{p}_r)) \\
&= \left( \frac{\tilde{c}_+ \tilde{u}_+}{\gamma - 1} + \frac{\tilde{u}_+^2}{2}, -\tilde{u}_+ - \frac{\tilde{c}_+}{\gamma - 1}, 1, 0 \right) (U_+ - U_l(\tilde{p}_r)) \\
&= f_1(\tilde{p}_r) + f_2(\tilde{p}_r) + f_3(\tilde{p}_r) + f_4(\tilde{p}_r) + \frac{\tilde{p}_+}{\gamma - 1}
\end{aligned}$$

with

$$\begin{aligned}
f_1(\tilde{p}_r) &:= -\left( \frac{\tilde{c}_+ \tilde{u}_+}{\gamma - 1} + \frac{\tilde{u}_+^2}{2} \right) \tilde{\rho}_r(\tilde{p}_r) \frac{\tilde{p}_r - \tilde{f}_{ext}}{\tilde{p}_r}, \\
f_2(\tilde{p}_r) &:= \left( \tilde{u}_+ + \frac{\tilde{c}_+}{\gamma - 1} \right) \frac{\tilde{A}_r}{\tilde{A}_l} \tilde{\rho}_r(\tilde{p}_r) \tilde{u}_r(\tilde{p}_r), \\
f_3(\tilde{p}_r) &:= -\left( \frac{\tilde{A}_r}{\tilde{A}_l} \right)^2 \frac{\tilde{p}_r}{\tilde{p}_r - \tilde{f}_{ext}} \tilde{\rho}_r(\tilde{p}_r) \frac{(\tilde{u}_r(\tilde{p}_r))^2}{2}, \\
f_4(\tilde{p}_r) &:= -\frac{\tilde{p}_r - \tilde{f}_{ext}}{\gamma - 1}.
\end{aligned}$$

We will list the derivatives, since they are required for Netwon's method.

$$\begin{aligned}
f_1'(\tilde{p}_r) &= -\left( \frac{\tilde{c}_+ \tilde{u}_+}{\gamma - 1} + \frac{\tilde{u}_+^2}{2} \right) \left( \tilde{\rho}_r'(\tilde{p}_r) \frac{\tilde{p}_r - \tilde{f}_{ext}}{\tilde{p}_r} + \tilde{\rho}_r(\tilde{p}_r) \frac{\tilde{f}_{ext}}{(\tilde{p}_r)^2} \right), \\
f_2'(\tilde{p}_r) &= \left( \tilde{u}_+ + \frac{\tilde{c}_+}{\gamma - 1} \right) \frac{\tilde{A}_r}{\tilde{A}_l} \left( \tilde{\rho}_r'(\tilde{p}_r) \tilde{u}_r(\tilde{p}_r) + \tilde{\rho}_r(\tilde{p}_r) \tilde{u}_r'(\tilde{p}_r) \right), \\
f_3'(\tilde{p}_r) &= -\left( \frac{\tilde{A}_r}{\tilde{A}_l} \right)^2 \left( \frac{-\tilde{f}_{ext}}{(\tilde{p}_r - \tilde{f}_{ext})^2} \tilde{\rho}_r(\tilde{p}_r) \frac{(\tilde{u}_r(\tilde{p}_r))^2}{2} + \frac{\tilde{p}_r}{\tilde{p}_r - \tilde{f}_{ext}} \tilde{\rho}_r'(\tilde{p}_r) \frac{(\tilde{u}_r(\tilde{p}_r))^2}{2} \right. \\
&\qquad \left. + \frac{\tilde{p}_r}{\tilde{p}_r - \tilde{f}_{ext}} \tilde{\rho}_r(\tilde{p}_r) \tilde{u}_r(\tilde{p}_r) \tilde{u}_r'(\tilde{p}_r) \right), \\
f_4'(\tilde{p}_r) &= -\frac{1}{\gamma - 1}
\end{aligned}$$

[2] Although the coupling condition have to be fulfilled between the left and right states, for simplicity we evaluate the pressure loss term at the neighbouring cells. The values should not differ significantly. See Remark 4 on Page 25 for details on $\tilde{f}_{ext}$.

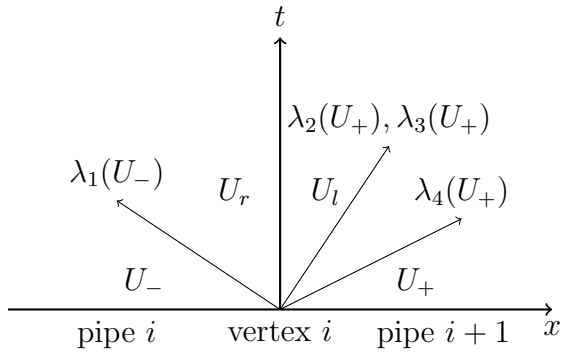


Figure C.3.: Linearized Riemann problem at a vertex $i$

with

$$\tilde{u}_r'(\tilde{p}_r) = \frac{1}{\tilde{c}_-\tilde{\rho}_-(\gamma-1)}\left(\frac{\left(\frac{\tilde{p}_r+(\gamma-1)\tilde{p}_-}{\tilde{c}_-\tilde{\rho}_-(\gamma-1)} - \tilde{c}_-\right)}{\sqrt{\left(\frac{\tilde{p}_r+(\gamma-1)\tilde{p}_-}{\tilde{c}_-\tilde{\rho}_-(\gamma-1)}\right)^2 - \frac{2(\tilde{p}_r-\tilde{p}_-)}{\tilde{\rho}_-(\gamma-1)}}} - 1\right),$$

$$\tilde{\rho}_r'(\tilde{p}_r) = \frac{c_-^2 - \frac{\gamma-1}{2}(\tilde{u}_- - \tilde{u}_r(\tilde{p}_r))^2 - (\gamma-1)(\tilde{p}_r+(\gamma-1)\tilde{p}_-)(\tilde{u}_- - \tilde{u}_r(\tilde{p}_r))\tilde{u}_r'(\tilde{p}_r)}{\left(c_-^2 - \frac{\gamma-1}{2}(\tilde{u}_- - \tilde{u}_r(\tilde{p}_r))^2\right)^2}.$$

## C.5. Flops in one spatial step of the homogeneous problem

Consider one spatial step for the hyperbolic model

$$U_j^{n+1} = U_j^n - \Delta t \cdot \left(A^+(U_j^n)\frac{U_j^n - U_{j-1}^n}{\Delta x} + A^-(U_j^n)\frac{U_{j+1}^n - U_j^n}{\Delta x}\right).$$

For the computations of one spatial derivative we need 8 flops. The multiplication of a $4 \times 4$ matrix with a 4-dimensional vector takes 32 flops. Then we have to add those products in the brackets, which costs 4 flops. Finally, we have to multiply with $\Delta t$ (4 flops) and add this to the old values (4 flops). This gives us in total:

$$2 \cdot 8 + 2 \cdot 32 + 4 + 4 + 4 = 92.$$

In addition, we have to consider the computations of $A^{+/-}$. There is a lot of effort required for the construction of these matrices. We recall the construction from Subsection 3.3.1:

$$\begin{aligned}
\lambda_i^+(U) &:= \max\{\lambda_i(U), 0\}, & \lambda_i^-(U) &:= \min\{\lambda_i(U), 0\},\\
\Lambda^+(U) &:= \operatorname{diag}(\lambda_1^+(U), \dots, \lambda_n^+(U)), & \Lambda^-(U) &:= \operatorname{diag}(\lambda_1^-(U), \dots, \lambda_n^-(U)),\\
A^+(U) &:= R(U)\Lambda^+(U)L(U), & A^-(U) &:= R(U)\Lambda^-(U)L(U)
\end{aligned}$$

with

$$\lambda_1 = \tilde{u} - \tilde{c}, \qquad \lambda_2 = \lambda_3 = \tilde{u}, \qquad \lambda_4 = \tilde{u} + \tilde{c}.$$

Thus, we need first to compute the velocity $\tilde{u}$ and the speed of sound $\tilde{c}$. We know from (2.36) that $\tilde{c}$ depends upon density $\tilde{\rho}$, pressure $\tilde{p}$ and the adiabatic exponent $\gamma$.

$$\tilde{u} = \frac{U_2}{U_1}, \qquad \tilde{c} = \sqrt{\gamma(\gamma-1)\left(\frac{U_3}{U_1} - 0.5\left(\frac{U_2}{U_1}\right)^2\right)}.$$

Even without counting the evaluation of the square root function we have to invest 1 flop for the computation of $\tilde{u}$, and 8 flops for $\tilde{c}$. Hence we need 11 flops to compute the eigenvalues.

We neglect the numerical of the evaluation of the min and max functions, remarking that we need more evaluations than in the case of AM.

We have four matrix multiplication. Each multiplication of two $4 \times 4$ matrices costs 128 flops. Hence we have to add $11 + 4 \cdot 128 = 523$ to the number of flops that we require for one spatial step:

$$\text{flops}_{FE} = 92 + 523 = 615.$$

The number of flops necessary for the two PDEs we need to numerically solve in the (AM) model is much smaller. Consider the one dimensional upwind scheme

$$y_j^{n+1} = y_j^n - \Delta t \cdot \left(a^+ \frac{y_j^n - y_{j-1}^n}{\Delta x} + a^- \frac{y_{j+1}^n - y_j^n}{\Delta x}\right).$$

We have only 2 flops for the computation of a spatial derivative. The computation of $a^{+/-}$ is a simple comparison[3] between two real numbers. We require two flops for the multiplication with the velocity $a^+$ and $a^-$, respectively, and one flop to add the spatial derivatives. Furthermore we need one flop for the multiplication with the $\Delta t$ and one flop for adding this product to the old state. Since we have to solve two PDEs by such an upwind scheme, this gives us in total:

$$\text{flops}_{AM} = 2 \cdot (2 \cdot 2 + 2 + 1 + 1 + 1) = 18.$$

[3] We neglect this effort, since we did this as well in the FE case.

## C.6. Comparison of the propagation speed of FE and AM

Figures C.4 - C.8 show the numerical results of Example 2 of Subsection 3.4.2 evaluated at times $\tilde{t}^* \in \{0\text{s}, 0.00125\text{s}, 0.0025\text{s}, 0.00375\text{s}, 0.005\text{s}\}$. In Figure C.4 we see the initial condition, whereas $\tilde{t}^* = 0.00125\text{s}$ passed in Figure C.5. While we have a finite speed of propagation with the hyperbolic model (green, dashed lines), we observe in the case of AM an instant increase of the velocity $\tilde{u}$ over the whole spatial domain. Hence, the speed at which information travel is infinite in the asymptotic model. This is a qualitative difference between the two models.

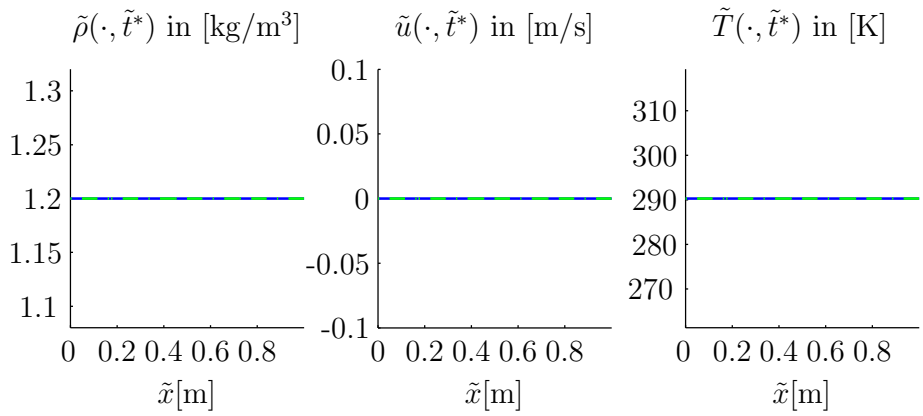


Figure C.4.: Num. results after $\tilde{t}^* = 0\text{s}$ (AM blue, FE green dashed lines)

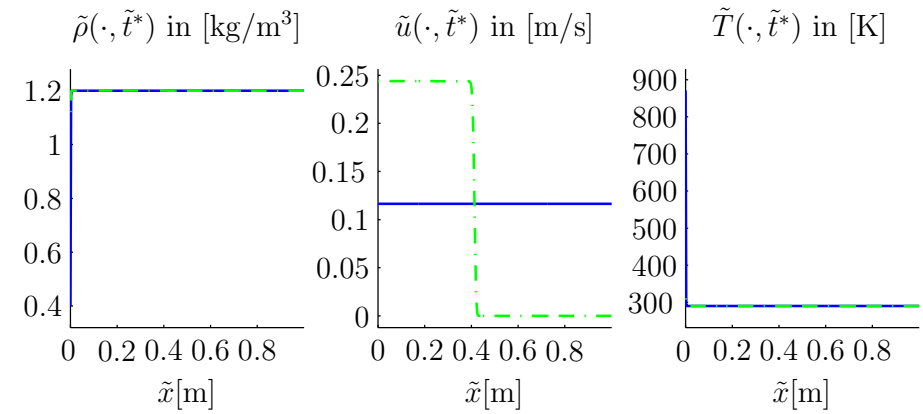


Figure C.5.: Num. results after $\tilde{t}^* = 0.00125\text{s}$ (AM blue, FE green dashed lines)

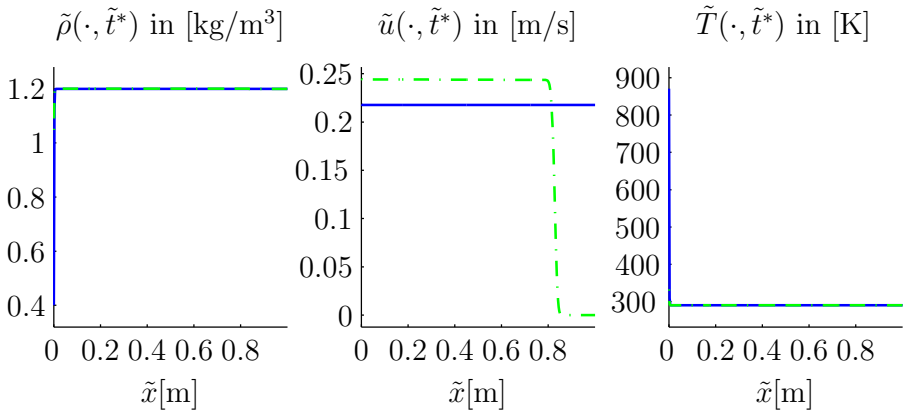


Figure C.6.: Num. results after $\tilde{t}^* = 0.0025$s (AM blue, FE green dashed lines)

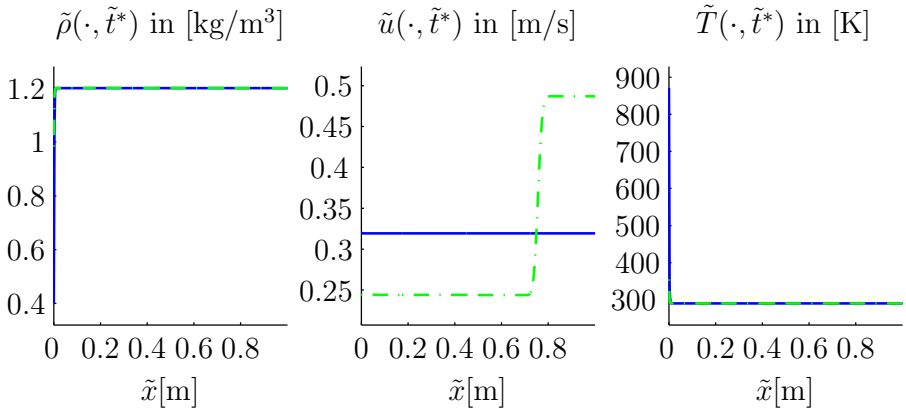


Figure C.7.: Num. results after $\tilde{t}^* = 0.00375$s (AM blue, FE green dashed lines)

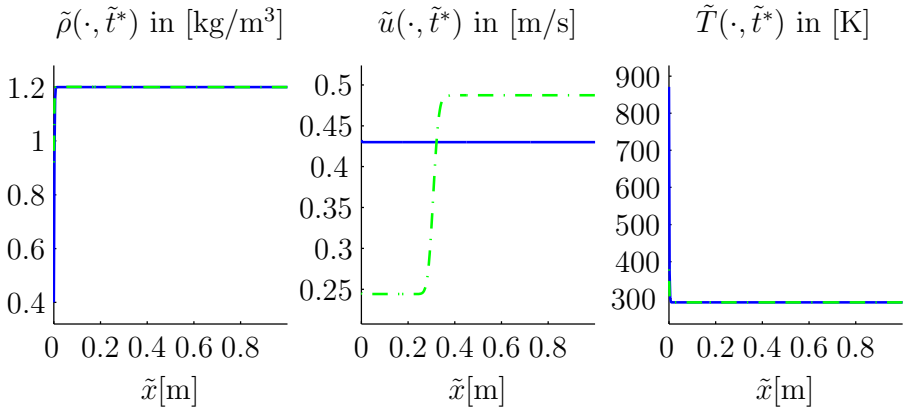


Figure C.8.: Num. results after $\tilde{t}^* = 0.005$s (AM blue, FE green dashed lines)

# D. Optimal control

## D.1. Information on the unscaled heat release coefficient

The value of the unscaled heat exchange coefficient $\tilde{h}_c = 100\frac{\text{kg}}{\text{Kms}^3}$ was found heuristically in order to match the temperature evolution in Figure 2.2. In order to deduce a relation between the scaled and unscaled coefficients, we consider the energy balance in the formulation of Lacoste and Natalini (see Equation (2.12)):

$$(\tilde{A}\tilde{\rho}\tilde{E})_{\tilde{t}} + (\tilde{A}\tilde{\rho}\tilde{u}\tilde{E} + \tilde{A}\tilde{u}\tilde{p})_{\tilde{x}} = -\tilde{h}\pi\tilde{d}(\tilde{T} - \tilde{T}_{\text{Wall}}) + \tilde{\chi}_f\tilde{q}_0\tilde{A}\tilde{\rho}\tilde{z}\tilde{K}(\tilde{T}).$$

Clearly, the heat exchange with the catalytic converter has to be multiplied with the cross section area. Hence,

$$-\tilde{\chi}_f\tilde{h}_c\tilde{A}(\tilde{T} - \tilde{T}_c)$$

models the energy balance of a simple heat exchange between the exhaust gas and the catalytic converter. Next, we proceed as it was done in the Section 2.4 and 2.5.1, i.e., we derive a model for a single pipe by assuming constant cross sections and scale the outcome. This leads us to the following relation between $h_c$ and $\tilde{h}_c$:

$$h_c = \frac{\tilde{h}_c\tilde{x}_{\text{ref}}}{\tilde{\rho}_{\text{ref}}\tilde{u}_{\text{ref}}\tilde{c}_v}.$$

In contrast to the dimensionless parameters $h^i$ and $C_f^i$ (see Equation (2.33)), the scaled heat exchange coefficient $h_c$ does not depend on a pipe-depending parameter (e.g., length or diameter). Therefore it is neglected by superscript notation, when denoting the parameters and variables affiliation to a pipe.

Lastly, we want to present the unscaled version of the ordinary differential equation (4.2), since the dimensionless factor for the heat exchange with the catalytic converter and the gas mixture does not only consist of $\tilde{h}_c$. We have

$$(\tilde{T}_c^i(t))_{\tilde{t}} = -\frac{\tilde{h}_c}{\tilde{\rho}_{\text{ref}}\tilde{c}_v}(\tilde{T}_c^i(\tilde{t}) - \tilde{T}_{\text{Gas}}^i(\tilde{t}))$$

for all $\tilde{t} \in (0, \tilde{t}_{\text{end}})$ and all pipes $i \in I_{cc}$.

## D.2. Identity which follows from Fubini's Theorem

**Lemma 2.** *For any Lebesgue-measurable functions $f, g : [0,1] \to \mathbb{R}$ the following identity holds:*

$$\int_0^1 f(x) \left( \int_0^x g(y)dy \right) dx = \int_0^1 g(x) \left( \int_x^1 f(y)dy \right) dx.$$

*Proof.* With the function

$$h : [0,1] \times [0,1] \to \{0,1\},$$
$$h(x,y) = \begin{cases} 1, & \text{if } y \leq x, \\ 0, & \text{if } y > x \end{cases}$$

we can rewrite the left hand side of the statement.

$$\int_0^1 f(x) \left( \int_0^x g(y)dy \right) dx = \int_0^1 \int_0^1 f(x)g(y)h(x,y)dydx.$$

By Fubini's Theorem (e.g., [For84, §7, Theorem 7]), we are allowed to change the order of integration and obtain

$$\int_0^1 \int_0^1 f(x)g(y)h(x,y)dydx = \int_0^1 \int_0^1 f(x)g(y)h(x,y)dxdy.$$

Isolating the $x$-independent terms from the inner integral leads to

$$\int_0^1 g(y) \int_0^1 f(x)h(x,y)dxdy = \int_0^1 g(y) \left( \int_y^1 f(x)dx \right) dy.$$

□

## D.3. First variation of $\mathcal{L}$ with respect to $T_c$ and $z$

For the sake of completeness in the derivation of the adjoint system, we compute the missing first variation of the Lagrangian $\mathcal{L}$ (4.12) - (4.21) with respect to $T_c$ and $z$. We derive the adjoint equations like in Section 4.4, i.e., for a pipe of length $L = 1$ with a catalytic converter ($\chi = 1$).

### D.3.1. First variation of $\mathcal{L}$ with respect to $T_c$

Before we start with the difference quotient, we first want to determine the differences of the $q, Q$ and $Q_t$, evaluated at $T_c + \epsilon\delta T_c$ and $T_c$:

$$\begin{aligned} q[\rho, z, T_c + \epsilon\delta T_c](x,t) - q[\rho, z, T_c](x,t) &= \epsilon\delta T_c(t) q_{T_c}, \\ Q[\rho, z, T_c + \epsilon\delta T_c](x,t) - Q[\rho, z, T_c](x,t) &= \epsilon\delta T_c(t) \int_0^x q_{T_c} dy, \\ Q_t[\rho, z, T_c + \epsilon\delta T_c](x,t) - Q_t[\rho, z, T_c](x,t) &= [\epsilon\delta T_c(t)]_t \int_0^x q_{T_c} dy \end{aligned}$$

with

$$q_{T_c} := \frac{h_c}{\gamma p_0}. \tag{D.1}$$

We compute the first variation of the Lagrangian with respect to $T_c$ step by step. In order to shorten the expressions, we define the following abbreviations for this section:

$$q := q[\rho, z, T_c], \quad q_\epsilon := q[\rho, z, T_c + \epsilon\delta T_c], \quad Q := Q[\rho, z, T_c], \quad Q_\epsilon := Q[\rho, z, T_c + \epsilon\delta T_c].$$

**a) The cost functional** (4.12)

It is straightforward to see

$$\mathcal{J}[T_c + \epsilon\delta T_c, z_{bc,l}] - \mathcal{J}[T_c, z_{bc,l}] = \int_0^{t_{end}} \epsilon\delta T_c (T_c - T_{opt}) dt + o(\epsilon). \tag{D.2}$$

**b) The $\xi_\rho$-integral** (4.13)

$$\begin{aligned} &- \int_0^{t_{\text{end}}} \int_0^1 \xi_\rho \big(\rho_t + (v + Q_\epsilon)\rho_x + q_\epsilon \rho\big) dx dt \\ &+ \int_0^{t_{\text{end}}} \int_0^1 \xi_\rho \big(\rho_t + (v + Q)\rho_x + q\rho\big) dx dt \\ &\quad = - \int_0^{t_{\text{end}}} \int_0^1 \xi_\rho \left( \rho_x \epsilon\delta T_c \int_0^x q_{T_c} dy + \epsilon\delta T_c \rho q_{T_c} \right) dx dt \\ &\quad = - \int_0^{t_{\text{end}}} \epsilon\delta T_c \int_0^1 q_{T_c} \left( \int_x^1 \xi_\rho \rho_x dy + \xi_\rho \rho \right) dx dt. \end{aligned} \tag{D.3}$$

**c) The $\xi_z$-integral** (4.14)

$$
\begin{aligned}
&-\int_0^{t_{\text{end}}}\int_0^1 \xi_z\big(z_t+(v+Q_\epsilon)z_x+\chi z K(T)\big)dxdt\\
&+\int_0^{t_{\text{end}}}\int_0^1 \xi_z\big(z_t+(v+Q)z_x+\chi z K(T)\big)dxdt\\
&\quad=-\int_0^{t_{\text{end}}}\int_0^1 \xi_z z_x \epsilon\delta T_c\int_0^x q_{T_c}dydxdt\\
&\quad=-\int_0^{t_{\text{end}}}\epsilon\delta T_c\int_0^1 q_{T_c}\int_x^1 \xi_z z_x dydxdt.
\end{aligned}
\tag{D.4}
$$

**d) The $\xi_v$-integral** (4.15)

With

$$
\Phi := \Phi[\rho, z, v, T_c], \qquad \Phi_\epsilon := \Phi[\rho, z, v, T_c+\epsilon\delta T_c]
$$

we deduce

$$
\begin{aligned}
&-\int_0^{t_{\text{end}}}\xi_v\left(v_t-\frac{1}{R(0)}\Phi_\epsilon\right)dt+\int_0^{t_{\text{end}}}\xi_v\left(v_t-\frac{1}{R(0)}\Phi\right)dt\\
&=-\int_0^{t_{\text{end}}}\xi_v\frac{1}{R(0)}\Bigg(\int_0^1\rho[\epsilon\delta T_c]_t\int_0^x q_{T_c}dydx+\int_0^1\epsilon\delta T_c\rho(v+Q)q_{T_c}\\
&\qquad\qquad+\epsilon\delta T_c\rho q\int_0^x q_{T_c}dydx+C_f\int_0^1\epsilon\delta T_c\rho(v+Q)\int_0^x q_{T_c}dydx\\
&\qquad\qquad+\chi C_c\int_0^1\epsilon\delta T_c\rho\int_0^x q_{T_c}dydx\Bigg)dt+o(\epsilon)\\
&=-\int_0^{t_{\text{end}}}\xi_v\frac{1}{R(0)}\Bigg(\int_0^1[\epsilon\delta T_c]_t q_{T_c}R(x)dx+\int_0^1\epsilon\delta T_c\rho(v+Q)q_{T_c}dx\\
&\qquad\qquad+\int_0^1\epsilon\delta T_c q_{T_c}\int_x^1\rho q dydx+C_f\int_0^1\epsilon\delta T_c q_{T_c}\int_x^1\rho(v+Q)dydx\\
&\qquad\qquad+\chi C_c\int_0^1\epsilon\delta T_c q_{T_c}\int_x^1\rho dydx\Bigg)dt+o(\epsilon)\\
&:=I_{\xi_v}.
\end{aligned}
\tag{D.5}
$$

We have to deal with the time derivative in this equation. Since we want to isolate the variation $\delta T_c$ we have to integrate by parts.

$$
\begin{aligned}
&-\int_0^{t_{\text{end}}}\int_0^1 \xi_v \frac{R(x)}{R(0)}[\epsilon\delta T_c]_t q_{T_c} dx \\
&= \int_0^{t_{\text{end}}}\int_0^1 \epsilon\delta T_c q_{T_c}\left[\xi_v\frac{R(x)}{R(0)}\right]_t dx - \left[\int_0^1 \epsilon\delta T_c q_{T_c}\xi_v\frac{R(x)}{R(0)}dx\right]_{t=0}^{t=t_{\text{end}}}.
\end{aligned}
$$

With (4.24) we can get rid of the time derivative of $\xi_v$ [1] .

$$
\begin{aligned}
&\left[\xi_v\frac{R(x)}{R(0)}\right]_t = (\xi_v)_t\frac{R(x)}{R(0)} + \xi_v\frac{R_t(x)}{R(0)} - \xi_v\frac{R_t(0)R(x)}{R(0)^2} \\
&= \left(\xi_v S(0) + \int_0^1 \xi_\rho\rho_x + \xi_z z_x dx\right)\frac{R(x)}{R(0)} + \xi_v\frac{R_t(x)}{R(0)} - \xi_v\frac{R_t(0)R(x)}{R(0)^2} \\
&= \frac{R(x)}{R(0)}\int_0^1 \xi_\rho\rho_x + \xi_z z_x dx + \xi_v\frac{1}{R(0)}\left(R(x)S(0) + R_t(x) - \frac{R_t(0)R(x)}{R(0)}\int_x^1 \rho dy\right).
\end{aligned}
$$

Finally, we obtain for the $\xi_v$ - integral (D.5):

$$
\begin{aligned}
I_{\xi_v} = \int_0^{t_{\text{end}}} \epsilon\delta T_c \int_0^1 q_{T_c}\Bigg[\frac{R(x)}{R(0)}\int_0^1 \xi_\rho\rho_x + \xi_z z_x dx + \xi_v\frac{1}{R(0)}\Bigg(R(x)S(0) + R_t(x) \\
-R(0)S(x) - \frac{R_t(0)R(x)}{R(0)} - \rho(v+Q)\Bigg)\Bigg] dxdt \\
- \left[\epsilon\delta T_c\xi_v\frac{1}{R(0)}\int_0^1 q_{T_c}R(x)dx\right]_{t=0}^{t=t_{\text{end}}} + o(\epsilon).
\end{aligned}
\tag{D.6}
$$

**e) The $\xi_{T_c}$-integral** (4.16)

$$
\begin{aligned}
&-\int_0^{t_{\text{end}}} \xi_{T_c}\big((T_c+\epsilon\delta T_c)_t - h_c(T_{gas} - (T_c+\epsilon\delta T_c))\big)dt \\
&+\int_0^{t_{\text{end}}} \xi_{T_c}\big((T_c)_t - h_c(T_{gas} - T_c)\big)dt \\
&= -\int_0^{t_{\text{end}}} \xi_{T_c}\big((\epsilon\delta T_c)_t + h_c\epsilon\delta T_c\big)dt \\
&= \int_0^{t_{\text{end}}} \epsilon\delta T_c\big((\xi_{T_c})_t - h_c\xi_{T_c}\big)dt - \Big[\epsilon\delta T_c\xi_{T_c}\Big]_{t=0}^{t=t_{\text{end}}}
\end{aligned}
\quad . \tag{D.7}
$$

[1] The variable $S$ is defined in (4.23).

**f) The summary of the computation for the first variation of $\mathcal{L}$ with respect to $T_c$**

Since everything is prepared, we can start with the derivative. Combining the terms (D.2),(D.3),(D.4),(D.6), and (D.7), we obtain:

$$\begin{aligned}\frac{\partial \mathcal{L}(W, z_{bc,l}, \Lambda)}{\partial T_c}(\delta T_c) = \lim_{\epsilon \to 0} \frac{1}{\epsilon} \Bigg[ \int_0^{t_{\text{end}}} \epsilon \delta T_c \Bigg( & (\xi_{T_c})_t - h_c \xi_{T_c} \\ & + (T_c - T_{opt}) - \int_0^1 q_{T_c} F dx \Bigg) dt \\ & - \left[ \epsilon \delta T_c \xi_v \frac{1}{R(0)} \int_0^1 q_{T_c} R(x) dx \right]_{t=0}^{t=t_{\text{end}}} \\ & - \left[ \epsilon \delta T_c \xi_{T_c} \right]_{t=0}^{t=t_{\text{end}}} - \nu_{T_c} \epsilon \delta T_c \Big|_{t=0} + o(\epsilon) \Bigg],\end{aligned}$$

where $F$ is defined (4.35). By using that $\delta T_c$ is arbitrary, we end up with

$$\boxed{-(\xi_{T_c})_t = -\int_0^1 q_{T_c} F dx - h_c \xi_{T_c} + (T_c - T_{opt})}$$

and the terminal condition

$$\boxed{\xi_{T_c} = 0 \quad \text{for} \quad t = t_{\text{end}}.}$$

## D.3.2. First variation of $\mathcal{L}$ with respect to $z$

Again, we first determine the differences of the $q, Q$ and $Q_t$ evaluated at $z + \epsilon \delta z$ and $z$, respectively.

$$\begin{aligned} q[\rho, z + \epsilon \delta z, T_c] - q[\rho, z, T_c] &= \epsilon \delta z q_z, \\ Q[\rho, z + \epsilon \delta z, T_c] - Q[\rho, z, T_c] &= \int_0^x \epsilon \delta z(y,t) q_z(y,t) dy, \\ Q_t[\rho, z + \epsilon \delta z, T_c] - Q_t[\rho, z, T_c] &= \int_0^x [\epsilon \delta z(y,t) q_z(y,t)]_t dy \end{aligned}$$

with

$$q_z := \chi \frac{q_0}{\gamma p_0} \rho K(T). \tag{D.8}$$

We now compute the variation of the Lagrangian step by step. As in the section before, we use the equivalent shortening expression:

$$q := q[\rho, z, T_c], \quad q_\epsilon := q[\rho, z + \epsilon \delta z, T_c], \quad Q := Q[\rho, z, T_c], \quad Q_\epsilon := Q[\rho, z + \epsilon \delta z, T_c].$$

**a) The $\xi_\rho$-integral** (4.13)

$$
\begin{aligned}
&-\int_0^{t_{\text{end}}}\int_0^1 \xi_\rho\big(\rho_t+(v+Q_\epsilon)\rho_x+q_\epsilon\rho\big)dxdt\\
&+\int_0^{t_{\text{end}}}\int_0^1 \xi_\rho\big(\rho_t+(v+Q)\rho_x+q\rho\big)dxdt\\
&\quad=-\int_0^{t_{\text{end}}}\int_0^1 \xi_\rho\left(\rho_x\int_0^x \epsilon\delta z q_z dy+\epsilon\delta z\rho q_z\right)dxdt\\
&\quad=-\int_0^{t_{\text{end}}}\int_0^1 \epsilon\delta z\left(q_z\int_x^1 \xi_\rho\rho_x dy+\xi_\rho\rho q_z\right)dxdt.
\end{aligned}
\tag{D.9}
$$

**b) The $\xi_z$-integral** (4.14)

$$
\begin{aligned}
&-\int_0^{t_{\text{end}}}\int_0^1 \xi_z\big((z+\epsilon\delta z)_t+(v+Q_\epsilon)(z+\epsilon\delta z)_x+\chi(z+\epsilon\delta z)K(T)\big)dxdt\\
&+\int_0^{t_{\text{end}}}\int_0^1 \xi_z\big(z_t+(v+Q)z_x+\chi zK(T)\big)dxdt\\
&\quad=-\int_0^{t_{\text{end}}}\int_0^1 \xi_z\left(\epsilon\delta z_t+(v+Q)\epsilon\delta z_x+z_x\int_0^x \epsilon\delta z q_z dy+\chi\epsilon\delta zK(T)\right)dxdt+o(\epsilon)\\
&\quad=\int_0^{t_{\text{end}}}\int_0^1 \epsilon\delta z\left((\xi_z)_t+(v+Q)(\xi_z)_x+\xi_z q-q_z\int_x^1 \xi_z z_x dy-\chi\xi_z K(T)\right)dxdt\\
&\qquad-\left[\int_0^{t_{\text{end}}}\epsilon\delta z(v+Q)\xi_z dt\right]_{x=0}^{x=1}-\left[\int_0^1 \epsilon\delta z\xi_z dx\right]_{t=0}^{t=t_{\text{end}}}+o(\epsilon).
\end{aligned}
\tag{D.10}
$$

**c) The $\xi_v$-integral** (4.15)

With

$$
\Phi := \Phi[\rho, z, v, T_c], \qquad \Phi_\epsilon := \Phi[\rho, z+\epsilon\delta z, v, T_c],
$$

we deduce

$$
\begin{aligned}
&-\int_0^{t_{\text{end}}} \xi_v \left(v_t - \frac{1}{R(0)}\Phi_\epsilon\right) dt + \int_0^{t_{\text{end}}} \xi_v \left(v_t - \frac{1}{R(0)}\Phi\right) dt \\
&= -\int_0^{t_{\text{end}}} \xi_v \frac{1}{R(0)} \left(\int_0^1 \rho \int_0^x [\epsilon\delta z q_z]_t dy dx + \int_0^1 \epsilon\delta z \rho (v+Q) q_z \right. \\
&\qquad + \rho q \int_0^x \epsilon\delta z q_z dy dx + C_f \int_0^1 \rho (v+Q) \int_0^x \epsilon\delta z q_z dy dx \\
&\qquad \left. + \chi C_c \int_0^1 \rho \int_0^x \epsilon\delta z q_z dy dx \right) dt + o(\epsilon) \\
&= -\int_0^{t_{\text{end}}} \xi_v \frac{1}{R(0)} \left(\int_0^1 [\epsilon\delta z q_z]_t R(x) dx + \int_0^1 \epsilon\delta z \rho (v+Q) q_z dx \right. \\
&\qquad + \int_0^1 \epsilon\delta z q_z \int_x^1 \rho q dy dx + C_f \int_0^1 \epsilon\delta z q_z \int_x^1 \rho (v+Q) dy dx \\
&\qquad \left. + \chi C_c \int_0^1 \epsilon\delta z q_z \int_x^1 \rho dy dx \right) dt + o(\epsilon) =: I_{\xi_v}. \qquad \text{(D.11)}
\end{aligned}
$$

Like in the case of $T_c$, we have to deal with the time derivative in this equation. Since we want to isolate the variation $\delta z$ we have to integrate by parts.

$$
\begin{aligned}
&-\int_0^{t_{\text{end}}} \int_0^1 \xi_v \frac{R(x)}{R(0)} [\epsilon\delta z q_z]_t dx dt \\
&= \int_0^{t_{\text{end}}} \int_0^1 \epsilon\delta z q_z \left[\xi_v \frac{R(x)}{R(0)}\right]_t dx dt - \left[\int_0^1 \epsilon\delta z q_z \xi_v \frac{R(x)}{R(0)} dx\right]_{t=0}^{t=t_{\text{end}}}.
\end{aligned}
$$

We replace the time derivative of $\xi_v$ like in the computation of the $\xi_v$-integral in the previous subsection (see Subsection D.3.2, **d)**). We obtain finally for the $\xi_v$ -integral (D.11)

$$
\begin{aligned}
I_{\xi_v} = &\int_0^{t_{\text{end}}} \int_0^1 \epsilon\delta z \left[\xi_v q_z \frac{1}{R(0)} \left(-\rho(v+Q) - R(0)S(x) + R(x)S(0) + R_t(x) \right.\right. \\
&\qquad \left.\left. - \frac{R_t(0)R(x)}{R(0)}\right) + q_z \frac{R(x)}{R(0)} \int_0^1 \xi_\rho \rho_x + \xi_z z_x dx\right] dx dt \\
&- \left[\int_0^1 \epsilon\delta z q_z \xi_v \frac{R(x)}{R(0)} dx\right]_{t=0}^{t=t_{\text{end}}} + o(\epsilon). \qquad \text{(D.12)}
\end{aligned}
$$

We can combine the terms (D.9),(D.10), and (D.12) to get:

$$\begin{aligned}\frac{\partial \mathcal{L}(W, z_{bc,l}, \Lambda)}{\partial z}(\delta z) = \lim_{\epsilon \to 0} \frac{1}{\epsilon} \Bigg[ \int_0^{t_{\text{end}}} \int_0^1 \epsilon \delta z \Big( & (\xi_z)_t + (v+Q)(\xi_z)_x \\ & - \xi_z \left(\chi K(T) - q\right) - q_z F \Big) dx dt \\ & - \left[ \int_0^{t_{\text{end}}} \epsilon \delta z (v+Q) \xi_z dt \right]_{x=0}^{x=1} \\ & - \left[ \int_0^1 \epsilon \delta z \xi_z dx + \int_0^1 \epsilon \delta z q_z \xi_v \frac{R(x)}{R(0)} dx \right]_{t=0}^{t=t_{\text{end}}} \\ & - \int_0^{t_{\text{end}}} \epsilon \delta z(0,t) \eta_2(t) dt - \int_0^1 \epsilon \delta z(x,0) \nu_2(x) dx + o(\epsilon) \Bigg].\end{aligned}$$

Using that $\delta z$ is arbitrary, we end up with

$$\boxed{-(\xi_z)_t - (v+Q)(\xi_z)_x = -q_z F - \xi_z \left(\chi K(T) - q\right)} \tag{D.13}$$

with terminal condition

$$\boxed{\xi_z = 0 \quad \text{for} \quad t = t_{\text{end}}} \tag{D.14}$$

and boundary condition

$$\boxed{\xi_z (v+Q) = 0 \quad \text{for} \quad x = 1.}$$

Furthermore, the spatial boundary condition for $\xi_z$ at $x = 0$ plays an important role. By these conditions we compute the adjoint $\eta_z$, which also appears in the optimality condition, i.e., it is used for the computation of the gradient.

$$\boxed{\xi_z (v+Q) = \eta_z \quad \text{for} \quad x = 0.} \tag{D.15}$$

### D.3.3. Coupling conditions for the adjoint equation for $\xi_z$

We follow the derivation from Subsection 4.4.3. Let us consider the first variation of the Lagrangian for the whole network (4.12)-(4.21) with respect to the ratio of unburnt gas in an inner pipe $i$. As outlined in D.3.2, we would deduce (D.13) and (D.14). Since $i \in \{2, \ldots, n_P - 1\}$, we have to neglect the boundary condition for the ratio of unburnt gas (4.17). Finally, we would be left only with the following integrals:

$$\begin{aligned}\frac{\partial \mathcal{L}(W, z_{bc,l}, \Lambda)}{\partial z^i}(\delta z) = & - \int_0^{t_{\text{end}}} \delta z^i(L^i, t) \left( (v^i(t) + Q^i(L^i, t)) \xi_z^i(L^i, t) + \zeta_z^{i+1}(t) \right) dt \\ & + \int_0^{t_{\text{end}}} \delta z^i(0, t) \left( (v^i(t) + Q^i(0, t)) \xi_z^i(0, t) + \zeta_z^i(t) \right) dt \overset{!}{=} 0.\end{aligned}$$

Using the fact that $\delta z^i$ is arbitrary, we obtain

$$(v^i(t) + Q^i(L^i, t))\xi_z^i(L^i, t) = -\zeta_z^{i+1}(t) \tag{D.16}$$

and

$$(v^i(t) + Q^i(0, t))\xi_z^i(0, t) = -\zeta_z^i(t). \tag{D.17}$$

Increasing the indices of all terms in D.17, we can combine this with D.16 to get:

$$\boxed{(v^i(t) + Q^i(L^i, t))\xi_z^i(L^i, t) = -\zeta_z^{i+1}(t) = (v^{i+1}(t) + Q^{i+1}(0, t))\xi_z^{i+1}(0, t).}$$

## D.4. First-discretize-then-optimize vs first-optimize-then-discretize

In this section, we want to demonstrate, by considering a simplified example, that both approaches can lead to the same discretization of the adjoint problem. Moreover, we show how to discretize the adjoint equations derived in Section 4.4, which are posed backwards in space and time, properly.

For this investigation, we consider a problem in which we control the boundary condition $\rho_{bc,l}$ of a physical quantity $\rho$, in order to match the latter with a desired state $\rho_{opt}$ at a fixed spatial position ($x = 1$). The optimal control problem is to minimize a tracking-type cost functional, subject to the constraints, consisting of a transport equation as well as initial and boundary conditions:

$$\min_{\rho_{bc,l} \in R_{ad}} \mathcal{J}(\rho(\rho_{bc,l})) := \frac{1}{2} \int_0^T (\rho(1, t) - \rho_{opt}(t))^2 dt,$$

subject to

$$\begin{aligned} \rho_t + u\rho_x &= -k\rho, && \text{in } (0, 1) \times (0, t_{\text{end}}), \\ \rho(x, 0) &= \rho_{ic}(x), && \text{on } [0, 1], \\ \rho(0, t) &= \rho_{bc,l}(t), && \text{on } (0, t_{\text{end}}], \end{aligned}$$

where $u > 0$ and $k > 0$ are given constants.

### D.4.1. First-discretize-then-optimize

1. **Discretize:**
   We discretize the PDE with the explicit upwind scheme (3.23):

$$\rho_j^{n+1} = \rho_j^n + \Delta t \left( -u \frac{\rho_j^n - \rho_{j-1}^n}{\Delta x} - k\rho_j^n \right)$$

with a uniform spatial grid size $\Delta x = J^{-1}$, and a uniform time step size $\Delta t = N^{-1}$. In order to respect the CFL condition, the number of space and time grid points ($J+1$ and $N+1$) have fulfil the relation

$$\frac{N}{J} \geq u.$$

Rewriting the state discretization in matrix-form yields for all time indices $n \in \{0, \ldots, N-1\}$

$$\rho^{n+1} = A\rho^n + b^n$$

with

$$\rho^n := \begin{pmatrix} \rho_0^n \\ \rho_1^n \\ \vdots \\ \rho_J^n \end{pmatrix}, \quad A := \begin{pmatrix} 0 & & & \\ c & d & & \\ & \ddots & \ddots & \\ & & c & d \end{pmatrix}, \quad b^n := \begin{pmatrix} \rho_{bc,l}(t^n) \\ \mathbf{1}_{\{0\}}(t^n)\rho_{ic}(x_1) \\ \vdots \\ \mathbf{1}_{\{0\}}(t^n)\rho_{ic}(x_J) \end{pmatrix},$$

$$c := u\frac{\Delta t}{\Delta x}, \qquad d := 1 - u\frac{\Delta t}{\Delta x} - \Delta t k,$$

where $\rho_{bc,l}(t^n)$ and $\rho_{ic}(x_j)$ are the evaluations of the boundary and initial condition at time step $t^n = n \cdot \Delta t$ / spatial grid point $x_j = j \cdot \Delta x$, respectively. The indicator function $\mathbf{1}_{\{0\}}(t)$ vanishes if $t \neq 0$. Finally, we consider

$$B\rho = b,$$

with

$$B := \begin{pmatrix} I & & & \\ -A & \ddots & & \\ & \ddots & \ddots & \\ & & -A & I \end{pmatrix}, \qquad \rho := \begin{pmatrix} \rho^0 \\ \rho^1 \\ \vdots \\ \rho^N \end{pmatrix}, \qquad b := \begin{pmatrix} b^0 \\ b^1 \\ \vdots \\ b^N \end{pmatrix},$$

where $I \in \mathbb{R}^{(J+1)\times(J+1)}$ is the identity matrix.

2. **Optimize:**
   The first variation of the discrete Lagrangian is

$$\begin{aligned} \frac{\partial \mathcal{L}^{dis}(\rho, \rho_{bc,l}, \xi, \eta, \nu)}{\partial \rho}(\delta\rho) &= \lim_{\epsilon \to 0} \frac{1}{\epsilon}\Big[\langle B(\rho + \epsilon\delta\rho) - b, \xi\rangle - \langle B\rho - b, \xi\rangle\Big] \\ &= \langle \delta\rho, B^T\xi\rangle = 0. \end{aligned}$$

Since the last identity holds for any admissible perturbation $\delta\rho \in \mathbb{R}^{(J+1)(N+1)}$, we obtain

$$B^T \xi = 0.$$

By this we have

$$\xi^n = A^T \xi^{n+1}$$

and therefore

$$\begin{aligned}\xi_j^n &= d\xi_j^{n+1} + c\xi_{j+1}^{n+1} \\ &= \xi_j^{n+1} + \Delta t \left( -u \frac{\xi_j^{n+1} - \xi_{j+1}^{n+1}}{\Delta x} - k\xi_j^{n+1} \right).\end{aligned}$$

### D.4.2. First-optimize-then-discretize

1. **Optimize:**
   Before starting with the computation, we state the Lagrangian functional of the considered optimal control problem:

$$\begin{aligned}\mathcal{L}(\rho, \rho_{bc,l}, \xi, \eta, \nu) = \frac{1}{2} \int_0^T (\rho(1,t) - \rho_{opt}(t))^2 dt - \int_0^T \int_0^1 \xi(\rho_t + u\rho_x + k\rho) dx dt \\ - \int_0^T \eta(\rho(0,t) - \rho_{bc,l}(t)) dt - \int_0^1 \nu(\rho(x,0) - \rho_{ic}(x)) dx.\end{aligned}$$

   We derive the adjoint equations, similar to the computation of Sections 4.4 and D.3.

$$\begin{aligned}0 \overset{!}{=} \frac{\partial \mathcal{L}(\rho, \rho_{bc,l}, \xi, \eta, \nu)}{\partial \rho}(\delta\rho) = &\int_0^{t_{\text{end}}} \delta\rho(1,t)(\rho(1,t) - \rho_{opt}(t)) dt \\ &+ \int_0^{t_{\text{end}}} \int_0^1 \delta\rho \left(\xi_t + u\xi_x - k\xi\right) dx dt \\ &- \int_0^1 \Big[\delta\rho\xi\Big]_0^{t_{\text{end}}} + \delta\rho(x,0)\nu dx \\ &- \int_0^{t_{\text{end}}} \Big[\delta\rho u\xi\Big]_{x=0}^{x=1} + \delta\rho(0,t)\eta dt.\end{aligned}$$

By the fundamental lemma of variational calculus, we obtain:

$$\begin{aligned} -\xi_t - u\xi_x &= -k\xi, && \text{in } (0,1)\times(0,t_{\text{end}}),\\ \xi(x,t_{\text{end}}) &= 0, && \text{on } [0,1],\\ \xi(1,t) &= \rho(1,t) - \rho_{opt}(t), && \text{on } [0,t_{\text{end}}). \end{aligned}$$

2. **Discretize:**
We discretize the state equation with the same explicit upwind scheme which was used in the first approach. Since the adjoint equation is posed backwards in space and time (boundary condition at $x = 1$, although the flow direction $u$ is positive; terminal condition at $t = t_{\text{end}}$), we have to transform the variables, such that the problem is posed forward in space and time. Then we can apply our standard explicit upwind scheme, which we used for the discretization of the state equation.

So let us introduce the new variables for space and time:

$$\hat{t} := t_{\text{end}} - t, \qquad \hat{x} := 1 - x.$$

With $\hat{\xi}(\hat{x},\hat{t}) = \xi(x,t)$ we obtain

$$\begin{aligned} \hat{\xi}_{\hat{t}} + u\hat{\xi}_{\hat{x}} &= -k\hat{\xi}, && \text{in } (0,1)\times(0,t_{\text{end}}),\\ \hat{\xi}(\hat{x},0) &= 0, && \text{on } [0,1],\\ \hat{\xi}(0,\hat{t}) &= \rho(1,t_{\text{end}}-\hat{t}) - \rho_{opt}(t_{\text{end}}-\hat{t}), && \text{on } (0,t_{\text{end}}]. \end{aligned}$$

In contrast to the original formulation, the system for the variable $\hat{\xi}$ is posed forward in the new space and time variables $\hat{x}$ and $\hat{t}$. Therefore, we can now apply our standard explicit upwind scheme:

$$\hat{\xi}_i^{m+1} = \hat{\xi}_i^m + \Delta t\left(-u\frac{\hat{\xi}_i^m - \hat{\xi}_{i-1}^m}{\Delta x} - k\hat{\xi}_i^m\right).$$

Retransformation leads to a discretization for the variable $\xi$:

$$\xi_j^n = \xi_j^{n+1} + \Delta t\left(-u\frac{\xi_j^{n+1} - \xi_{j+1}^{n+1}}{\Delta x} - k\xi_j^{n+1}\right).$$

## D.5. Parameters used for Armijo line search

We shortly discuss the principle of the Armijo line search method on the basis of [GK99] and [NW06] and give details about the parameter values used for the

optimization in the Algorithm 3 on Page 95.

Having found a search direction $d \in \mathbb{R}^N$, along which one assumes to find an improvement of the current state $x \in \mathbb{R}^N$ with respect to the evaluation of the functional $f : \mathbb{R}^N \to \mathbb{R}$, one still need to determine "how far" one has to follow that direction, i.e., one needs to find a step size $s$. There are several algorithms to fulfil this task, such as the (strong) Wolfe-Powell-rule and the Armijo-rule. For the sake of simplicity, we applied the latter in our optimization algorithm. The task is, given $\kappa \in (0,1), \beta \in (0,1)$, to find a step size $s \in \max\{\beta^l \mid l = 0, 1, 2, \ldots\}$, such that

$$f(x + sd) \leq f(x) + \kappa s \nabla f(x) d^T. \tag{D.18}$$

We choose

$$\beta = 0.25, \qquad \kappa = 10^{-7},$$

i.e., we reduce the step length by 75%, each time the Armijo condition (D.18) is violated. The value for $\kappa$ is chosen heuristically and reduces the demand of a "larger" decrease of the objective functional $f$.

# E. Android App

For the purpose of demonstrating that the asymptotic model (2.57) can be simulated in real time on small device, we - Ruslan Krenzler[†] and Martin Rybicki - programmed an Android App[1] "Single Pipe Flow". As the name of the application already indicates, the computational domain consists of a single pipe with constant cross section. However, the pipe can also contain a catalytic converter (see top right figure).

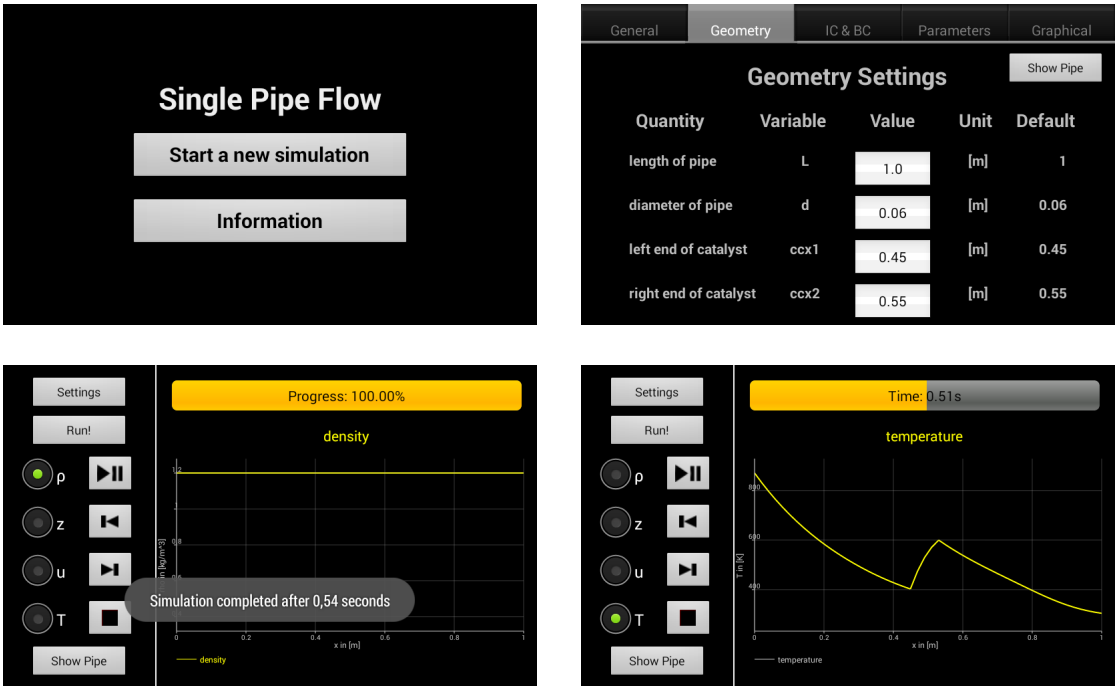


Figure E.1.: Screenshots of the running Android App on a Samsung Galaxy S2 i9100.

[†]Ruslan Krenzler is a PhD student at the University of Hamburg. Website: `http://www.math.uni-hamburg.de/home/krenzler/`

[1]For details and download see `http://www.math.uni-hamburg.de/home/rybicki/apps`

## Short summary in English

See p. 105ff.

## Zusammenfassung auf Deutsch

In dieser Arbeit wird die Strömung von Abgasen in einem Auspuffrohr untersucht. Dabei ist inbesondere das Aufheizverhalten des Katalysators nach dem Kaltstart von Interesse.

Um dieses zu untersuchen wird zunächst ein numerisch effizientes Modell benötigt. Die Grundlage für unsere Herleitung eines solches Modells bildet ein hyperbolisches System von partiellen Differentialgleichungen (u.a. bestehend aus den reaktiven Eulergleichungen), welches von Lacoste und Natalini in Zusammenarbeit mit dem italienischen Autozulieferer Magenti Marelli hergeleitet wurde (vgl. [LN04]). In Hinblick auf schnelle numerische Umsetzung bietet dieses Modell noch Verbesserungspotential. Zum einen kann man durch einen Netzwerk-Ansatz auf ortsabhängige Querschnittsfunktionen zur Abbildung der Auspuffgeometrie verzichten. Zum anderen lässt sich durch einen kleinen Machzahl Grenzwert die Komplexität des Modells so vereinfachen, dass es keine Informationen über die Ausbreitung der Schallwellen mehr enthält, ohne jedoch gleichzeitig Aussagekraft über die verbleibenden physikalischen Prozesse zu verlieren. Bei dem somit erhalten asymptotischen Modell sind wir in der Lage klassische numerische Verfahren (explizite Upwind Verfahren) mit deutlich größeren Orts- und Zeitschrittweiten für numerischen Simulationen zu verwenden.

Im zweiten Teil der Arbeit verifizieren wir sowohl ein numerisches Verfahren für das neue asymptotische Modell als auch das Modell selbst, indem wir es mit den numerischen Ergebnissen des prä-asymptotischen Modells vergleichen.

Die Arbeit wird abgeschlossen durch die Beantwortung der Frage, inwieweit man Katalysatoren bei einem Kaltstart optimal aufheizen kann. Für das Optimalsteuerungsproblem werden zunächst formal, mittels eines Lagrange-Kalküls, die Optimalitätsbedingungen hergeleitet. Anschließend werden mit Hilfe des projezierten Gradientenverfahrens zwei prototypische Beispiele demonstiert, welche zeigen, mit welchem Luft-Kraftstoffgemisch im Motor man ein optimales Aufheizverhalten des Katalysators erhält.

# Lebenslauf

Name: Martin Rafeal Rybicki
E-Mail: martin.rybicki@yahoo.de

| | |
|---|---|
| 12.05.1986 | geboren in Neustadt, Polen (poln. Wejherowo). |
| 06/2005 | Erhalt der Allgemeinen Hochschulreife (Abitur) am Gymnasiun Süderelbe, Hamburg. |
| 10/2005 - 03/2007 | Studium Diplom-Wirtschaftsmathematik an der Universität Hamburg. |
| 10/2006 - 03/2010 | Studium Diplom-Mathematik mit Anwendungsfach VWL an der Universität Hamburg. |
| 03/2007 | Vordiplom Wirtschaftsmathematik mit der Note „gut“(1,6). |
| 08/2007 | Vordiplom Mathematik mit der Note „sehr gut“. |
| 08/2007 - 03/2008 | Teilnahme am Erasmus-Austauschprogramm: Studium der Mathematik an der University of Bath, in Bath, England. |
| 09/2010 | Diplom im Mathematik mit der Note „sehr gut“. |
| 10/2010 - 07/2014 | Promotionsstudium am Fachbereich Mathematik der Universität Hamburg. |